In presenting the dissertation as a partial fulfillment of the requirements for an advanced degree from the Georgia Institute of Technology, I agree that the Library of the Institute shall make it available for inspection and circulation in accordance with its regulations governing materials of this type. I agree that permission to copy from, or to publish from, this dissertation may be granted by the professor under whose direction it was written, or, in his absence, by the Dean of the Graduate Division when such copying or publication is solely for scholarly purposes and does not involve potential financial gain. It is understood that any copying from, or publication of, this dissertation which involves potential financial gain will not be allowed without written permission.

7/25/68

MOBILITIES, LONGITUDINAL DIFFUSION COEFFICIENTS, AND REACTION RATES OF MASS-IDENTIFIED POSITIVE AND NEGATIVE OXYGEN IONS IN OXYGEN

A THESIS

Presented to

The Faculty of the Division of Graduate

Studies and Research

by

Robert Marvin Snuggs

In Partial Fulfillment

of the Requirements for the Degree

Doctor of Philosophy

in the School of Physics

Georgia Institute of Technology

March, 1970

MOBILITIES, LONGITUDINAL DIFFUSION COEFFICIENTS,

AND REACTION RATES OF MASS-IDENTIFIED POSITIVE

AND NEGATIVE OXYGEN IONS IN OXYGEN

Approved:

_____ _____

Chairman

____ _____

_____ _____

Date approved by Chairman: May 22, 1970

This thesis is gratefully dedicated

to my wife, Wanda, and my parents,

Mr. and Mrs. Robert M. Snuggs, Jr.

ACKNOWLEDGMENTS

It is with pleasure that acknowledgment is made of the interest and assistance of those who have contributed to the work described in this thesis. The author wishes to acknowledge the guidance and encouragement of his thesis advisors, Dr. Earl McDaniel and Dr. David Martin, throughout this research. The comments of Dr. Ron Felton, who served on the thesis reading committee, were valued.

The assistance of Dr. Don Volz and Mr. John Schummers, who aided the author in obtaining the data presented here and with whom many fruitful discussions were held, is greatly appreciated. The contributions of those who preceded the author in this laboratory, Dr. Dan Albritton, Dr. Tom Miller, and Dr. John Moseley, are acknowledged.

A special acknowledgment is made of the contribution of Dr. Ian Gatland to the analysis presented in Chapter III.

The research reported here was sponsored in part by the Office of Naval Research in Project SQUID, Purdue University, and in part by the U. S. Air Force Office of Scientific Research. The author was the recipient of a NASA fellowship for three years.

TABLE OF CONTENTS

LIST OF ILLUSTRATIONS

Figure Page

SUMMARY

The drift velocities and mobilities of mass-identified O_2^+, O_4^+, O^-, O_2^-, O_3^-, O_4^- and K^+ ions in oxygen gas at 300°K and at pressures on the range from 0.03 to 6.27 Torr have been determined as a function of E/N, where E is the electric field strength and N is the gas molecule number density. The longitudinal diffusion coefficients for O_2^+, O^-, O_2^- and K^+ ions in oxygen have been measured as a function of E/N at the same temperature and on the same pressure range. The rates for the ion-molecule reactions

$$O^- + O_2 \rightarrow O_2^- + O$$

and

$$O^- + 2O_2 \rightarrow O_3^- + O_2$$

have also been obtained, and order of magnitude estimates for the rates of the reaction

$$O_2^+ + 2O_2 \rightarrow O_4^+ + O_2$$

and its reverse reaction

$$O_4^+ + O_2 \rightarrow O_2^+ + 2O_2$$

have been determined.

The measurements were made with a drift tube mass spectrometer of ultra-high vacuum construction. Most of the results were obtained by a time-of-flight method. This method uses a pulsed electron-impact ion source combined with an electric shutter to create, repetitively, bursts of oxygen ions of accurately known initial spatial extent and temporal duration. Potassium ions are produced by a thermionic emitter. Each ion swarm migrates down the drift tube under the influence of a weak uniform electric field. During this migration the swarm spreads due to diffusion, and may undergo ion-molecule reactions with the neutral gas. The ion population is sampled on the axis at the end of the drift tube by a small exit aperture and mass-selected by an rf quadrupole spectrometer. The ions are individually detected. The time of arrival of an ion at the detector is recorded by a 256-channel time analyzer. By repetitive pulsing of the ion source, a histogram of arrival times can be built up. From such time profiles the drift velocities, diffusion coefficients and some of the ion-molecule reaction rates were obtained. Ion-molecule reaction rates were also determined by an attenuation method, in which the decrease in primary ion current was measured as the drift distance was increased by moving the ion source further away from the exit aperture.

The mobility of O_2^+ was obtained on the E/N range from 7 to 550×10^{-17} V cm^2 and over a pressure range of 0.20 to 0.03 Torr. The zero-field reduced mobility for O_2^+ was determined to be 2.24 ± .09 cm^2/V sec. The mobility of O^- was obtained on the E/N range from 4 to

175 x 10^{-17} V cm^2 and over a pressure range of 0.26 to 0.05 Torr. The zero-field reduced mobility for O^- was shown to be 3.20 ± .13 cm^2/V sec. The mobility of O_2^- was measured on the E/N range from 3 to 140 x 10^{-17} V cm^2 and over a pressure range of 0.63 to 0.10 Torr. The zero-field reduced mobility for O_2^- was determined to be 2.16 ± .09 cm^2/V sec. The mobility of O_3^- was obtained on the E/N range from 4 to 15 x 10^{-17} V cm^2 and over a pressure range of 1.05 to 2.61 Torr. The zero-field reduced mobility for O_3^- was shown to be 2.55 ± .10 cm^2/V sec. The mobilities of O_4^+ and O_4^- were measured on the E/N range from 2 to 5 x 10^{-17} V cm^2 and over a pressure range of 3.13 to 6.27 Torr. The zero-field reduced mobility for O_4^+ was shown to be close to that for O_2^+; the mobility of O_4^- was determined to be similar to that for O_2^-. The mobility of K^+ was obtained on the E/N range from 3 to 300 x 10^{-17} V cm^2 and over a pressure range of 6.27 to 0.05 Torr. The zero-field reduced mobility for K^+ was determined to be 2.68 ± .11 cm^2/V sec.

Longitudinal diffusion coefficients were measured for O_2^+, O^-, O_2^- and K^+ in O_2 on the E/N range from 3 to 500 x 10^{-17} V cm^2 and over a pressure range of 0.26 to 0.03 Torr. All coefficients at low E/N were within 16 per cent of the values predicted from the mobilities by the Einstein relation. At higher E/N the coefficients increased, in some cases quite rapidly, as E/N was increased.

The rate constant for the reaction

$$O^- + 2O_2 \rightarrow O_3^- + O_2$$

was measured on the E/N range from 6 to 29 x 10^{-17} V cm^2 and at pressures from 0.31 to 0.84 Torr. The rate coefficient was found to be 1.0 ± 0.2 x 10^{-30} cm^6/sec over the entire E/N range. The reaction

$$O^- + O_2 \rightarrow O_2^- + O$$

was observed with a rate that increased sharply with E/N. This is as might be expected of an endothermic reaction. The reaction is endothermic because the electron affinity of O^- is about 1 eV greater than that for O_2^-. The rate coefficient was found to increase from 2.5 ± 1.5 x 10^{-14} cm^3/sec at E/N of 62 x 10^{-17} V cm^2 to a value of 3.4 ± 1.0 x 10^{-12} cm^3/sec at E/N of 140 x 10^{-17} V cm^2. Order of magnitude rate coefficients for the reaction

$$O_2^+ + 2O_2 \rightarrow O_4^+ + O_2$$

and

$$O_4^+ + O_2 \rightarrow O_2^+ + 2O_2$$

were estimated, at thermal energies, to be 7.5 x 10^{-30} cm^6/sec and 5.0 x 10^{-14} cm^3/sec, respectively.

Impurity ions which could not be eliminated were seen at pressures greater than 0.6 Torr and over all E/N. The impurity ions were identified as CO_3^- and CO_4^-, CO_3^- being much more intense. Mobilities were determined for both CO_3^- and CO_4^- at pressures on the range from

2.6 to 3.1 Torr and on the E/N range of 2.5 to 7.0 x 10^{-17} V cm^2. CO_3^- and CO_4^- had zero-field mobilities of 2.50 ± .10 and 2.45 ± .10 cm^2/V sec, respectively. The CO_3^- appears to arise primarily from a reaction involving O_3^-, and CO_4^- from a reaction involving O_4^-. The impurity molecule which reacts with the negative oxygen ions to form these impurity ions is thought to be CO_2. The source of CO_2 is unknown, but is speculated to be the stainless steel walls of the drift tube.

CHAPTER I

INTRODUCTION

General Considerations

Ions in a weakly ionized gas in thermal equilibrium with the gas at an absolute temperature T move, like the gas molecules, in a random fashion with a most probable speed, v_p, determined by their thermal energy:

$$\frac{1}{2} m v_p^2 = \kappa T, \tag{1}$$

where m is the mass of each ion and κ is Boltzmann's constant. The requirement "weakly ionized" implies that ion-ion interactions are negligible; "thermal equilibrium" implies that there is no applied electric field. The net motion of the ions and molecules is zero over a period of time large with respect to the average time between collisions.

When an external electrostatic field is applied, an ion will gain energy from the field between collisions with the gas molecules and will, on the average, lose energy during collisions. We will refer to the average energy of an ion in excess of its thermal energy as its field energy. Over a sufficient number of collisions an ion will reach a limiting average velocity in the direction of the field. This velocity is known as the drift velocity, v_d. For the work reported

here the gas pressure is always high enough and the electric field low enough that this limiting velocity is attained by the ion in a distance very short compared to its total distance of drift.

It is found that a parameter useful in interpreting the data of ion swarm experiments is the ratio of the electric field strength E to the gas number density N. In fact, it can be rigorously shown that, at a given temperature T, the parameter E/N determines the drift velocity and the field energy as well as other transport properties of the ion.

Although E/N is the fundamental parameter which will appear in theoretical expressions, existing experimental drift velocity data have been almost universally recorded as a function of E/p, where p is the gas pressure. While p is proportional to N, it is also proportional to the gas temperature. Since it is E/N that determines the transport properties of the ions, a temperature normalization is required if data taken at different temperatures are to be compared. A common practice is to normalize to a gas temperature of 0°C, although other normalizations have been used. In this case, data may be conveniently presented as a function of E/p_o, where the reduced pressure p_o is related to the pressure p at which the measurement is made by

$$p_o = p\left(\frac{273.16}{T}\right). \tag{2}$$

This temperature normalization is not entirely satisfactory, however, because the drift velocity may depend on the temperature. This

normalization often causes confusion when an actual temperature dependence is at issue.

If one uses E/N, there is no ambiguity in comparing experimental results. The conversion relations between E/N and E/p are

$$E/N = (1.0354 \times 10^{-2} \times T)(E/p) \tag{3}$$

or, equivalently,

$$E/N = 2.828 \times E/p_o \tag{4}$$

where E/N is in units of 10^{-17} Vcm^2, T in degrees Kelvin, and E/p or E/p_o in V/cm Torr. The suggestion has been made by Huxley, Crompton, and Elford[1] that the units of E/N be denoted by the "townsend" or "Td", where 1 Td = 10^{-17} Vcm^2. Although this designation has not yet been universally adopted, it will be used in this thesis. Furthermore, the parameter E/N will be used exclusively in discussing the data. Graphical presentations of results for which data as a function of E/p_o have been published will include for convenience both E/N and E/p_o abscissa scales.

When the field energy of the ion is small compared to its thermal energy, it is found[2] that the drift velocity is directly proportional to the electric field strength,

$$v_d = KE. \tag{5}$$

The constant of proportionality, K, is called the mobility of the ion. The field energy is negligible if[2]

$$\left[\frac{M}{m} + \frac{m}{M}\right] eE\lambda << \kappa T, \tag{6}$$

where M and m are the molecular and ionic masses, respectively, e is the ionic charge and λ is the mean free path[3] of the ion between collisions. This expression leads to the conclusion that the field energy of an ion in its parent gas is much less than its thermal energy, at 300°K, below an E/N of about 10 Td.

At higher values of E/N, where the ions are no longer in thermal equilibrium with the gas, the drift velocity may no longer be proportional to the electric field strength. The drift velocity at moderately high E/N is still physically meaningful, but K, as defined by Equation (5), which may no longer be constant, serves mainly as a convenient quantity for comparing sets of data. The custom has evolved of using K to represent the value of v_d/E even at high E/N in order to focus attention on the variation of K with E/N. In employing this custom, however, care must be taken to clearly specify whether one is referring to the low field constant of proportionality or to the high-E/N variation of the ratio v_d/E.

The mobility K is inversely proportional to the molecular number density N, and in order to facilitate comparisons between data taken at various temperatures and pressures, experimental results are usually presented as the mobility which would result if N were 2.687×10^{19} cm^{-3},

which corresponds to 0°C and 760 Torr. This practice leads to the definition of a reduced mobility K_o given by the equation

$$K_o = K(p/760)(273.16/T), \tag{7}$$

where p and T are the pressure and temperature at which the measurement is performed. The assumption of ideal gas behavior is implied in this normalization.

The zero-field reduced mobility is defined as the limiting (constant) value which is approached by K_o as E or E/N approaches zero. Before an extrapolation of data taken at finite E/N is made to E/N = 0, the mobility measurements should be made down to sufficiently low E/N to show clearly that a constant value for K_o has been attained. There is no guide for the extrapolation of K_o to zero field except for such a straight line extrapolation. In this thesis the term mobility or reduced mobility will be used to refer simply to that quantity obtained from the ratio v_d/E. When reference to the limiting constant value at low E/N is desired, the term zero-field reduced mobility will be used.

Up to this point we have considered a single ion and defined the drift velocity as its time-average speed in the direction of the applied field, taken over many collisions under steady state conditions. Alternatively, we might consider all of the ions in a swarm at some instant in time, and define the drift velocity as the instantaneous mean velocity of this distribution. The drift velocity of the first definition is accessible to experimental measurement; that of the second definition

is more desirable from the theoretical point of view. Hence, we repeat the fundamental ergodic postulate stated by Miller,[4] namely that a time average of the velocity of one ion over many collisions is equivalent to an instantaneous average of the velocity vectors of all the ions in the swarm.

The density $d(\vec{r},\vec{v},t)$ of ions in six-dimensional phase space is governed by the Boltzmann equation.[5] The drift velocity is defined by

$$v_d(\vec{r},t) = \frac{1}{n(\vec{r},t)} \int d(\vec{r},\vec{v},t)\vec{v}d\vec{v} \tag{8}$$

where

$$n(\vec{r},t) = \int d(\vec{r},\vec{v},t)d\vec{v} \tag{9}$$

is the ion number density in three-dimensional configuration space. In the cases of interest here, $d(\vec{r},\vec{v},t)$ may be separated according to the equation

$$d(\vec{r},\vec{v},t) = f(\vec{v})\, n(\vec{r},t). \tag{10}$$

$f(\vec{v})$ is called the velocity distribution function. This separation removes the $\vec{r}$ and t dependences from v_d, so that then

$$v_d = \int f(\vec{v})\vec{v}d\vec{v}. \tag{11}$$

Note also that Equations (9) and (10) require that

$$\int f(\vec{v})d\vec{v} = 1. \tag{12}$$

If the Boltzmann equation is linear in $d(\vec{r},\vec{v},t)$, a small density gradient will result in a diffusion current density $\vec{j}_D$ given by

$$\vec{j}_D = -\overleftrightarrow{D} \cdot \vec{\nabla}_r \, n(\vec{r},t), \tag{13}$$

where $\overleftrightarrow{D}$ is the diffusion tensor. Only the diagonal components of $\overleftrightarrow{D}$ are non-zero, and when the ions are in thermal equilibrium with the gas, these components are equal. The components of $\overleftrightarrow{D}$ associated with the directions perpendicular to the electric field are always equal and are referred to as the transverse diffusion coefficients, D_T. The component associated with the field direction is called the longitudinal diffusion coefficient, D_L.

Ion-molecule reactions with the gas can add an additional complication to the description of the ion swarm. Ions of a particular type might be disappearing through conversion to other species, or appearing through conversion from other species, and indeed, both processes can simultaneously be occurring in some cases.

The reaction frequency will be denoted by α, in units $(\text{sec})^{-1}$. The reaction frequency depends on the collision frequency and hence on the number density of the gas. The dependence of α on N is determined by the interactions involved. In many cases it is found that α is

proportional to N or to N^2. If α is proportional to N, the reaction is said to be two-body, while if α is proportional to N^2, it is said to be three-body. The constant of proportionality, k, is called the reaction rate coefficient. The units of k will depend on the N-dependence of α.

In Chapter III account is taken of the drift, diffusion and reactions of each ion species and a set of transport equations is shown which describes all of the different species in the swarm. The equation for the pth species is

$$\frac{\partial n_p}{\partial t} = \vec{\nabla} \cdot \overleftrightarrow{D}_p \cdot \vec{\nabla} n_p - v_{dp} \frac{\partial n_p}{\partial z} - \alpha_p n_p + \sum_q \alpha_{pq} n_q + \beta_p \qquad (14)$$

where n_p is the number density of the pth ionic species; $\overleftrightarrow{D}_p$ is the diffusion tensor and v_{dp} is the drift velocity of the pth ionic species; β_p is a source term describing an input of ions of the pth species; α_{pq} is the reaction frequency for conversion of the qth ionic species to the pth species; α_p is the depleting reaction frequency for the pth species.

These equations for the geometry used in this investigation have been solved under the assumption of an appropriate form for β_p. The general goal of this research will be to determine v_d, D_L, α_{pq}, and α_p for the various ions in oxygen gas, by means of detailed comparisons of experimental swarm measurements with the analytic solution of (14).

Review of Past Oxygen Ion Swarm Research

Mobilities

1901. Mobility measurements on ions in oxygen were begun as early as the turn of the twentieth century. Zeleny[6] developed a technique in which a stream of gas was passed between two concentric cylinders which were kept at different potentials, and which at one place was traversed by a beam of X-rays perpendicular to the axis. The ions which were produced between the two cylinders by the X-rays were carried along by the stream of gas parallel to the axis. At the same time, the influence of the electric field was causing the ions to move at right angles to the axis of the tubes. The distance that the ions were carried along the tube by the gas stream while they were crossing between the two cylinders under the influence of the electric field was a measure of the relative velocities of the gas and of the ions. This information was used in determining the velocity with which the ions moved in a given electric field. Zeleny obtained a mobility of 1.36 cm^2/V sec for a positive oxygen ion in oxygen and 1.80 for a negative ion.

However, the influence of such phenomena as gas turbulence and diffusion and the experimental uncertainties caused by vaguely defined volumes of ionization, inadequate purification of the gas, and poor base vacuum, make these values of historical importance only.

1910. Franck[7] used a gauze modification of the Rutherford method to measure mobilities in oxygen. He obtained 1.29 for the mobility of a positive ion and 1.79 for a negative ion. This experiment

also suffered from many of the imperfections mentioned in the discussion of Zeleny's investigation and is of only historical interest.

1932. Bradbury[8] reported a mobility of 1.58 for a positive ion in oxygen and 2.19 for a negative ion. He used a mechanically chopped beam of X-rays to produce pulses of ions in his drift tube. These values are also mainly of historical importance because they incur many of the errors mentioned in Zeleny's work and also suffer the uncertainty of inaccurate timing techniques.

1935. Nielsen and Bradbury[9] used an electrical shutter method in which the shutter took the form of a fine wire grid, alternate wires being connected to the opposite ends of a high frequency alternating potential source. Ions pass through the grid only when the potential between adjacent grid wires is small. The amplitude of the alternating voltage is sufficiently high to sweep all arriving uncaptured electrons to the grid wires but still permit transmission of the more sluggish negative ions. Nielsen and Bradbury reported a mobility of 3.3 for a negative ion which they labeled as O_2^-. (The Bradbury-Nielsen technique has been used recently by Crompton and Elford[10] for determination of the mobility of positive potassium ions in nitrogen and neon.)

1952. Doehring[11] obtained a value of 2.48 for the mobility of a negative ion in oxygen. He used a "four-grid" electrical shutter method, similar to that used more recently by Beaty[12] for measurements in argon. No deduction was made regarding the nature of the ions involved.

1953. Varney[13] reported a zero-field reduced mobility of 2.25 for a positive ion in oxygen. He used a pulsed Townsend discharge method, in which a field is applied between parallel-plate electrodes, and a pulse of electrons is released from the cathode by the radiation from an external spark of short duration. A typical Townsend avalanche results, and an exponential distribution of positive ions is left between the plates. The time needed to sweep out these ions is measured and thereby the drift velocity is obtained. Because of the high voltage used to create the ions this technique is limited to high E/N.

1955. Huber[14] observed a positive ion in oxygen with a mobility of 2.2. She used a discharge tube. The discharge was triggered by an alpha particle source.

1956. Schulz-DuBois[15] used the ambipolar diffusion method[16] to obtain the mobility of a positive ion in oxygen. He obtained a value of 2.2.

1957. In the experiments performed by Burch and Geballe,[17] who utilized a pulsed Townsend discharge, there was evidence of three separate species of negative ions. Three distinct and pressure independent negative ion mobilities consistent with zero-field values of 3.4, 2.6, and 1.95 were found. Although they had no mass analysis, Burch and Geballe labeled the intermediate mobility as O_3^-, the fastest ion as O^- and the slowest as O_2^-. Positive ions were also investigated in their experiment. No difference was noted between the mobilities of the supposed O_2^+ and O_2^- ions.

Also in 1957, McDaniel and Crane[18] measured a mobility for a negative ion in oxygen. The value was 2.46 and was ascribed to a single ionic species which McDaniel and McDowell[19] later labeled as O_3^-.

1958. Maushart[20] measured a mobility of 2.12 for a positive ion in oxygen. He used a moveable alpha particle source to produce his ions. The drift velocity was calculated from the difference in drift time between different source positions.

1962. Chanin, Phelps, and Biondi[21] measured mobilities for two negative ions in oxygen. They attained values of 3.0 and 2.7 for the mobilities. They labeled the fast ion O^- and the slower ion O_2^-. In their measurement electrons are released from the cathode by an ultraviolet light pulse. They drift through the gas-filled tube under the action of the applied electric field. Some of the electrons are captured by neutral molecules to form negative ions; the remainder reach the collector electrode after passing through a control grid. The negative ions then drift across the tube. A Bradbury-Nielsen shutter is used to sample the ion current as a function of time after the light pulse. No mass analysis was used.

1963. Eiber[22] used an electrical shutter consisting of two coplanar sets of fine wires having very small gaps between adjacent wires to determine a crude ratio of e/m (where m is the mass of the ions and e is their electric charge) for the positive and negative ions produced in oxygen. One positive and three negative ions were observed by Eiber. The positive ion, O_2^+, has a zero-field mobility of 2.15. The mobilities of the negative ions were 3.2, 2.5, and 2.25 and the ions were identified as O^-, O_2^-, and O_3^-, respectively.

Mentzoni[23] used the ambipolar diffusion method to measure the mobility of a positive ion in oxygen. He obtained a value of 2.8 for the zero-field mobility.

1964. Rees[24] used a Bradbury-Nielsen grid to allow a short burst of ions and electrons into his drift tube. A second Bradbury-Nielsen grid was used to sample the current as a function of time relative to the opening of the first grid. Four species of negative ions were observed and they had zero-field mobilities of 3.01, 2.52, 2.39 and 2.18 which were labeled O^-, O_3^-, O_2^-, and an impurity, respectively.

Voshall, Pack, and Phelps[25] performed an experiment which superseded the work of Chanin, Phelps and Biondi. They determined a mobility of 2.42 for a negative ion which they labeled as O_2^-. They used grids at two positions along the drift tube to obtain two different ion current waveforms. The drift velocity can be obtained from the difference in transit time. This should eliminate end effects.

Beaty, Branscomb and Patterson[26] reported mobilities of negative ions produced by a spark in oxygen. Three kinds of ions were observed with mobilities in good agreement with both Eiber and Burch and Geballe. No mass analysis was used.

1965. Samson and Weissler[27] attained a mobility of 2.4 for a positive ion in oxygen. Monochromatic radiation of wavelength just small enough to ionize the gas was used to produce a burst of ions. A shutter consisting of two grids sampled the ion current as a function of time of drift down the drift tube.

1967. The first reports on results from oxygen mobility experiments in which ions were mass-analyzed with good resolution concurrent with a measurement of their drift velocities were presented by McKnight[28] at the 19th Gaseous Electronics Conference. Electrons were produced from a hot filament and reacted with the neutral gas molecules to produce ions. The ions were then gated into a drift cell through a double grid, withdrawn from an aperture, and their mass and intensity determined as a function of drift time by a quadrupole mass analyzer and a gated particle multiplier. Comparison of experimental time spectra with numerical calculations allowed the determination of ion drift times and reaction rates. Data were taken at fairly low E/N, and zero-field reduced mobilities were quoted for O^-, O_2^-, and O_3^- ions. The values obtained were 3.4, 2.1, and 2.9, respectively.

1968. Shafer and Beaty[29] used a double shutter drift tube with a differentially pumped quadrupole mass spectrometer to measure the mobilities of negative ions in oxygen at room temperature. O^-, O_2^-, O_3^-, and O_4^- were found in sufficient quantities to permit measurement of their drift velocities. The mobilities of O^-, O_2^-, and O_3^- were found to be in agreement with the measurements of Burch and Geballe and of Eiber. The mobility of O_4^- was similar to that for O_2^-.

Dutton and Howells[30] used a four-gauze electrical shutter system to measure the drift velocities of positive and negative ions produced in a glow discharge in oxygen. They reported the presence of two pressure independent mobilities for positive ions in oxygen. Their data gave a mobility of 2.15 for both species. They labeled the ions as

O_2^+ and O_4^+. Two negative ion mobilities were also measured, with values 2.5 and 2.4. They were labeled O_3^- and O_2^-, respectively. No mass analysis was used.

1969. Rees and Fleming[31] investigated the drift velocities of positive oxygen ions in oxygen with a drift tube of the Bradbury-Nielsen type. The positive ions were produced using an alpha particle source. Their data indicated the presence of two ions with mobilities of 2.15 and 2.20 which they labeled O_2^+ and O_4^+, respectively.

Varney[32] performed a mass-analyzed investigation of the mobilities of the positive and negative ions in oxygen. Basically the experimental set up consisted of an electron source, an ion-forming region, a drift space in which ions may be aged under selected conditions, a double shutter drift velocity device, a small exit aperture, and a quadrupole type mass spectrometer with an electron multiplier. A value of 2.4 was obtained for the mobilities of both O_2^+ and O_2^-. The O^- data yielded a mobility of 6.1.

McKnight[33] found the mobility of O_4^- to be virtually identical to that of O_2^- ion, with a zero-field mobility of 2.15. McKnight[34] has also obtained new data for O_3^- which give a zero-field mobility of 2.5 instead of his previously reported value of 2.9.

It is evident that the data from the experiments just reviewed are inconsistent. The most obvious problem is that of ion identification. Even when the detected ion was definitely identified, there were in most cases no assurances that the ion had not participated in an ion-molecule reaction during its drift, thus giving rise to an

"apparent drift velocity," that is, some sort of an average of the true drift velocities of the ions involved in the reaction. Furthermore, many of the experimenters did not obtain data at low enough E/N to justify the inference of a zero-field reduced mobility. Also, the results from many of their investigations exhibited considerable scatter and it is difficult to decide with any precision what the zero-field reduced mobility of the ions are.

Before the transport properties of the several ions in oxygen can be determined unambiguously, data must be taken under the following conditions:

(1) It must be demonstrated that the data reach low enough E/N to insure that K_o is truly constant, independent of E/N. There is no guide for determining the zero-field reduced mobility from data which do not meet this requirement.

(2) The data must clearly indicate that any drift velocities ascribed to a given ion were not perturbed by that ion having spent part of its drift time as another species.

(3) The ionic identity must be unambiguously determined. Due to the simultaneous presence of as many as four different negative ion species and two positive ions in oxygen under the conditions of most drift velocity experiments, the inclusion of a mass spectrometer will almost certainly be required. The possibility of the presence of impurities further confirms the necessity for mass analysis.

Longitudinal Diffusion Coefficients

While many experiments have been performed on the drift velocities of oxygen ions in oxygen, no data on the longitudinal diffusion coefficients appear to have been published. At low E/N, the components of the diffusion tensor are equal and are given by the Einstein relation[35]

$$\frac{D}{K} = \frac{\kappa T}{e} , \tag{15}$$

where κ is Boltzmann's constant, T is the absolute temperature and e is the ionic charge. No experiment has produced data for which the longitudinal diffusion in oxygen has been shown to be consistent with (15).

Ion-Molecule Reaction Rates

1957. Burch and Geballe[36] made reaction rate determinations for negative ions in oxygen by observation of the transient ion currents in a Townsend discharge and comparison of these observations with analytically generated transients. They reported the three-body reaction

$$O^- + 2O_2 \rightarrow O_3^- + O_2 \tag{16}$$

to have a rate of 9×10^{-31} cm^6/sec at an E/N of 40 Td, decreasing to 1×10^{-32} cm^6/sec at an E/N of 100 Td. The pressure dependence was consistent with the assumption of a three-body reaction. The reaction

$$O^- + O_2 \rightarrow O_2^- + O_2 \qquad (17)$$

was also reported. The rate coefficient varied from 1×10^{-15} cm^3/sec at an E/N of 55 Td to a value of 1×10^{-12} cm^3/sec at an E/N of 120 Td. This investigation was performed with no mass analysis.

1964. Beaty et al.[26] obtained a rate coefficient of 9×10^{-31} cm^6/sec for reaction (16). Presumably, this rate coefficient was obtained at low E/N. They used no mass analysis.

Yang and Conway[37] studied the formation of O_4^+ by reaction of O_2^+ with oxygen. O_2^+ and O_4^+ were observed in a mass spectrometer using a high pressure source with titanium tritide as the ionizing medium. They found that the measured ion intensities for O_2^+ and O_4^+ were consistent with the equilibrium requirement for the following reaction

$$O_2^+ + 2O_2 \rightleftarrows O_4 + O_2. \qquad (18)$$

For a reaction of the form given by Reaction (18), the equilibrium constant[38] is given by

$$K_E = \frac{n_2 \times N}{n_1 \times N^2} \qquad (19)$$

where n_2 is the number density of O_4^+, n_1 is the number density of O_2^+, and N is the number density of O_2. They also examined the equilibrium constant as a function of gas temperature. This information can be used to calculate[39] the binding energy of O_4^+. A bond energy of 0.42 eV was thus determined.

1966. Moruzzi and Phelps[40] obtained a rate coefficient of 1.4×10^{-31} cm^6/sec at an E/N of 13.4 Td for reaction (16) in a mass analyzed experiment. They found rate coefficients for reaction (17) of 1.8×10^{-13} and 5.5×10^{-13} cm^3/sec at E/N values of 70.7 and 84.9 Td, respectively. The rates of both reactions showed the correct pressure dependence.

1968. Dutton and Howells[30] in their non-mass analyzed mobility experiment obtained results which showed that at a value of E/N between 60 and 12 Td and at pressures above 3.43 Torr a value of the drift velocity is attained which depends only on the value of E/N. Likewise, at an E/N of 45 to 250 Td and at pressures below 2.04 Torr, a value of the drift velocity dependent only on the value of E/N was obtained. The authors hypothesized that a single ion was predominant in each of these regions. They further assumed that O_4^+ was the ion present at high pressure and O_2^+ was the ion present at low pressure. At pressures between 2 and 3 Torr and at E/N between 45 and 60 Td, drift velocity values were found which depended not only on E/N but also on the pressure. These drift velocity values lay between the values obtained at higher and lower pressures for the species labeled O_4^+ and O_2^+. If two ion species are present at equilibrium concentrations in a gas, the intermediate drift velocity is the weighted mean of the individual drift velocities. This fact can be expressed as

$$v_d = \frac{n_2 v_{d2} + n_1 v_{d1}}{n_1 + n_2} \qquad (20)$$

where v_d is the pressure-dependent intermediate velocity, v_{d2} and n_2 the drift velocity and concentration of O_4^+ and v_{d1} and n_1 the corresponding quantities for O_2^+. Rearranging Equation (20) gives an expression for the ratio of the ionic species at the E/N and pressure at which v_d is measured. Knowledge of the relative abundance of the two species permits calculation of the equilibrium constant. Their values are consistent with reaction (18). The equilibrium constant was examined as a function of E/N and by the use of Wannier's[41] expression to relate E/N to temperature, a binding energy for the species which they labeled O_4^+ was obtained. They calculated a value of 0.45 eV.

1969. Durden, Kebarle, and Good[42] examined reaction (18) with a high pressure (4-10 Torr) mass spectrometer. Ions are produced in the high pressure region by a focused and pulsed electron beam. This region is field-free. Some of the ions and gas drift out of the field-free region through an exit aperture by diffusion and mass flow. The ions are now in a differential pumping stage where they are focused by an electric field and subjected to mass analysis and detection while the neutral gas is evacuated by a high capacity pump. Rate coefficients are determined by examining the ratio of the O_2^+ current to the O_4^+ current as a function of time delay between the electron pulse and a pulse which opens the mass spectrometer. From information about the rate of approach to equilibrium and the equilibrium coefficient, values were obtained for the forward and backward reaction rates. The forward reaction coefficient was found to be 2.8×10^{-30} cm^6/sec and the

backward reaction was found to be 2.8×10^{-13} cm^3/sec. The reaction rates showed the correct pressure dependence for reaction (18) to be valid.

Unpublished data by McKnight[34] give a rate coefficient for reaction (16) of 9×10^{-31} cm^6/sec over an E/N range of 3.5 to 30 Td. The rate coefficient for reaction (17) was found to be 5×10^{-11} cm^3/sec at E/N of 300 Td and to decrease to 4×10^{-13} cm^3/sec at E/N of 80 Td. This work involved mass analyzed data.

McKnight and Sawina[33] reported rate coefficients for the reactions

$$O_2^- + 2O_2 \rightleftarrows O_4^- + O_2. \qquad (21)$$

The rate for the forward reaction was measured under conditions where the reaction rate forming O_4^- was much faster than the breakup of the O_4^- complex. From equilibrium concentrations of O_2^- and O_4^- the backward reaction rate was obtained. A value of 3×10^{-31} cm^6/sec was found for the forward rate coefficient and 2×10^{-14} cm^3/sec for the backward reaction. This work had the benefit of mass analysis.

Unpublished data by Woo[43] gives a value of 9×10^{-31} cm^6/sec for reaction (16). He had no mass analysis.

The reaction

$$O^+ + O_2 \rightarrow O_2^+ + O \qquad (22)$$

is mentioned because of its historical importance. The rate constant of this reaction has been determined[44,45] to be about 2.0×10^{-11} cm^3/sec. Because of the large rate coefficient, the O^+ ion is observed in the present experiment only under drift conditions of high fields, low pressures and short drift distances. Under these conditions the ionic motion has not reached steady state, so no meaningful drift velocities and reaction rates can be obtained for O^+.

Impurities

Impurities which could not be eliminated have been seen by most experimenters[29,34,40] who investigated the negative ions of oxygen with mass analysis. The two dominant impurity ions observed have been identified as CO_3^- and CO_4^-. Beaty and Schafer[29] determined a mobility for CO_3^- and found it to be slightly less than that of O_3^-. CO_3^- and CO_4^- have been observed to be formed from negative oxygen ions through the following reaction schemes:

$$O_3^- + CO_2 \rightarrow CO_3^- + O_2 \tag{23}$$

$$O^- + O_2 + CO_2 \rightarrow CO_3^- + O_2 \tag{24}$$

$$O_4^- + CO_2 \rightarrow CO_4^- + O_2 \tag{25}$$

$$O_2^- + CO_2 + O_2 \rightarrow CO_4^- + O_2 \tag{26}$$

with reaction rates of 4×10^{-10} cm^3/sec[46], 3×10^{-29} cm^6/sec[40],

4.3×10^{-10} cm^3/sec[47], and 2×10^{-29} cm^6/sec[40], respectively. The source of the CO_2 is not known, but is speculated to be the metal surfaces of the apparatus.

Summary

After almost 70 years of investigations, the situation in oxygen is still confused. The mobilities for the positive ion experiments are in fair agreement. However, very few low E/N data are available, and no mass analyzed data are available. The possibility of the presence of two positive ions with similar mobilities has been advocated but no mass analyzed data have substantiated this hypothesis. Very little work has been done on the reactions for positive oxygen ions.

The non-mass analyzed negative oxygen ion experiments disagree among themselves and it is difficult to decide which experimenters have drawn the correct conclusions. The probable presence of impurities which might have affected the results places doubt on the accuracy of these results. The four mass-analyzed experiments give mobility results which have high scatter and which sometimes disagree by a factor of 2. The reaction rates for the negative ions in these mass analyzed experiments disagree by an order of magnitude in some cases.

Goals of the Present Research

The general objective of the present research is to evaluate as precisely as possible the drift velocities, longitudinal diffusion coefficients, and reaction rates of oxygen ions in oxygen at room temperature. Specifically, this may be broken down into four goals:

(1) To determine unambiguous zero-field reduced mobilities for the two positive oxygen ions and four negative ions in oxygen.

(2) To measure the variation of the mobilities with E/N over as wide as possible a range.

(3) To evaluate the longitudinal diffusion coefficients over as wide a range of E/N as possible.

(4) To assess the ion-molecule reaction situation and to determine the reaction rates involved.

CHAPTER II

APPARATUS

General Description

The apparatus has already been discussed in detail in three reports,[48-50] so a detailed description will not be given here. A brief description will be presented, along with a discussion of modifications made for the present research.

Figure 1 shows a sectioned view of the apparatus. The main ultra-high-vacuum chamber is constructed of stainless steel and is evacuated by oil diffusion pumps which are separated from the chamber by water-cooled baffles and molecular sieve traps. Metal gaskets provide the vacuum seals. The vacuum chamber contains the ion source, drift tube, and sampling apparatus.

Prior to beginning an investigation the entire assembly is baked at an average temperature of 250°C. Bakeout is accomplished by the heating mantles shown in an overall view of the apparatus, Figure 2. Heating tapes are used on the small exposed parts and on the gas feedline. The sorbent traps are outgassed at about 375°C. After cooling, the base vacuum in the drift region is typically 1×10^{-9} Torr with the isolation valve open. Closing the isolation valve shuts the drift region off from the diffusion pumps except for the 0.035 cm diameter exit aperture on the axis at the base of the drift tube. The pressure in the drift tube with the isolation valve closed does not rise above

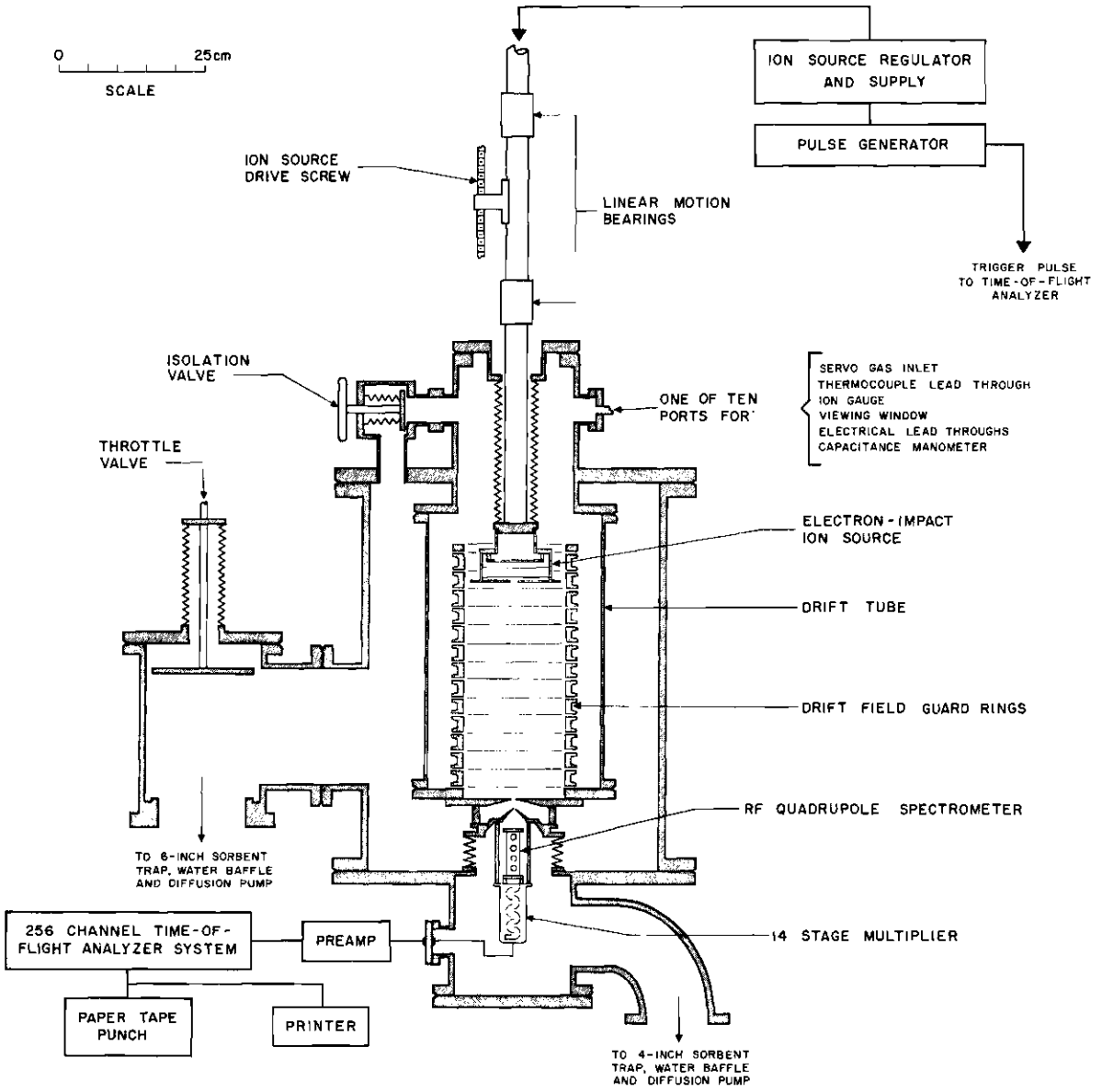

Figure 1. Sectioned View of the Drift Tube, the Outer Vacuum Enclosure, and the Analysis Chamber

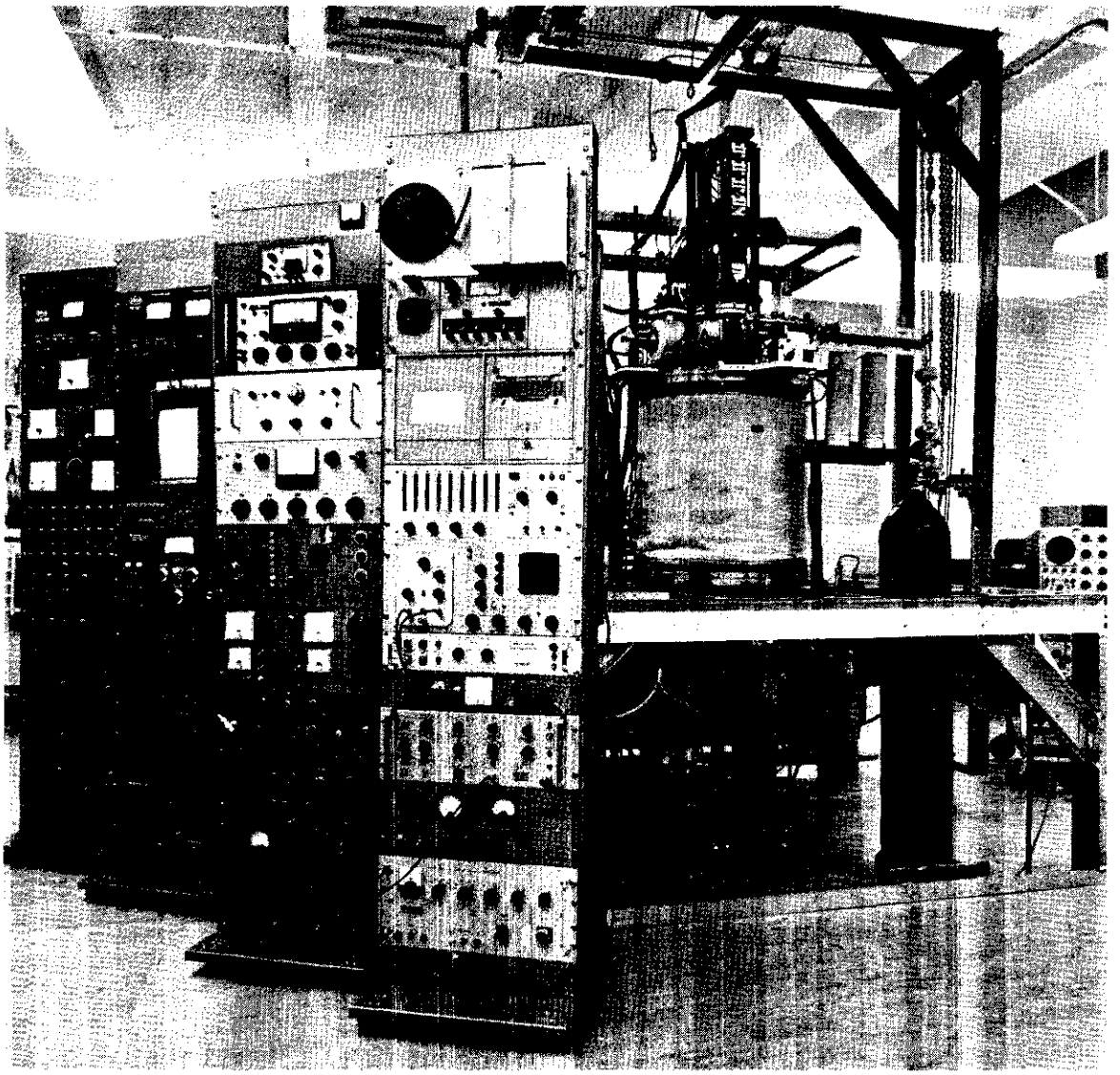

Figure 2. Overall View of the Apparatus

9×10^{-8} Torr. Important to the achievement of low base pressures are the facts that (a) the use of organic materials is avoided, (b) all insulators are made of ultra-high-vacuum quality ceramics, and (c) all welds are heliarc welds made from the inside.

A very pure sample of the gas to be investigated is admitted into the drift tube through a servo-controlled leak valve and the sample gas continuously flows from the tube through the exit aperture. An MKS "Baratron" capacitance manometer continually monitors the pressure and causes the servo-valve to react in order to maintain a predetermined pressure in the range 0.02 to 10.00 Torr in the drift tube. This pressure can be maintained within $\pm 10^{-4}$ Torr over extended periods of time. The oxygen gas used for this work was the Ultra-pure grade supplied by Air Products and Chemicals, Inc., Allentown, Pennsylvania. The only impurities in this gas present to greater than five parts per million are argon which is present at a concentration of less than 20 parts per million and nitrogen at a concentration of less than 19 parts per million. Two dry ice and acetone traps in the gas feedline were used to remove water vapor. The gas which had gone through the traps produced no detectable impurity ions which could be attributed to impurities in the incoming gas.

An ion swarm can be followed from creation to detection in Figure 3. A pulsed electron-impact ion source is used repetitively to create short bursts of primary oxygen ions inside the source. Alkali ions can be produced by a thermionic emitter when desired. These ions are usually gated out of the source into the drift region by a double

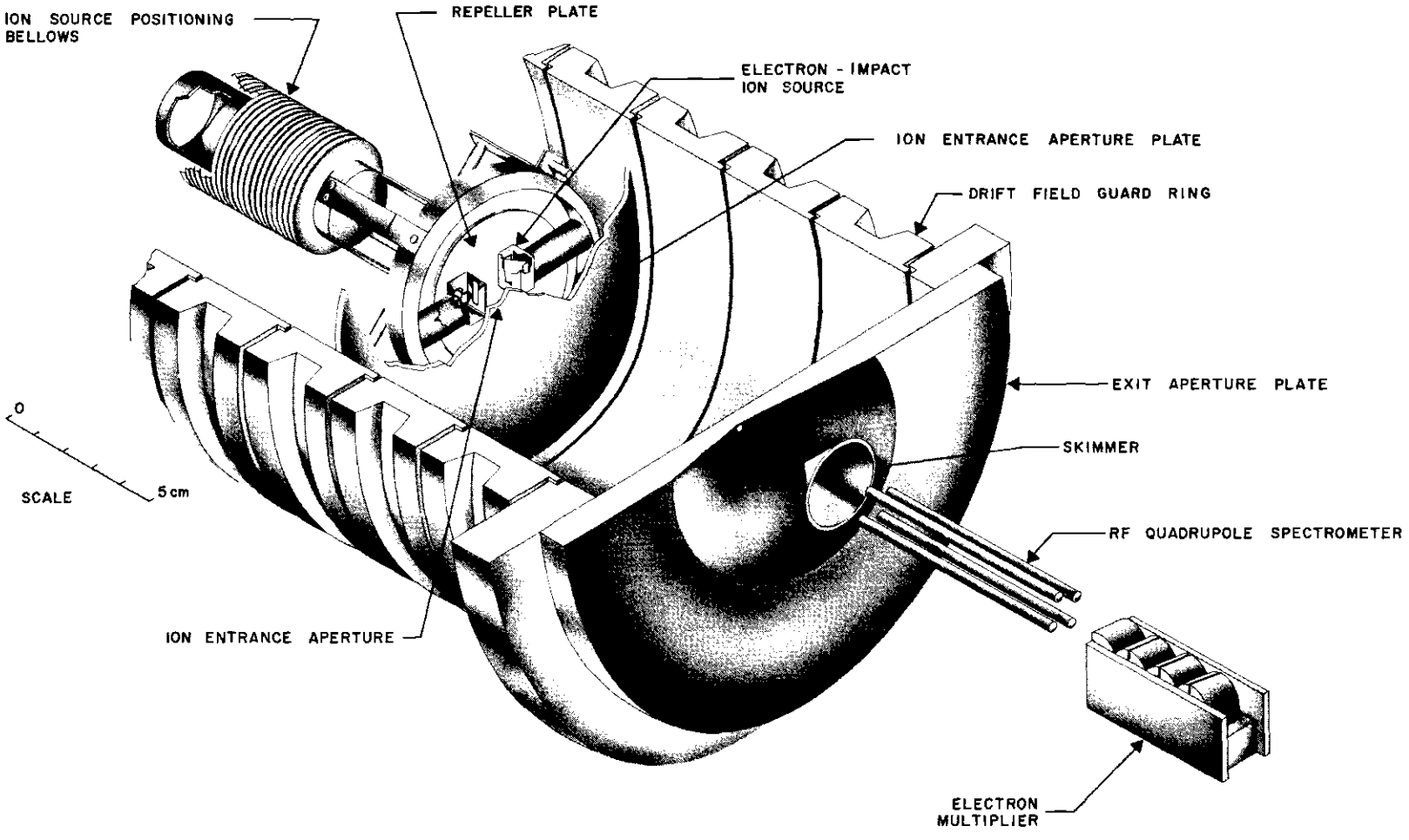

Figure 3. Perspective Drawing of the Drift Region and the Mass Analysis and Detection Components

grid "electric shutter"[51] located at the ion entrance aperture. The drift region is the space defined by the ion entrance aperture plate, the exit aperture plate, and the drift field guard rings. Each ion swarm migrates down the drift region under the influence of a weak uniform electric field maintained by the drift field guard rings. During this migration the swarm spreads due to diffusion, and may undergo ion-molecule reactions with the neutral gas. When the ions reach the bottom of the drift tube, those close to the axis are swept out through the exit aperture, and the core of the emerging jet of ions and gas molecules is cut out by a conical skimmer and directed into an rf quadrupole mass spectrometer. Ions of only a selected charge-to-mass ratio traverse the length of the spectrometer; all other ions are rejected in the mass selection process. The selected ions are then detected individually by an electron multiplier operated as a pulse counter, and the resulting pulses are electronically sorted as to their arrival time by a 256-channel time-of-flight analyzer.

The pressure in the region between the exit aperture plate and the skimmer (the differential pumping region) is typically 5×10^{-4} Torr, and the pressure in the analysis region below the skimmer is typically 5×10^{-6} Torr. Hence, the ions undergoing analysis maintain their distribution in time, since very few collisions are made outside the drift region.

Because of diffusion and geometrical losses, only an extremely small fraction of the number of ions originally present in the swarm reach the detector. However, a histogram of arrival times can be built

up by superimposing the data from a large number of source pulses (typically 10^4-10^6) for a given source position. Such a histogram is referred to as an arrival time spectrum or a time profile. Such spectra are obtained for various positions of the source along the axis of the drift tube. Following this, measurements are taken for other values of drift field intensity and gas pressure. Finally, the mass spectrometer is tuned to other ionic masses, and the above sequence of measurements is repeated until arrival time spectra are acquired for each type of ion present in the drift tube under the conditions of drift field intensity, source position, and gas pressure desired.

A typical set of superimposed arrival time spectra for seven different source positions is shown in Figure 4. For this illustration, the same counting time has been used for each spectrum. The points represent data from the time analyzer; the smooth curves are obtained from an analysis described in Appendix IV. This analysis will be shown to provide an excellent description of the experimental arrival time spectra under the conditions of source input and ion-molecule reactions where it is applicable. Alkali ions are ideal for illustrating the diffusion-induced changes in the time profiles because they do not react with the gas molecules.

The drift velocity may be obtained to an excellent approximation from the known distance traveled by a swarm divided by the mean time of the resulting spectrum. Differencing of two or more spectra will (ideally) eliminate end effects. The widths of the spectra are determined by the longitudinal diffusion coefficient (but may also be

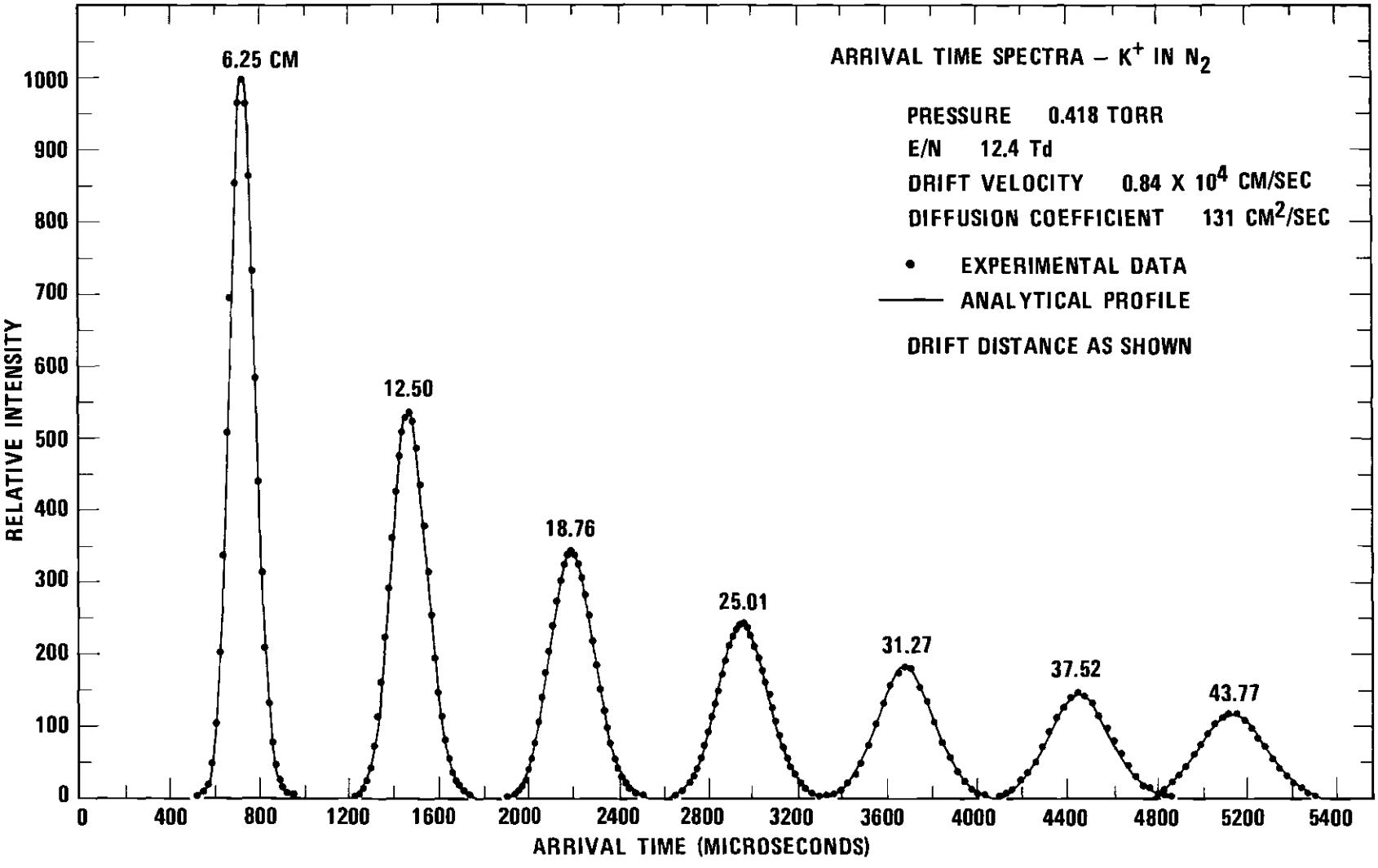

Figure 4. Arrival Time Spectra for Potassium Ions in Nitrogen for Seven Drift Distances. The Points Represent the Experimental Data; the Smooth Curves Represent the Analytical Profiles.

affected by ion-molecule reactions when they are present). The change in the relative total number of ions making up each of the spectra at the various drift distances is governed by the transverse diffusion coefficient (but may also be affected by reactions if they are present). Hence, at low E/N, where the diffusion coefficient can be calculated if the mobility is known, reaction rates may be obtained by examination of the shapes of the spectra or by determining the rate of growth or attenuation of the profiles as the ion source is moved along the drift tube axis. Both an attenuation technique and a profile fit method are used in this investigation.

Figure 5 is a schematic diagram of the ion source. The source contains two nonmagnetic stainless steel boxes, one mounted on each pole of a ring magnet which produces a field of about 100 gauss in the magnet gap. When the source is operated to form ions of the gas filling the tube, electrons are evaporated from a filament in the box on the left side, and are periodically admitted into the ionization region through a slit in a control plate which is used to gate the passage of the electrons. Because of the magnetic field, the electrons are constrained to move in tight helices. The electron beam has the shape of a narrow ribbon perpendicular to the drift tube axis, and thus the primary ionization is restricted to a narrow, well-defined region in the gas. After traversing the ionization gap, the electrons are collected in the box on the right side of the source. A thermionic alkali-emitter is mounted on the back of the repeller plate, as is shown in Figure 5.

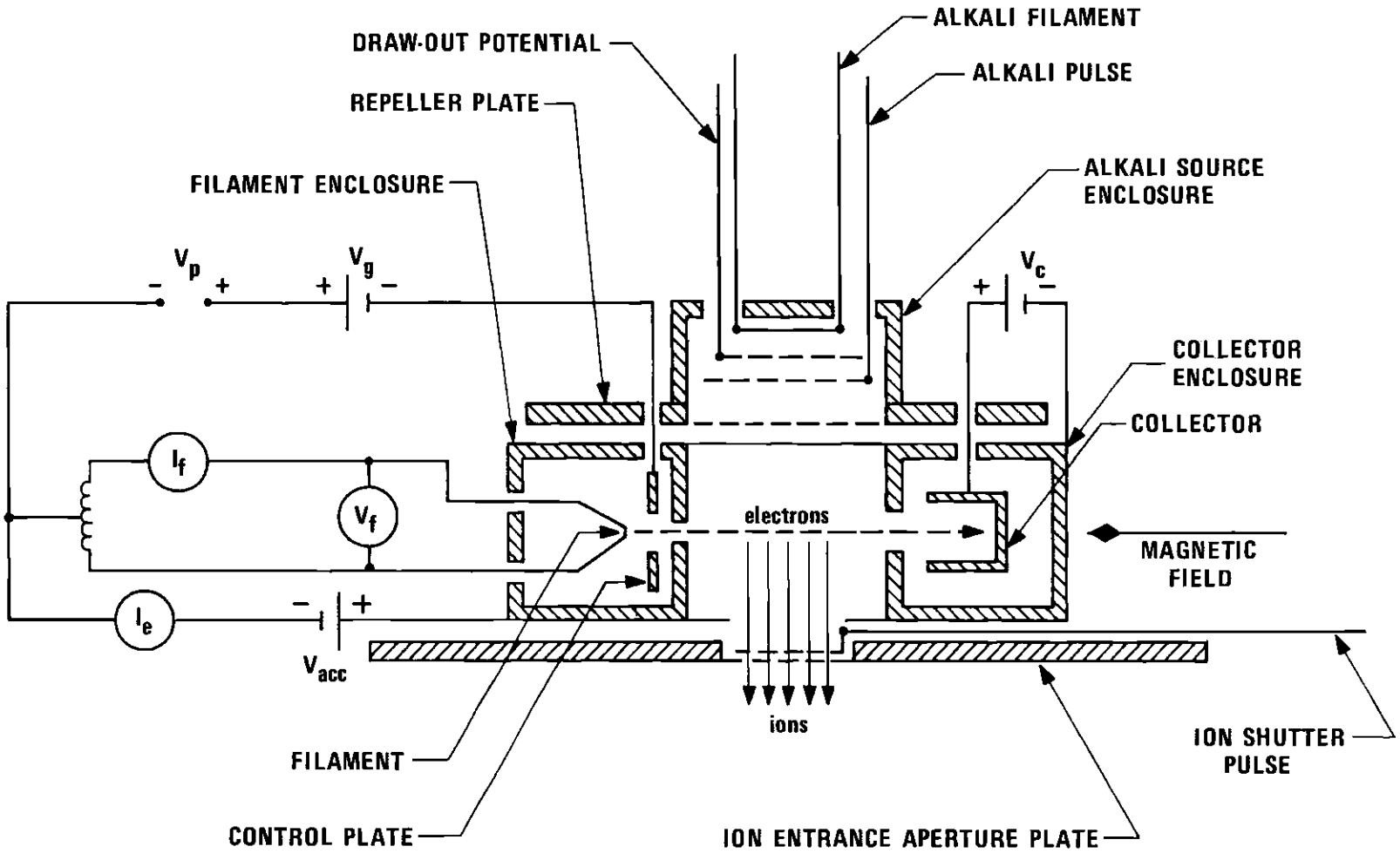

Figure 5. Schematic Diagram of the Ion Source. The Alkali Source is Mounted Above the Electron Impact Ion Source.

Alkali ion mobility and diffusion results can be used to check on possible systematic errors, as will be discussed later, and are representative of ions which undergo no ion-molecule reactions with the gas, as has already been mentioned. The thermionic emitter (a platinum gauze filament coated with Kingman Feldspar ($K_2O \cdot Al_2O_3 \cdot 6SiO_2$) heated to about 850°C) emits only singly-charged ground-state ions, mainly K^+. Three grids extract, pulse, and slow the emitted ions.

The source frame is maintained at the local equipotential in the drift field, and a suitable potential is applied to the repeller plate at the top of the source to cause the ions which are formed to move toward the ion entrance aperture plate. The field inside the ion source is normally maintained equal to the field in the drift region, but tests have been made with smaller fields in the source, thus giving rise to a longer "residence time" and resulting in visible effects due to reactions in the source. A double grid shutter is mounted in the 3/4-inch hole in the ion entrance aperture plate. This grid consists of two closely-spaced wire meshes mounted perpendicular to the drift tube axis. Normally, a potential is applied between these meshes to prevent the ions from passing through the hole. Periodically, however, this potential is removed briefly by an electrical pulse so that a burst of ions may flow through the grid and enter the drift space. The repetition rate of the pulses applied to the control plate and the shutter is 10^2-10^4/sec, and the width of the pulses is usually less than 1 microsecond, a time which is negligible compared to typical drift times.

Short pulse widths and an electron beam current of only about 10 microamperes during each pulse are utilized in order to restrict the number of ions in each burst to a value which does not produce appreciable space charge effects in the drift space. An approximate calculation gives an ionic density in the source of less than 1×10^6 ions/cm^3 under typical conditions. If the ionic density is increased much beyond this limit, effects of space charge appear in the experimental spectra. Further, an approximate calculation reveals that a density no greater than 1×10^6 ions/cm^3 must be maintained if the space charge field is to be at least an order of magnitude lower than the applied drift field, at the smallest field used.

The electron beam in the ion source has a fairly small energy spread (several eV), and its energy can be set at any desired value within wide limits. This feature provides closer control on the production of excited and multiply-charged ions than is possible with many other kinds of ion sources.

The ion source is mounted on the end of a moveable shaft. A stainless steel bellows (see Figure 1) allows movement of the source over a total distance of almost 44 cm while maintaining the ultra-high-vacuum integrity of the vacuum system. The ion source can be placed within a few thousandths of an inch at any of 16 pre-determined positions along the drift tube axis to yield drift distances over the range from 1 to 44 cm.

The drift space which the ions enter after leaving the ion source is bounded by a set of 14 guard rings with 17.5 cm inside diameter.

The rings are similar to those used by Crompton, Elford, and Gascoigne,[52] and they maintain an axial electric field which is free of distortion to a fraction of 1 per cent in the region traversed by the ion swarm. (Calculations of the field established by these electrodes may be found in the report by Albritton.[48]) Concealed alumina spacers and dowel pins electrically separate the guard rings and provide alignments accurate to a few thousandths of an inch. All surfaces exposed to the ion swarm, here and in other parts of the apparatus, are gold-plated to reduce surface potential variations.

Ions leave the drift space through a knife-edged hole in the exit aperture plate at the bottom of the drift tube. This aperture is similar to a simple molecular beam effusion orifice, and its design minimizes mass discrimination effects in the ionic mass sampling. Strong differential pumping is applied between the drift tube exit aperture and the skimmer, and between the skimmer and the mass spectrometer, so that very few collisions occur after the ions have passed out of the drift tube. The apparatus may be operated with no guiding or focusing field applied between the drift tube exit aperture plate and the skimmer, in order that the ions not be accelerated until they have passed through the skimmer and entered the analysis region, where the pressure is below 10^{-5} Torr. This procedure guards against the possibility that weakly-bound ions might be dissociated in energetic collisions with gas molecules. However, it has been found with oxygen that a voltage of 30-40 volts can be placed on the skimmer without producing detectable dissociation. With this skimmer potential, a

substantial increase in signal was observed. The holes in the exit aperture plate and in the tip of the skimmer are both quite large, so that only a small fraction of the ions which enter the mass spectrometer have grazed a surface.

After the ions have passed through the skimmer, they are focused into a Varian radio-frequency quadrupole mass filter. Before entering the quadrupole they are brought to an energy of about 3 eV for most efficient operation of the quadrupole. The resolving power of the quadrupole is easily variable up to a maximum resolution of 50. The quadrupole has the ability continuously to sweep any desired range of masses out to mass 250, thus facilitating the search for impurity ions.

Ions of the species selected by the mass filter are next accelerated through a few kilovolts and strike an electron multiplier which is used as a pulse counter. Pulse-counting techniques permit the collection of data even though the number of ions may be extremely small. This capability allows the apparatus to be operated at very low E/N and with sufficiently small ion currents that space charge effects are negligible.

The time interval between the entry of a given ion swarm into the drift space and the detection of one of its members is measured and stored by a Technical Measurements Corporation 256-channel time-of-flight analyzer. The channel width of this analyzer is variable in steps of a factor of 2 from 0.25 to 64 microseconds. The time sweep of the analyzer is triggered by the pulse which opens the double grid shutter to admit the ion swarm into the drift region.

As has been mentioned, the drift distance may be varied from 1 to 44 cm. A variable drift distance is very useful because end effects produced both in the ion source and in the mass selection and detection system can be eliminated by comparing results obtained with different distances. In addition, a long drift distance is an aid to accurate determination of ion-molecule reaction rates.

The drift tube may be operated over a pressure range of about 0.02 to 10 Torr. The lower limit is imposed by the requirement that the product of gas pressure and drift distance be sufficiently large that steady state drift conditions obtain over most of the drift distance. The upper limit arises from the inability of the diffusion pumps to handle the gas load imposed on them at higher pressures. It is important to be able to operate over a wide range of pressures so that the pressure dependence of ion-molecule reactions occurring in the drift tube may be accurately determined. Furthermore, the reaction pattern in a given gas might make it mandatory to operate at either a high or a low gas pressure in order to obtain meaningful results for a given ionic species in that gas.

The electric field may be varied from about 0.2 to 6.5 V/cm. This ability, combined with the wide pressure range, gives this apparatus a range of E/N encompassing almost three orders of magnitude--2 to 800 Td.

Modifications Incorporated for the Present Research

Ion Source

The ion source and its method of operation are basically the same as that described by Miller[49] and Moseley.[50] However, several changes have been made to improve its operation or to deal with problems peculiar to the use of oxygen in the drift tube.

Thoriated-iridium had always been used as the electron-emitting filament material in previous investigations with this drift tube. This material was also used for most of the positive ion oxygen measurements at pressures less than 0.3 Torr. However, at pressures greater than 0.5 Torr, the thoriated-iridium filament was found to have a life time of only a few hours in oxygen. Because it takes several days to bake the apparatus after replacement of a filament, a filament with a longer life time was desired. A platinum-rhodium filament coated with a $BaZrO_3$-$BaCO_3$-$SrCO_3$ mixture as described by MacNair[53] was installed. This filament has been used for one year and at pressures up to 10 Torr, and it has not yet failed. However, the $BaZrO_3$ coated filament takes about 90 watts of power as compared to 13 watts for the thoriated iridium filament. This increase in power used by the filament causes the temperature in the drift tube to increase by 10°C during eight hours of operation. Temperature gradients of 3 to 4°C exist in the drift tube after eight hours of operation. These temperature variations typically impose a maximum of about five hours on periods of continuous operations.

The filament and its control grid are enclosed in a housing which is attached to the magnet. Current is carried to the filament and voltages to the control grid through the housing by Kovar feedthroughs. Part of each feedthrough was originally exposed to the electron beam. Immediately after the oxygen research was begun, these feedthroughs were observed to have become electrically leaky. When the source was disassembled, the feedthroughs were found to have a purple conducting coating on them. To prevent the replacement feedthroughs from becoming similarly coated, they were geometrically shielded from the electron beam, and no further leakage has since been observed.

In order to acquire good attenuation data, it is necessary for the source to be stable. This goal has been difficult to achieve with the filament supply employed by the previous investigators who used this apparatus. Albritton[54] tried to minimize instabilities of the source by using an emission-regulation circuit of the type designed by Nier.[55] However, this technique did not show enough sensitivity in the pulse mode and failed to give good stability. Miller[49] and Moseley[50] regulated the line voltage to the transformer which provided a.c. current to the filament. This technique worked better, but instability of the source was still a problem. During the oxygen research reported here, a Harrison Laboratory model 6263A regulated constant voltage, constant current d.c. power supply was used to provide current to the filament. The supply was used in the constant current mode. This supply achieved a marked improvement in the stability of the

thoriated-iridium filament. However, stability was again a problem when the $BaZrO_3$ coated filament was in use. The difference in stability of the two filaments probably arises because the $BaZrO_3$ filament requires about six times the power needed by the thoriated iridium filament to produce the same number of electrons.

The batteries which originally produced the voltages for the control grid, filament bias, collector bias, and the Tyndall shutter were replaced by Hewlett Packard model 6217A constant voltage, current limiting, d.c. power supplies in order to improve stability.

The experiments described in this thesis were the first with this apparatus that required the source to produce negative ions. It was found that the same source which had produced O_2^+ ions would also produce O_2^- and O^- ions in sufficient quantities to permit a pulsed experiment, and would not simultaneously allow electrons into the drift region.

In the previous research performed with this apparatus, it was unnecessary to operate at drift tube pressures greater than 1 Torr. However, in the present research, pressures up to 10 Torr were required. Operation at high pressures exposed certain expected shortcomings of the electron impact ion source. At pressures greater than 6 Torr, it was impossible to get enough positive ion intensity to perform a pulsed experiment. The inability to create ions under these conditions is caused by the mean free path of the electron being so short that the electrons cannot acquire enough energy to cause ionization.

A radioactive or discharge source would probably be preferable for measurements at high pressures.

The Tyndall shutter seems to lose its ability to control the passage of ions at pressures above 3 Torr. This phenomenon is probably caused by the scattering mean free path becoming less than the spacing of the grid wires, so that ions are carried into the drift region by scattering in spite of the potentials on the grids.

Another interesting observation was that the field of the source magnet successfully prevents electrons from drifting with the negative ions into the drift region, at pressures less than 4 Torr. However, at higher pressures the electron scattering is sufficient to override the influence of the magnet, and some electrons drift into the drift region with the negative ions. As a result, appreciable attachment occurs along the entire length of the drift tube at pressures above 4 Torr.

Exit Aperture

Some of the reaction rates investigated in oxygen were of such magnitude that it was necessary to work at pressures higher than had been obtained previously. Higher pressure operation is enabled by reducing the diameter of the exit aperture from 0.079 cm to 0.035 cm. The previous upper limit on pressure was 0.8 Torr. The new upper limit is 10 Torr. However, satisfactory operation at this pressure was attained only after the two-inch isolation valve had been torqued to ten ft.-lbs. (With the previous larger exit aperture, the valve had never been closed more than hand tight.)

Negative Ions

In routine operation, the switch from the investigations of positive ions to negative ions is a very simple procedure and takes only a few minutes. The change is greatly facilitated by the use of the same source for production of ions of either polarity. All necessary changes can be made external to the vacuum system and consist of the following steps:

(1) The skimmer is changed from negative polarity to positive.

(2) The potentials of the guard rings are now set so that the top guard ring is negative with respect to the bottom guard ring, which is still maintained at ground.

(3) The voltage settings on the power supplies for the electron multiplier are changed. The signal end supply goes from ground to +4500 volts. The pre-acceleration supply goes from -3000 to +1500 volts.

(4) The polarity of the bias for the Tyndall shutter is changed from negative to positive. The polarity of the pulse applied to open the Tyndall shutter must be reversed, but the amplitude and shape of the pulse are the same as before.

(5) The filament bias is changed from 40 volts to the value found to optimize attachment for the particular negative ion species being observed.

Electron Multiplier

The EMI model 9643B discrete electron multiplier (DEM) used in previous investigations with this apparatus was replaced by a Mullard

Type B419BL channel electron multiplier (CEM). The CEM is an electrostatic device which employs a continuous semi-conductor dynode surface--only two electrical connections are required to establish the necessary voltage distribution for electron multiplication. This is opposed to the conventional DEM which has discrete dynodes and requires a voltage divider network.

The CEM operates in the following manner. A negative ion with sufficient energy enters the low positive potential (for positive ions this end is at a high negative voltage) end of the CEM and generates electrons on collision with the walls of the tube. By applying voltage between the ends of the tube, a uniform electric field along the axis of the tube is obtained. The initial electrons are accelerated along the axis of the tube and gain enough energy to release secondary electrons on subsequent impact on the wall and the process is repeated down the tube. CEMs are designed so that gains of 10^8 are typical. The tube is curved to minimize after-pulses due to ion feedback. The CEM has several advantages over the DEM:

(1) At sufficiently high operation voltage the gain of the CEM reaches a limiting value so that the heights of separate pulses all tend to a common limit, producing a sharp peak in the pulse height distribution. The practical consequence of the narrow pulse height distribution is the fact that it can be used to more effectively discriminate against noise.

(2) The gain of the CEM is 10^8 versus 10^6 for the DEM.

(3) DEMs lose a considerable percentage of their gain under exposure to air. Consequently, the DEM must be frequently replaced, or rejuvenated if possible. CEMs maintain their excellent performance characteristics when exposed to air. For the present experiment this also means a considerable saving in time. Every time the system was let up to atmosphere, the DEM had to be removed and placed in an auxiliary vacuum system in order to prolong its lifetime.

The CEM has one disadvantage for some types of applications: there is an inherent limit to the count rate above which there is a progressive degradation of gain with increased count rate. However, for the present experiment this limiting count rate is never approached.

The standard CEM also has the disadvantage that it has a small input aperture (1 to 2 mm in diameter). However, larger input apertures can be achieved without increasing the overall dimensions of the CEM by fitting a cone-shaped funnel to the input end. Because the response of a CEM depends on the angle of incidence of the input flux, the physical size of the funnel may not correspond to the dimensions of the effective aperture. It has been found by Fitzwilson et al.[56] that the effective aperture is considerably smaller than the geometrical aperture. However, they also found that by placing a grid above the funnel at the same potential as the funnel, the effective area is made very close to the geometrical area. This technique was used in this experiment.

The Mullard Type B410BL is a CEM consisting of a planar spiral tube having an internal diameter of 2.2 mm with a 10 mm diameter input cone and a closed output end.

The channeltron was operated in a pulsed mode. The number of counts detected ceased to be a function of voltage across the CEM at and above 2.7 kV. We operated with 3.0 kV. The incident energy of the ions ceased to have an effect on the number of counts detected at 1.2 kV. For positive ions, 3.0 kV pre-acceleration was used in order that the signal could be taken out at ground. For negative ions 1.5 kV was used. This caused the signal to be taken out at 4.5 kV, and necessitated the use of a blocking capacitor between the signal lead of the channeltron and the input of the pre-amplifier.

CHAPTER III

ANALYSIS

Moseley and Gatland[57,58] have developed a solution to the transport equation describing the drift, diffusion, and reaction of an ion swarm under the influence of a uniform electric field E in a gas of uniform number density N. An expression was obtained for an ion swarm which is instantaneously created with uniform density across an axially thin circular disk, drifts in unbounded space in a direction perpendicular to the disc, and possibly undergoes a depleting reaction with the gas molecules. This solution is outlined in Appendix IV.

In this earlier analysis the possibility of interactions creating ions of the species under consideration during drift was not considered; all the reaction rates were for reactions which deplete the ion species supplied by the source. Gatland[59] has recently obtained solutions for the situation in which the species supplied by the source reacts with the gas to produce a second ion species; and this second species reacts to produce a third species, etc. These solutions are then used to obtain a solution to the case in which forward-backward reactions are present. This analysis developed by Gatland is described in the next section.

Analysis of Gatland

The transport equation is described in Appendix IV and the related terms are defined there. These same terms are used in this section.

General Analysis

When reactions occur, ions of a given species, labeled 2, may be created at various positions and times, from another ion species, labeled 1, reacting with the gas. The reaction input to species 2 will then be given by

$$\beta_2 (x,y,z,t) = \alpha_{21} n_1 (x,y,z,t) \tag{27}$$

where n_1 is the number density of ionic species 1 and α_{21} is the reaction frequency for converting 1 to 2 at the appropriate gas density. The ions of species 2 may in turn react with the ambient gas to produce ions of species 3 and these in turn produce species 4, etc. Suppose that the ions of species 1 are produced by an initial source input given by

$$\beta = (b/\pi r_o^2) S(r_o - r) \delta(z - z_o) \delta(t - t_o) \tag{28}$$

where $S(\phi) = 0$ if $\phi < 0$, $S(\phi) = 1$ otherwise.

Let $b/\pi r_o^2 = s$, be the planar source density. Then a set of differential equations (in cylindrical coordinates) can be written down as follows:

$$\frac{\partial n_1}{\partial t} = \mathcal{D}_1 n_1 + \beta \tag{29}$$

and

$$\frac{\partial n_p}{\partial t} = \mathcal{D}_p n_p + \alpha_{p,p-1} n_{p-1} \tag{30}$$

for $p > 1$ where

$$\mathcal{D}_p = D_{Tp}\left[\frac{1}{r}\frac{\partial}{\partial r}\left(r\frac{\partial}{\partial r}\right) + \frac{1}{r^2}\frac{\partial^2}{\partial \phi^2}\right] + D_{Lp}\frac{\partial^2}{\partial z^2} - v_{dp}\frac{\partial}{\partial z} - \alpha_p \tag{31}$$

for all p. The diffusion coefficients, drift velocity and depleting reaction frequency for the pth species use that subscript and $\alpha_{p,p-1}$ is the reaction frequency for converting ions of species p-1 into species p. This set of differential equations may be solved sequentially using the Green's function method. The ion density for the pth species is found to be

$$n_p(r,z,t) = s \prod_{\substack{q=1 \\ o}}^{p-1} \left[\alpha_{q+1,q} \int_{t_o}^{t_{q+1}} dt_q\right][\pi b_p]^{-1/2} \times \tag{32}$$

$$\exp[-d_p - (z-z_o-c_p)^2/b_p] \times$$

$$\left[1 - \sum_{m=o}^{\infty}\sum_{i=o}^{m} \frac{1}{m!i!}\left(\frac{r^2}{a_p}\right)^m\left(\frac{r_o^2}{a_p}\right)^i \exp\left(-\frac{r_o^2 + r^2}{a_p}\right)\right]$$

where

$$a_p = \sum_{q=1}^{p} 4D_{T_q}(t_q - t_{q-1}) \tag{33a}$$

$$b_p = \sum_{q=1}^{p} 4D_{Lq}(t_q - t_{q-1}) \tag{33b}$$

$$c_p = \sum_{q=1}^{p} v_{dq}(t_q - t_{q-1}) \tag{33c}$$

$$d_p = \sum_{q=1}^{p} \alpha_q(t_q - t_{q-1}) . \tag{33d}$$

The product symbol Π_o implies that the time integrations are taken in the order

$$\int_{t_o}^{t} dt_{p-1} \int_{t_o}^{t_{p-1}} dt_{p-2} \cdots \int_{t_o}^{t_2} dt_1 .$$

The solution (32) has been established for p = 1 in Appendix IV. Assuming that it is valid for p - 1 it may then be proven for p so that its general validity follows by induction. Because in the present experiment the ion swarm is sampled on axis, the result of interest is the axial ionic number density, $n_p(o,z,t)$,

$$n_p(o,z,t) = s \prod_{\substack{o \\ q=1}}^{p-1} \left[\alpha_{q+1,q} \int_o^{t_{q+1}} dt_q \right] [\pi b_p]^{-1/2} \times \tag{34}$$

$$\exp[-d_p - (z-c_p)^2/b_p][1-\exp(-r_o^2/a_p)].$$

The initial source of ions of species 1 is assumed to be created instantaneously at $t_o = 0$ in the plane $z_o = 0$.

The quantity measured experimentally is the flux Φ of ions leaving the drift tube through an exit aperture of area A at a fixed distance from the source plane:

$$\Phi_p(o,z,t) = Aj_p(o,z,t) \tag{35}$$

where $j_p(o,z,t)$ is ion current density.

The ionic current density is related to the ionic number density by

$$j_p = -D_{Lp}\left(\frac{\partial n_p}{\partial z}\right) + v_{dp} n_p . \tag{36}$$

Differentiation and substitution into Equation (36) gives

$$\Phi_p(o,z_p,t_p) = As \prod_{\substack{o \\ q=1}}^{p-1} \left[\alpha_{q+1,q} \int_o^{t_{q+1}} dt_q \right] [\pi b_p]^{-1/2} \left[2 \frac{D_{Lp}}{b_p} (z - c_p) + v_{dp} \right] \times$$

$$\exp[-d_p - (z - c_p)^2/b_p][1-\exp(-r_o^2/a_p)]. \tag{37}$$

Forward-Backward Reactions

So far the possibility of forward-backward reactions has been ignored. For two species, A and B, which convert into each other by interactions with the parent gas, the following coupled set of differential equations is obtained:

$$\frac{\partial n_A}{\partial t} = \mathcal{D}_A n_A + \alpha_{AB} n_B + \beta \tag{38}$$

$$\frac{\partial n_B}{\partial t} = \mathcal{D}_B n_B + \alpha_{BA} n_A \tag{39}$$

assuming that only species A is introduced by the source. Now n_A and n_B can be expanded in terms of $\alpha_{BA}\alpha_{AB}$,

$$n_A = \sum_{p=o}^{\infty} (\alpha_{AB}\alpha_{BA})^p \, n'_{2p+1} \tag{40}$$

$$n_B = \alpha_{BA} \sum_{p=o}^{\infty} (\alpha_{AB}\alpha_{BA})^p \, n'_{2p+2} \, . \tag{41}$$

Substituting these series into the differential Equations (38) and (39) and equating powers of $(\alpha_{AB}\alpha_{BA})^p$ for p = 0,1,2, etc. yields the following set of equations:

$$\frac{\partial n'_1}{\partial t} = \mathcal{D}_A n'_1 + \beta \tag{42}$$

$$\frac{\partial n'_{2p+2}}{\partial t} = \mathcal{D}_B n'_{2p+2} + n'_{2p+1} \tag{43}$$

$$\frac{\partial n'_{2p+3}}{\partial t} = \mathcal{D}_A n'_{2p+3} + n'_{2p+2} \tag{44}$$

for $p \geq 0$. Now define

$$n_{2p+1} = (\alpha_{AB}\alpha_{BA})^p \, n'_{2p+1} \tag{45}$$

$$n_{2p+2} = \alpha_{BA}(\alpha_{AB}\alpha_{BA})^p \, n'_{2p+2} \tag{46}$$

so that

$$n_A = \sum_{p=o}^{\infty} n_{2p+1} \tag{47}$$

$$n_B = \sum_{p=o}^{\infty} n_{2p+2} \tag{48}$$

and let $\mathcal{D}_{2p+1} = \mathcal{D}_A$; $\mathcal{D}_{2p+2} = \mathcal{D}_B$; $\alpha_{2p+1,2p} = \alpha_{AB}$; and $\alpha_{2p+2,2p+1} = \alpha_{BA}$. Then Equations (42), (43), and (44) are converted into Equations (29) and (30). Thus we have series solutions for n_A and n_B given by Equations (47) and (48). Physically the pth term, n_{2p+1}, in the series for n_A is the density of ions which have been converted from species A to species B, and back again p times.

Results

Evaluation of the time integrals in Equation (34) must be effected by numerical or approximate methods in the general case. However, for two species involved in a forward-backward reaction system, the integration variables occur only in the combination

$$u = t_{p-1} - t_{p-2} + t_{p-3} \ldots + (-1)^p t_1 \tag{49}$$

(assuming $t_o = 0$).

Therefore, for p odd Equation (33) can be put in the form

$$a_p = a_A = 4D_{TA}t - 4(D_{TA}-D_{TB})u \tag{50a}$$

$$b_p = b_A = 4D_{LA}t - 4(D_{LA}-D_{LB})u \tag{50b}$$

$$c_p = c_A = v_{dA}t - (v_{dA}-v_{dB})u \tag{50c}$$

$$d_p = d_A = \alpha_A t - (\alpha_A-\alpha_B)u. \tag{50d}$$

For p even, $a_p = a_B$; $b_p = b_B$, $c_p = c_B$, and $d_p = d_B$ where a_B, b_B, c_B, and d_B are defined in the same way as a_A, b_A, c_A, and d_A but with the subscripts A and B interchanged. All but one of the integrations in Equation (34) may be carried out. This is most easily effected by a change of variables

$$u = y - x \tag{51}$$

and by repeated use of the expression

$$\int_0^{\omega} dy \int_0^{y} dx\; g(y-x)\,\frac{x^n}{n!}\,\frac{(y-x)^m}{m!} = \int_0^{\omega} du\; g(u)\,\frac{u^m}{m!}\,\frac{(\omega-u)^{n+1}}{(n+1)!}\,. \tag{52}$$

Let Equation (52) be applied to the case of p = 6. From Equation (34) one can determine that n_6 can be written as

$$n_6 = \alpha_{65}\alpha_{54}\alpha_{43}\alpha_{32}\alpha_{21} \int_0^{t} dt_5 \int_0^{t_5} dt_y \int_0^{t_4} dt_3 \times \tag{53}$$
$$\int_0^{t_3} dt_2 \int_0^{t_2} dt_1\; g(t_5-t_4+t_3-t_2+t_1)$$

where $g(t_5 - t_4 + t_3 - t_2 + t_1) = s[\pi b_6]^{-1/2} \exp[-d_6 - (z-c_6)^2/b_6][1-\exp(-r_o^2/a_6]$.

Let $y = t_2$ and $x = t_1$; then

$$n_6 \propto \int_0^{t} dt_5 \int_0^{t_5} dt_4 \int_0^{t_4} dt_3 \left[\int_0^{t_3} dy \int_0^{t_2} dx\; g(t_5-t_4+t_3-y+x)\right] \tag{54}$$

and by Equation (52)

$$n_6 \propto \int_0^{t} dt_5 \int_0^{t_5} dt_4 \int_0^{t_4} dt_3 \left[\int_0^{t_3} g(t_5-t_4+t_3-u)(t_3-u)du\right]. \tag{55}$$

Now let $t_3 = y$ and $u = x$; then

$$n_6 \propto \int_0^t dt_5 \int_0^{t_5} dt_4 \int_0^{t_4} dy \int_0^{t_3} dx\ g(t_5-t_4+y-x)(y-x). \tag{56}$$

Again use Equation (52) and

$$n_6 \propto \int_0^t dt_5 \int_0^{t_5} dt_4 \left[\int_0^{t_4} du\ g(t_5-t_4+u)\ \frac{u}{1!}\ \frac{(t_4-u)}{1!} \right]. \tag{57}$$

By a further change of variables and application of Equation (52), we obtain

$$n_6 \propto \int_0^t dt_5 \int_0^{t_5} du\ g(t_5-u)\ \frac{(t_5-u)^2}{2!}\ \frac{u}{1!} \tag{58}$$

and finally

$$n_6 \propto \int_0^t du\ g(u)\ \frac{u^2}{2!}\ \frac{(t-u)^2}{2!}\ . \tag{59}$$

Note that

$$\alpha_{21} = \alpha_{43} = \alpha_{65} = \alpha_{BA}$$

and

$$\alpha_{32} = \alpha_{54} = \alpha_{AB}\ .$$

Define

$$\gamma = \alpha_{AB}\alpha_{BA}. \tag{60}$$

Then

$$n_6 = \alpha_{BA} \int_o^t du\ g(u)\ \frac{u^2}{2!}\ \frac{(t-u)^2}{2!}\ \gamma^2. \tag{61}$$

Expressions can be obtained for all n_p in a similar manner. Substitute these expressions for the various n_p in Equation (47) and (48) to obtain

$$n_A = g(0) + \int_o^t du\ g(u)\left[\gamma(t-u) + u\ \frac{\gamma^2(t-u)^2}{2!} + \frac{u^2}{2!}\ \gamma^3\ \frac{(t-u)^3}{3!} + \cdots\right] \tag{62}$$

and

$$n_B = \alpha_{BA} \int_o^t du\ g(u)\left[1 + u(t-u)\gamma + \frac{u^2}{2!}\ \gamma^2 + \frac{u^3}{3!}\ \frac{(t-u)^3}{3!}\ \gamma^3 + \cdots\right]. \tag{63}$$

Equation (62) and (63) can be written in the following compact form:

$$n_A = \int_o^t du\ g(u)\left[\delta(u) + \sum_{p=o}^{\infty} \frac{u^p}{p!}\ \frac{(t-u)^{p+1}}{(p+1)!}\ \gamma^{p+1}\right] \tag{64}$$

and

$$n_B = \alpha_{BA} \int_o^t du\ g(u)\ \sum_{p=o}^{\infty} \frac{u^p}{p!}\ \frac{(t-u)^p}{p!}\ \gamma^p \tag{65}$$

where the delta function is taken to lie wholly inside the range of integration.

One of the difficulties in evaluating Equations (64) and (65) might be in the determination of the number of terms necessary to calculate in the summation. However, the infinite series in (64) and (65) can be converted to Bessel functions which can be easily evaluated. The summation term in (64) can be expressed in the following form

$$\gamma(t-u) \sum_{k=o}^{\infty} \frac{[4\gamma u(t-u)/4]^k}{k!(k+1)!} . \tag{66}$$

Put

$$\eta = \sqrt{4\gamma u(t-u)} \tag{67}$$

and multiply numerator and denominator of Equation (66) by $\eta/2$. Then (66) can be written as

$$\frac{2\gamma(t-u)}{\eta} \sum_{k=o}^{\infty} \frac{(\eta/2)^{2k+1}}{k!(k+1)} . \tag{68}$$

One recognizes that the series in (68) is equivalent to $I_1(\eta)$,[60] where $I_1(\eta)$ is the modified Bessel function of the first kind of order 1.

Similar analysis shows that the summation term in (65)

$$\sum_{p=o}^{\infty} \frac{u^p (t-u)^p \gamma^p}{p!\ p!} = I_o(\eta) \tag{69}$$

where $I_o(\eta)$[60] is the modified Bessel function of the first kind of order o. Substitution of the Bessel functions into (64) and (65) gives

$$n_A(o,z,t) = s\int_o^t du\left[\delta(u) + 2\alpha_{AB}\alpha_{BA}\frac{I_1(\eta)}{\eta}(t-u)\right][\pi b_A]^{-1/2} \qquad (70)$$

$$x\ \exp[-d_A-(z-c_A)^2/b_A][1-\exp(-r_o^2/a_A)]$$

$$n_B(o,z,t) = s\alpha_{BA}\int_o^t du\ I_o(\eta)[\pi b_B]^{-1/2} \qquad (71)$$

$$\exp[-d_B-(z-c_B)^2/b_B][1-\exp(-r_o^2/a_B)]\ .$$

Note that

$$a_B(u) = a_A(t-u) \qquad (72a)$$

$$b_B(u) = b_A(t-u) \qquad (72b)$$

$$c_B(u) = c_A(t-u) \qquad (72c)$$

$$d_B(u) = d_A(t-u) \qquad (72d)$$

$$\eta(u) = \eta(t-u). \qquad (72e)$$

Therefore upon substitution of (72) into (71) and a change of variables from t-u to u, Equation (71) can be written as

$$n_B(o,z,t) = s\alpha_{BA}\int_o^t du\ I_o(\eta)[\pi b_A]^{-1/2}\ x \qquad (73)$$

$$\exp[-d_A - (z-c_A)^2/b_A][1-\exp(-r_o^2/a_A)]$$

Equation (70) is the number density for a source produced species labeled A which has reacted to form species B, C, etc. and which has been produced in the drift tube by species B. Equation (73) is the number density for species B which is produced from species A in the drift tube and which reacts to form species A, D, etc. A computer program has been written which calculates Equations (70) and (73). The ionic current densities for species A and B are also calculated by the computer program. This computer program will be used in the next section to calculate hypothetical time profiles for species B for a number of situations in order to make comparisons with the results of several approximate calculations. The program is also used in Chapter VI to calculate time profiles for comparison with experimental data.

Reaction Rate Techniques

Although in principle determination of v_{dA}, v_{dB}, D_{LA}, D_{LB}, D_{TA}, D_{TB}, α_A, α_B, α_{AB}, and α_{BA} by comparison of the experimental data with Equations (70) and (73) involves a many parameter fit, in practice the effects of many of these parameters on the spectra can be separated and the number of parameters needed to determine certain features of the spectra are greatly reduced.

The drift velocities of species A and B can be determined by the analysis discussed in Appendix IV and Chapter IV by making mobility measurements at appropriate pressures and drift distances. Therefore techniques were developed which determined the values of D_T, D_L, and α's. Several techniques have been developed for evaluating the reaction rates and the transverse diffusion coefficients from certain parts of

the product ion spectra which are taken under certain experimental conditions. Values for D_L can be determined independently of α and D_T from another feature of the product ion spectra.

Some of the techniques which determine reaction rates and transverse diffusion coefficients are restricted to the examination of that part of the product ion spectra for which the following statement is true.

$$(v_{dA}-v_{dB})^2t^2 >> b_A. \tag{74}$$

When Equation (74) is valid, the following approximation can be made.[61]

$$\frac{1}{[\pi b_A]^{1/2}} \exp[-(z-c_A)^2/b_A] = \frac{1}{v_{dA} - v_{dB}} \delta(u-u_1), \tag{75}$$

where

$$u_1 = \frac{v_{dA}t - z}{v_{dA} - v_{dB}}. \tag{76}$$

The region of time of the product ion spectrum for which Equation (74) is valid can be found by noting the following:

$$\frac{b_A}{(v_{dA}-v_{dB})^2t^2} = \frac{4D_{LA}(t-u) + 4D_{LB}u}{(v_{dA}-v_{dB})^2t^2} \leq \frac{4(D_{LA}+D_{LB})t}{(v_{dA}-v_{dB})^2t^2}.$$

Thus the delta function is valid if the difference in the drift distances $(v_{dA}t-v_{dB}t)$ is large compared to the square root of the sum of the diffusion areas $(4D_{LA}t + 4D_{LB}t)^{1/2}$.

Now let

$$a_o = 4D_{TA}t \qquad a_1 = 4D_{TA}(t-u_1) + 4D_{TB}u_1$$

$$b_o = 4D_{LA}t \qquad d_1 = \alpha_A(t-u_1) + \alpha_B u_1 \tag{77}$$

$$c_o = v_{dA}t \qquad \eta_1 = [4\alpha_{AB}\alpha_{BA}u_1(t-u_1)]^{1/2}$$

$$d_o = \alpha_A t \, .$$

Application of Equation (75) allows Equations (70) and (73) to be written as

$$n_A(o,z,t) = \frac{s}{(\pi b_o)^{1/2}}[1-\exp(-r_o^2/a_o)]\exp[-d_o]\exp[-(z-c_o)^2/b_o]$$
$$+ \frac{s}{|v_{dA}-v_{dB}|}[1-\exp(-r_o^2/a_1)]\exp[-d_1]2\alpha_{AB}\alpha_{BA}(t-u_1)\frac{I_1(\eta_1)}{\eta_1} \tag{78}$$

and

$$n_B(o,z,t) = \frac{s\alpha_{BA}}{|v_{dA}-v_{dB}|}[1-\exp(-r_o^2/a_1)]\exp[-d_1]I_o(\eta_1) \, . \tag{79}$$

If we now substitute Equation (76) into (77) the following expressions are found:

$$a_1 = \frac{4D_{TA}(z-v_{dB}t) + 4D_{TB}(v_{dA}t-z)}{v_{dA} - v_{dB}}$$

$$d_1 = \frac{\alpha_A(z-v_{dB}t) + \alpha_B(v_{dA}t-z)}{v_{dA} - v_{dB}} \tag{80}$$

$$\eta_1^2 = \frac{4\alpha_{AB}\alpha_{BA}}{(v_{dA}-v_{dB})^2}(z-v_{dB}t)(v_{dA}t-z).$$

Also let us make the following definition

$$a_1' = \frac{4D_{TB}v_{dA} - 4D_{TA}v_{dB}}{v_{dA} - v_{dB}}. \tag{81}$$

Now take the natural logarithm of Equation (79)

$$\ell n(n_B) = \ell n[1-\exp(-r_o^2/a_1)] - d_1 + \ell n\, I_o(\eta_1) + \text{constant}. \tag{82}$$

Differentiation of (82) yields

$$\frac{\partial \ell n(n_B)}{\partial t} = -\frac{\alpha_B v_{dA} - \alpha_A v_{dB}}{v_{dA} - v_{dB}} - \frac{r_o^2/a_1}{[\exp(r_o^2/a_1) - 1]}\frac{a_1'}{a_1} - \frac{1}{I_o}\frac{\partial I_o}{\partial \eta_1}\frac{\partial \eta_1}{\partial \eta_1^2}\frac{\partial \eta_1^2}{\partial t}. \tag{83}$$

Now let us examine Equation (83) under certain experimental situations. The most restrictive case will be examined first.

Assume (1) that species B does not react (i.e. $\alpha_B = \alpha_{AB} = 0$) and also assume (2) that v_{dA} and v_{dB} are related to D_{TA} and D_{TB} by $D_{TB}/D_{TA} = v_{dB}/v_{dA}$ (the Einstein relation is a special case for this restriction). Assumption (1) makes $I_o(\eta_1)$ = constant and (2) causes $a_1' = 0$. Thus Equation (83) reduces to

$$\frac{\partial \ell n(n_b)}{\partial t} = \frac{\alpha_A v_{dB}}{v_{dA} - v_{dB}} . \qquad (84)$$

Therefore, knowing the log of the product ion current density as a function of time at times where Equation (74) is valid and knowing the drift velocities, the depletion reaction frequency for species A, α_A, can be calculated. Note that α_A could include the depletion of A to B, A to C, etc. In Chapter VI, the case of A going only to B will be used in the analysis of Reaction (16) and (17).

Figure 6 is a computer generated product ion spectrum calculated on the basis of Equation (73). The drift velocities used to generate the spectrum were typical of O^- and O_2^-. The slope is independent of time as predicted by Equation (84) for a large part of the product ion spectrum (from t = 380 to 710 microseconds). Experimentally, one would like Equation (74) to be valid for a large part of the spectra in order that a good value of the slope can be obtained from the experimental data. Physically, as seen in Figure 6, Equation (74) is valid for a large region of the spectrum if the total width of the spectrum is large compared to the longitudinal diffusion spreading of the ionic species. This condition requires a large difference in drift velocities or very long drift times in order to obtain a substantial region where Equation (74) is valid. The reaction rate computed from the slope of the log of the product ion current is the same as the reaction rate used to generate the spectrum.

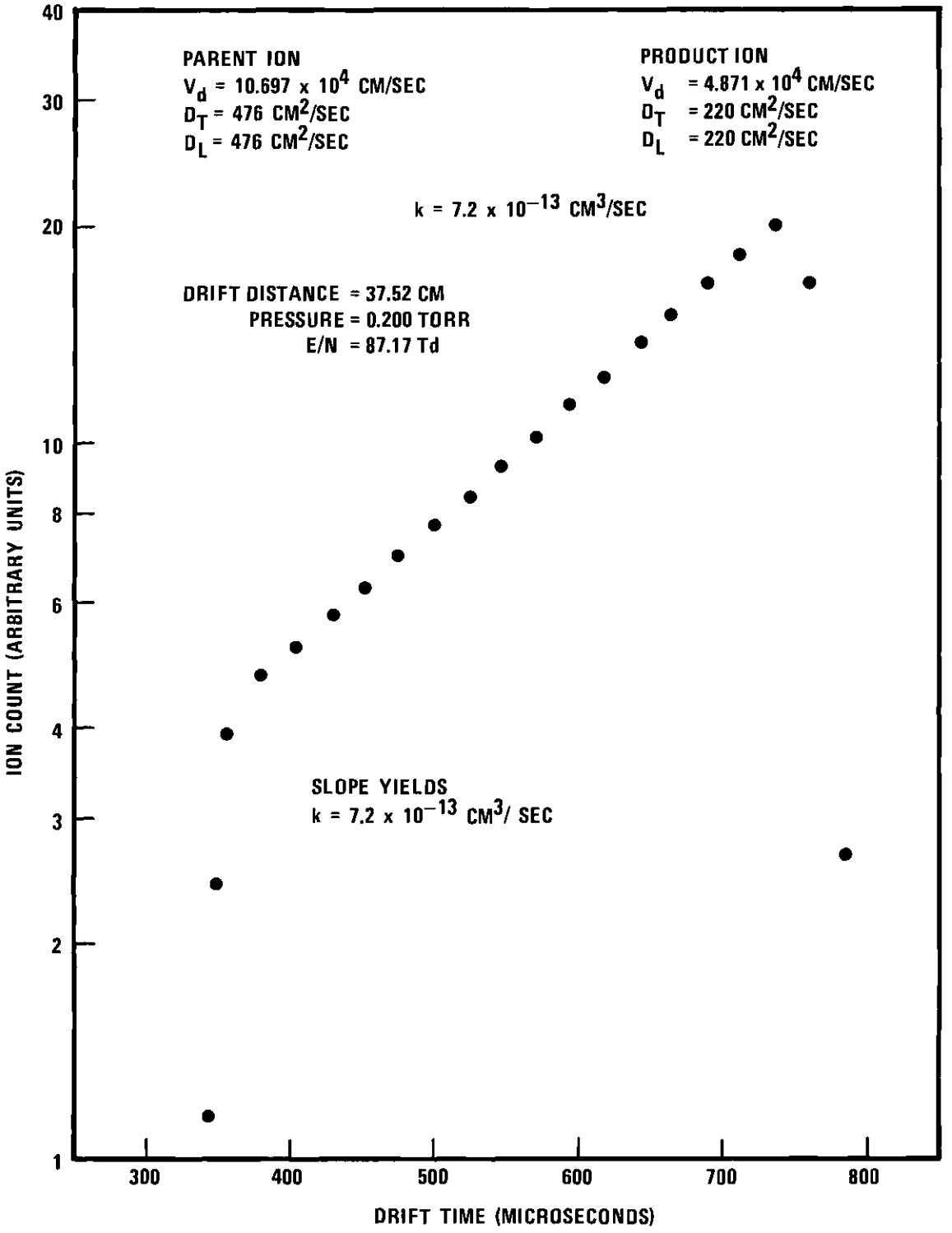

Figure 6. Analytic Product Ion Spectrum with Einstein Diffusion Assumed

Figure 7 shows the effect of variation of the value of D_L for the parent ion. Variation of D_{LA} by a factor five has a negligible effect on the slope in the region where Equation (74) is valid. Variation of D_{LA} does change the manner in which the ion current falls from its value at 740 microseconds.

Now let us remove the assumption that $D_{TB}/D_{TA} = v_{dB}/v_{dA}$. The removal of this assumption allows Equation (83) to be written as

$$\frac{\partial \ell n(n_B)}{\partial t} = \frac{\alpha_A v_{dB}}{v_{dA} - v_{dB}} - \frac{r_o^2/a_1}{[\exp(r_o^2/a_1) - 1]} \frac{a_1'}{a_1} . \qquad (85)$$

Because of the form of a_1 and a_1' the slope is now a function also of D_{TA}, D_{TB}, z, and t. Figure 8 shows a comparison of two computer generated spectra. One spectrum was generated with the Einstein values for the D_{TA} and D_{TB}. The other spectrum was generated with a value of D_{TA} five times the Einstein value. The comparison shows that the slope for the non-Einstein value of D_{TA} has a greater value than for the Einstein case. The agreement with Equation (85) is exact between t = 380 and 710 microseconds. The value of the slope for the non-Einstein spectra was calculated at t = 560 microseconds from the computer generated time spectra. Examination of the non-Einstein spectrum shows that the slope does vary with time. This time variation of the slope might in some experimental situations allow determination of D_{TA} and α_A. However, for our investigation of Reaction (17), this variation did not show enough sensitivity to allow determination of D_{TA} and α_A from the experimental data by examination of the time variation.

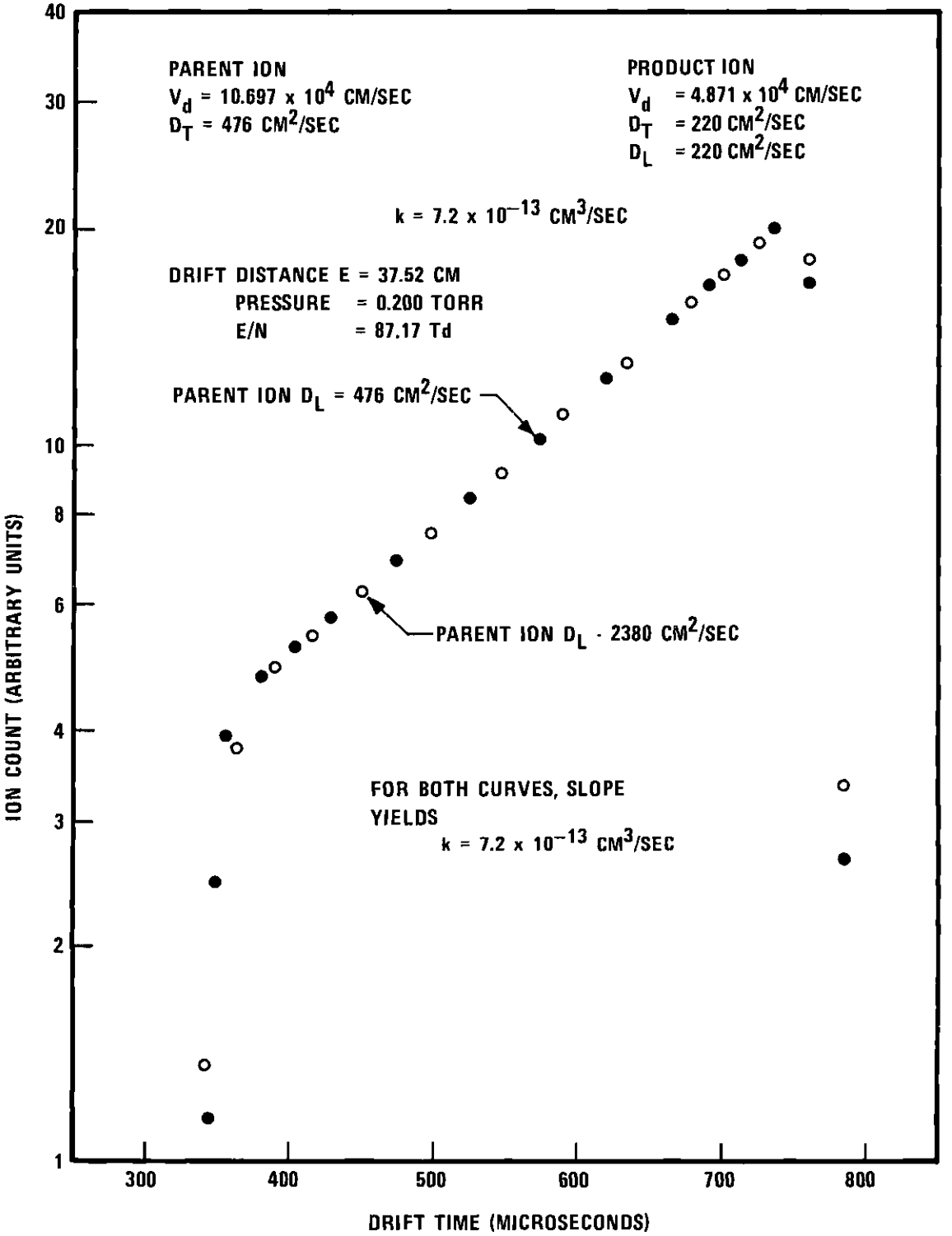

Figure 7. Comparison of Analytic Product Ion Spectra for Two Values of D_L

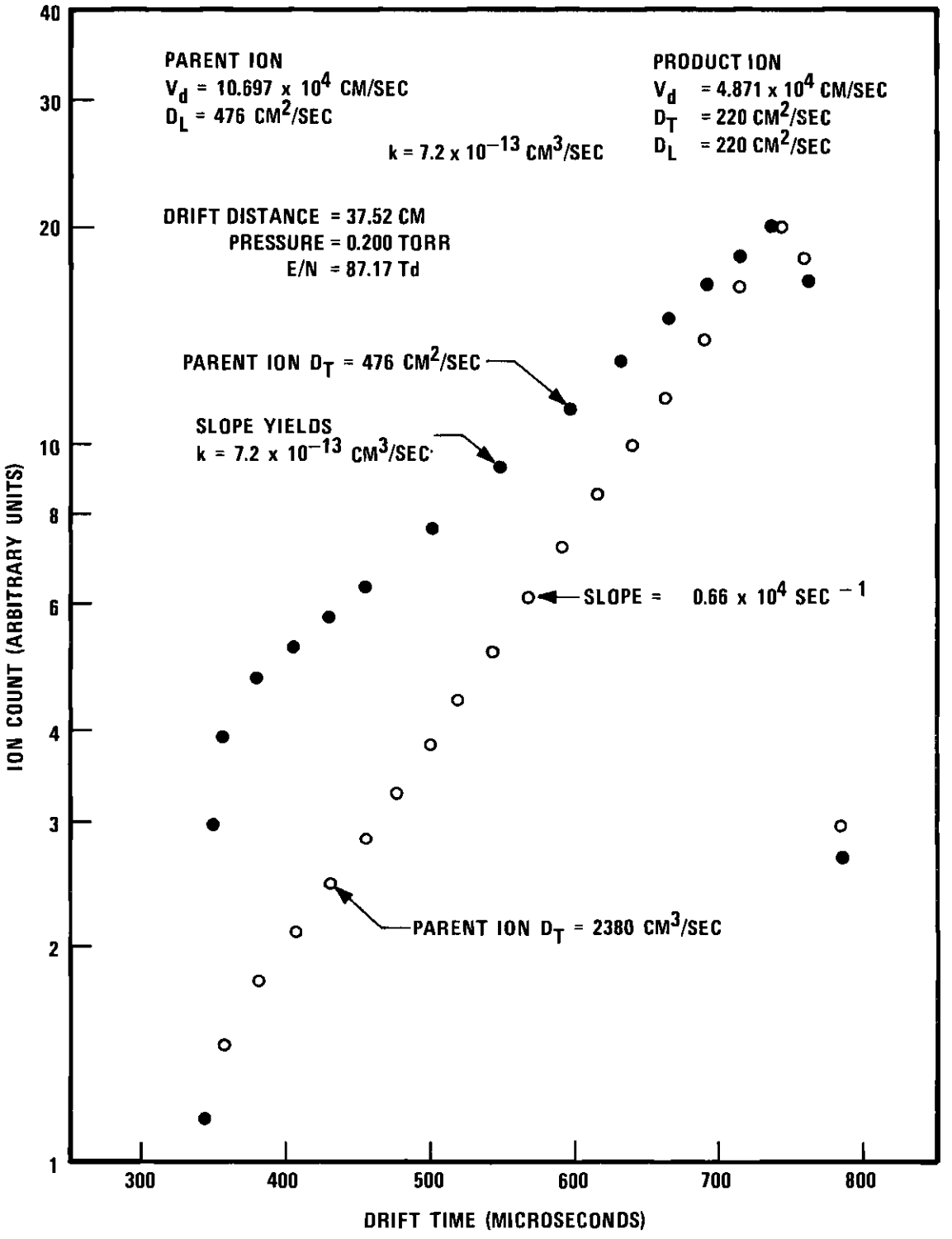

Figure 8. Comparison of Analytic Product Ion Spectra for Two Values of D_T

Equation (85) is also a function of z. Therefore, observation of the variation of the slope as a function of z can lead to the determination of D_{TA} and α_A. Figure 9 shows two computer generated spectra calculated for two values of z. Notice that the slopes of the two spectra are different. The slopes shown on the figure were calculated from the computer generated spectra at $t = t_c = z(v_{dA}+v_{dB})/2v_{dA}v_{dB}$. t_c is the midpoint in time of each spectrum. The variations of the slope of the time spectra with variations in z were too small for accurate determinations of D_{TA} and α_A for Reaction (17).

Large variations in the slope have been obtained for Reaction (17) by varying the pressure. If z and E/N are held constant while the pressure is changed, large variations in the slope were observed. Recall that for Reaction (17) $\alpha \propto N$ and $D_T \propto 1/N$. Therefore, the reaction rate and ND_T are constant for the spectra at the two pressures. Figure 10 illustrates the variation of the slope of the log of the ion current as a function of pressure. One of the computer generated spectra was calculated for a pressure of 0.100 Torr and the other spectra was calculated for 0.200 Torr. An iterative technique has been developed to obtain values of D_{TA} and α_A for Reaction (17) and this technique is described in Chapter VI. Consistency checks were made with the time and drift distance variations for Reaction (17).

Figure 11 shows the effects caused by dropping the assumption that species B does not react to form species C. The Einstein diffusion coefficients are assumed for both computer generated spectra. The time spectrum which was generated with $\alpha_B \neq 0$ has a smaller slope than that

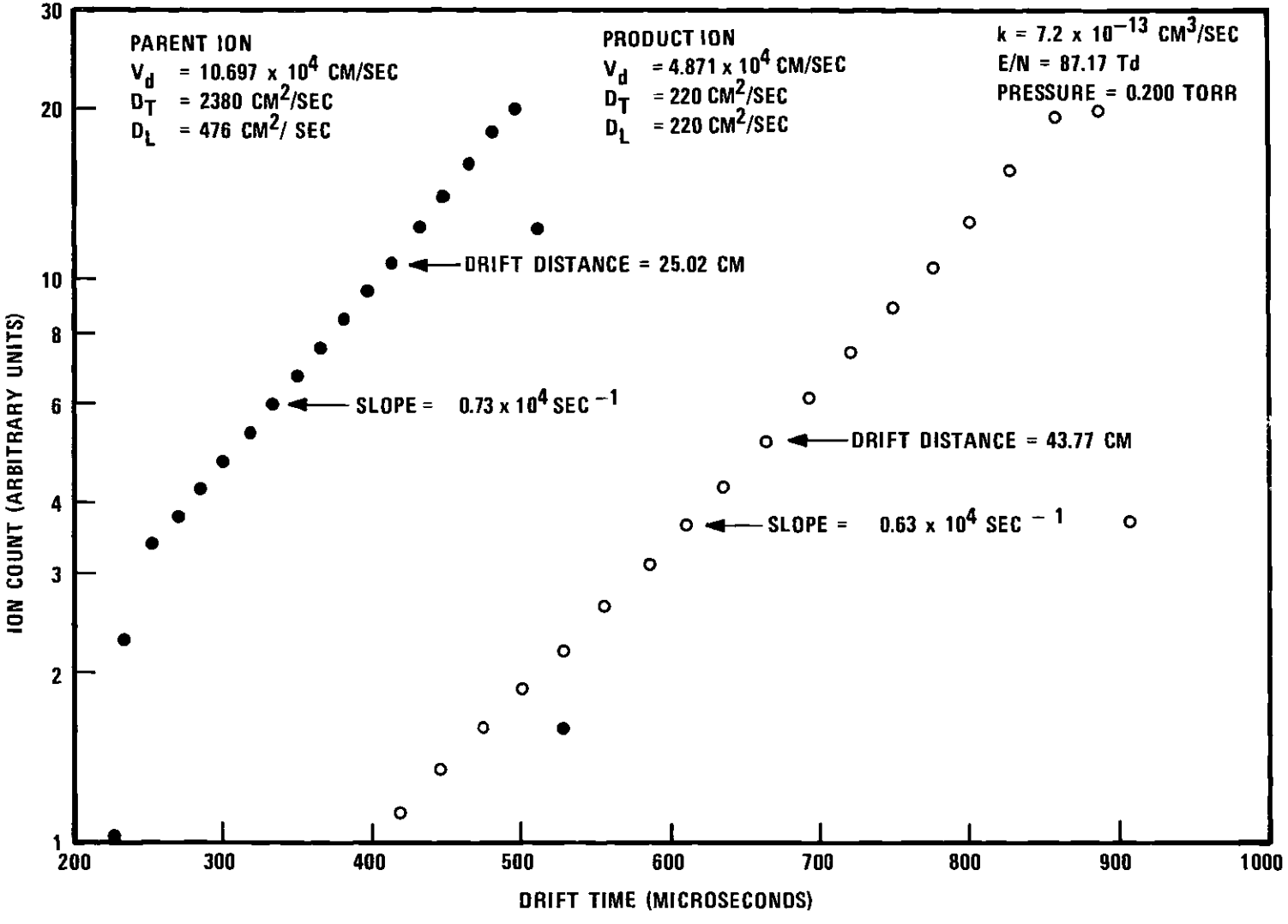

Figure 9. Comparison of Analytic Product Ion Spectra at Two Drift Distances

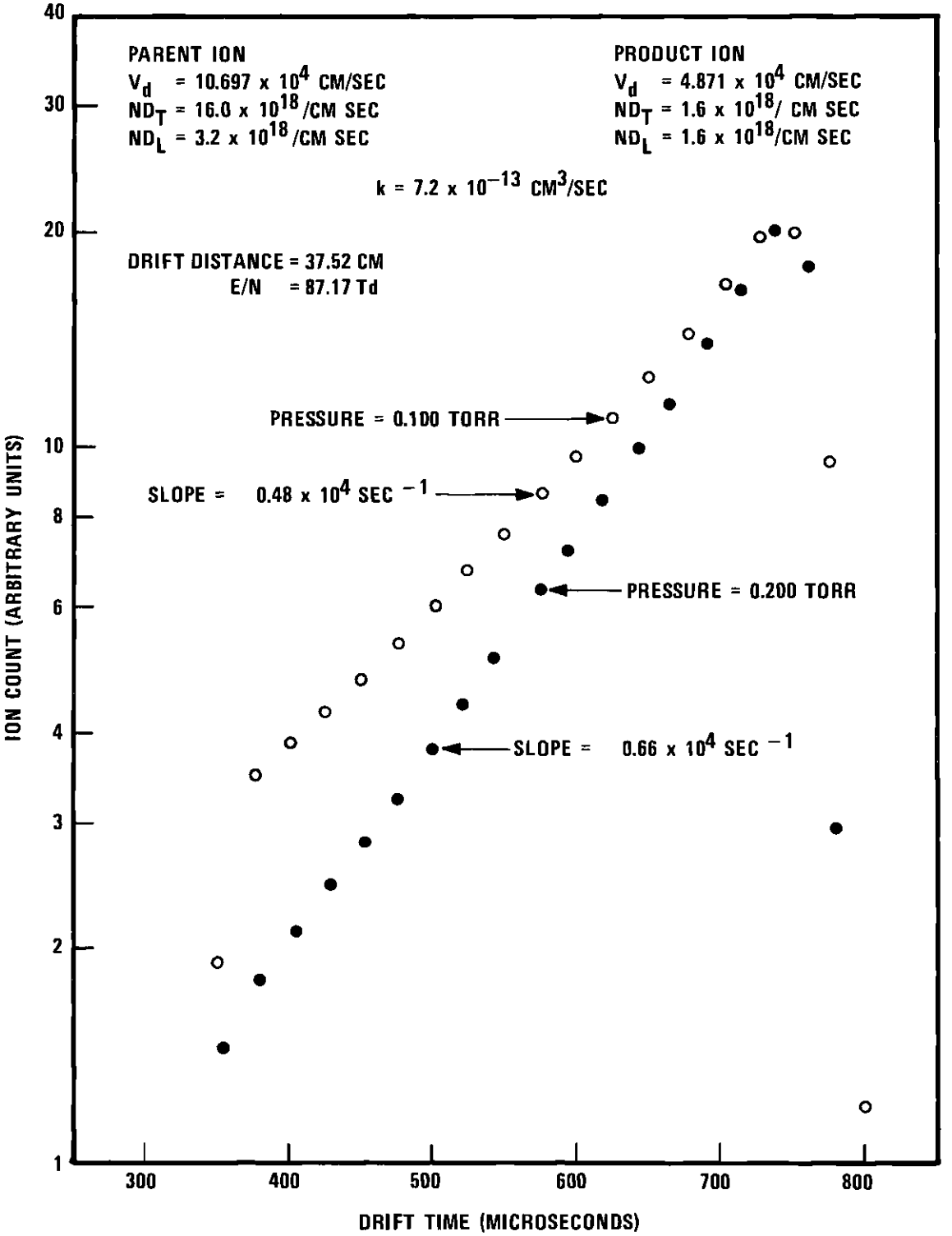

Figure 10. Comparison of Analytic Product Ion Spectra at Two Pressures

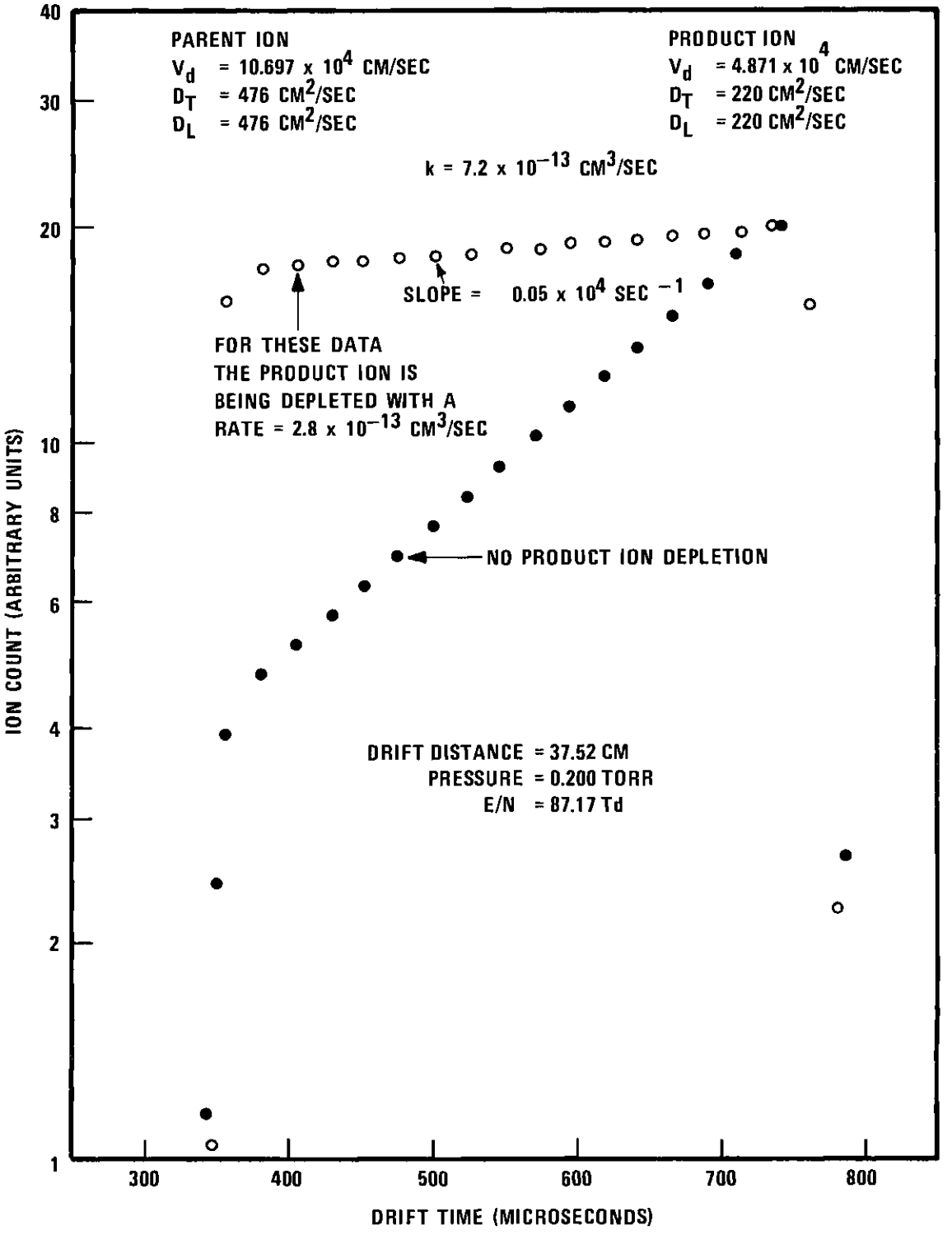

Figure 11. Analytic Product Ion Spectra Which Show Effects of Product Ion Depletion

for $\alpha_B = 0$. The slope for the spectrum with $\alpha_B \neq 0$ agrees with the following expression

$$\frac{\partial \ell n(n_B)}{\partial t} = - \frac{\alpha_B v_{dA} - \alpha_A v_{dA}}{v_{dA} - v_{dB}} \tag{86}$$

which is obtained from Equation (83).

Now let us investigate the forward-backward reaction scheme. For this case, both the product ion spectra and the parent ion spectra will show the effects of α_{AB} and α_{BA}. Assume that species A is being depleted only to species B and that B is being depleted only to A. Therefore $\alpha_A = \alpha_{BA}$ and $\alpha_B = \alpha_{AB}$. Also note that when $t = t_c$, $\partial n_1^2/\partial t = 0$. Thus, Equation (83) can be written

$$\left.\frac{\partial \ell n(n_B)}{\partial t}\right|_{t=t_c} = - \frac{\alpha_{AB} v_{dA} - \alpha_{BA} v_{dB}}{v_{dA} - v_{dB}} - \frac{r_o^2/a_1}{[\exp(r_o^2/a_1) - 1]} \frac{a_1'}{a_1} \tag{87}$$

where a_1' is defined as before and a_1 is defined at $t = t_c$. In the Einstein region, the slope of the log of the product ion current at $t = t_c$ depends on the difference in the reaction frequencies. Experimentally, it may be difficult to locate the mean time t_c and compute an accurate slope there. However, Equation (87) may have approximate validity over a time range about t_c. The size of this time range depends on the magnitudes of α_{AB}, α_{BA}, v_{dA}, v_{dB}, D_{TA}, and D_{TB} and must be evaluated for each case.

If Equation (74) is valid over a long time interval, a foot (or tail depending on which species is faster) will appear on the parent ion spectra which is due to the dissociation of the product ion. Gatland[62] has recently developed an analysis of Equation (78) which is useful in the determination of forward-backward reaction frequencies from the shape of the parent ion spectra.

For the parent ions which are source produced, the following assumption is made

$$\left(\frac{v_{dA}^2}{4\pi D_{LA} t}\right)^{1/2} \exp[-(z-v_{dA}t)^2/4D_{LA}t] = \delta(t-z/v_{dA}). \tag{88}$$

Then Equation (78) can be written as

$$n_A(0,z,t) = \frac{s}{v_{dA}} [1 - \exp(-r_o^2 v_{dA}/4D_{TA}z)]\exp[-\alpha_A z/v_{dA}] \times$$

$$\left\{ \delta(t-z/v_{dA}) + \frac{\alpha_{AB}\alpha_{BA}}{|v_{dA}-v_{dB}|} \frac{z(1-h)}{2} \left[\frac{2I_1(\eta_1)}{\eta_1}\right] \frac{[1 - \exp(-r_o^2/r_T^2)]}{[1 - \exp(-r_o^2 v_{dA}/4D_{TA}z)]} \times \right.$$

$$\left. \exp\left[-\left(\frac{\alpha_B}{v_{dB}} - \frac{\alpha_A}{v_{dA}}\right) \frac{z(1+h)}{2}\right] \right\}$$

where

$$h = 2\,\frac{t - z/v_{dA}}{z/v_{dB} - z/v_{dA}} - 1$$

and

$$r_T^2 = \frac{1}{2}\left[\frac{4D_{TB}z}{v_{dB}} + \frac{4D_{TA}z}{v_{dA}}\right] + \frac{1}{2}\left[\frac{4D_{TB}z}{v_{dB}} - \frac{4D_{TA}z}{v_{dA}}\right] h.$$

Designate the source produced parent ions by n_{AS}. Thus

$$n_{AS}(0,z,t) = \frac{s}{v_{dA}}\,[1 - \exp(-r_o^2 v_{dA}/4D_{TA}z)]\exp(-\alpha_A z/v_{dA})\ \delta(t-z/v_{dA}).$$

Now calculate the total detected source produced parent ions, I, by integrating the flux over all positive values of t. Therefore,

$$I = As\ [1 - \exp(-r_o^2 v_{dA}/4D_{TA}z)]\exp(-\alpha_A z/v_{dA}). \qquad (89)$$

Equation (89) is only an approximate measure of the ion current because of assumption (88), however, for typical values of v_d, D_L, D_T, and r_o Equation (89) differs from Equation (117) by less than one part in 10^3. Experimentally, the spectra for n_A will have a large peak and the area under this peak can be taken as an approximate experimental measure of I.

Designate the reaction produced parent ion current by Φ_{AR}. Then

$$\Phi_{AR} = \frac{I\alpha_{AB}\alpha_{BA}z(1-h)}{2|v_{dA}-v_{dB}|}\quad \exp\left[\left(\frac{\alpha_B}{v_{dB}} - \frac{\alpha_A}{v_{dA}}\right)\frac{z}{2}(1+h)\right] \times \qquad (90)$$

$$\frac{2I_1(\eta_1)}{\eta_1}\ \frac{\{1 - \exp[-1/(\beta_o+\beta_1 h)]\}}{\{1 - \exp[-1/(\beta_o-\beta_1)]\}}$$

where

$$\beta_o = \frac{4D_{TB}z}{2v_{dB}r_o^2} + \frac{4D_{TA}z}{2v_{dA}r_o^2}$$

and

$$\beta_1 = \frac{4D_{TB}z}{2v_{dB}r_o^2} - \frac{4D_{TA}z}{2v_{dA}r_o^2} .$$

Define

$$\phi = - \left(\frac{\alpha_B}{v_{dB}} - \frac{\alpha_A}{v_{dA}} \right) \frac{z}{2}$$

$$\psi = - \frac{\beta_1}{\beta_o^2[\exp(1/\beta_o) - 1]}$$

$$\rho = \ell n \left(\frac{I \ \alpha_{AB}\alpha_{BA} z \ \Delta t}{2|v_{dA} - v_{dB}|} \right)$$

$$\rho_1 = \phi + \psi$$

$$\rho_o = \rho + \phi + \psi$$

where Δt = channel width of the multichannel analyzer. The factor Δt is introduced because the quantity Φ is not what is measured, but $\Phi \Delta t$ is measured. It is also assumed in this analysis that $\alpha_{AB}\alpha_{BA}$ is much

less than one and for this assumption $2I_1(\eta_1)/\eta_1$ is approximately equal to one. Therefore Equation (90) becomes

$$\Phi_{AR}(0,z,t)\ \Delta t = (1-h)\exp(\rho_o + \rho_1 h).$$

It can be shown that Equation (87) which describes the slope of the log of the product ion current at time t_c reduces to

$$\left.\frac{\partial \ln(n_B)}{\partial t}\right|_{t=t_c} = \frac{2}{z/v_{dA} - z/v_{dB}}\ (\phi + \psi). \tag{87}$$

Therefore examination of n_B can provide values of ϕ and ψ. Now plot the experimental data which correspond to $\Phi_{AR}\Delta t$ in the following manner

$$\ln\left[\frac{\Phi_{AR}\Delta t}{1 - h}\right] = \rho_o + \rho_1 h. \tag{91}$$

This plot can provide values of ρ_o and ρ_1. Because $\rho_1 = \phi + \psi$, a consistency check can be made between the parent and the product ion data. Note from the previous definitions that

$$\frac{\alpha_{AB}\alpha_{BA}}{v_{dA}v_{dB}} = \frac{2|v_{dA}-v_{dB}|\exp(\rho_o-\rho_1)}{\Delta t\ Iz\ v_{dA}v_{dB}}$$

and

$$\frac{\alpha_A}{v_{dA}} - \frac{\alpha_B}{v_{dB}} = \frac{2\phi}{z} .$$

If no competing reactions are present, $\alpha_A = \alpha_{BA}$ and $\alpha_B = \alpha_{AB}$. Assume that the data are taken at a pressure where $\alpha_A/v_{dA} >> \alpha_B/v_{dB}$. Then a value for α_B can be found from

$$\frac{\alpha_B}{v_{dB}} = \left| \frac{1}{v_{dB}} - \frac{1}{v_{dA}} \right| \frac{\exp(\rho_o - \rho_1)}{\Delta t \; I \; \phi} \tag{92}$$

and α_A from

$$\frac{\alpha_A}{v_{dA}} = \frac{2\phi}{z} + \frac{\alpha_B}{v_{dB}} . \tag{93}$$

Because the drift velocities of O_2^+ and O_4^+ were very similar, Equations (87), (92), and (93) were not useful in the investigation of Reaction (18).

Let us now consider the case when the drift velocities and times involved are such that the region of validity of Equation (74) is small. In an attempt to develop a method for this situation, the expressions for the total number of ions of a given ionic species were examined for properties which might give good estimates of the reaction frequencies. Experimentally, the total ion current cannot be measured and still maintain the mass analysis. The total ion current is sampled on axis. Errors caused by differences in the total ion current and the ion current sampled on axis will be discussed later in this section.

The following set of equations describes the total ion current of two species involved in a forward-backward reaction scheme.

$$\frac{\partial N_A}{\partial t} = -\alpha_{BA} N_A + \alpha_{AB} N_B \tag{94}$$

$$\frac{\partial N_B}{\partial t} = -\alpha_{AB} N_B + \alpha_{BA} N_A \tag{95}$$

where N_A and N_B are the total ion current for species A and B, respectively. Assume the boundary conditions $N_A = C$ and $N_B = 0$ at $t = 0$. Then the solutions to Equations (94) and (95) are

$$N_A(t) = C\left[1 - \frac{\alpha_{BA}}{\alpha_{AB} + \alpha_{BA}} \{1-\exp[-(\alpha_{AB}+\alpha_{BA})t]\}\right] \tag{96}$$

and

$$N_B(t) = C \frac{\alpha_{BA}}{\alpha_{AB} + \alpha_{BA}} \{1-\exp[-(\alpha_{AB}+\alpha_{BA})t]\}. \tag{97}$$

One of the most useful properties of Equations (96) and (97) is their ratio for $t >> 1/(\alpha_{AB}+\alpha_{BA})$. For this assumption we find the following:

$$\frac{N_B}{N_A} = \frac{\alpha_{BA}}{\alpha_{AB}} = K_E \tag{98}$$

where K_E is the equilibrium constant which was defined in Chapter I. If it is noted that $N_B = C - N_A$ and Equation (98) is used, Equation (94) can be written as

$$\frac{dN_A}{dt} = -\alpha_{BA} N_A \left[1 + \frac{1}{K_E}\right] + \frac{\alpha_{BA}\, C}{K_E} . \tag{99}$$

Integration of (99) between times t_1 and t_2 and rearranging terms yields

$$\alpha_{BA}(t_2-t_1) = - \frac{K_E}{K_E + 1} \ln \left(\frac{[K_E+1]N_A(t_1) - C}{[K_E+1]N_A(t_2) - C} \right). \qquad (100)$$

Equation (100) suggests that the forward-backward reaction rates can be determined if the ratio of N_B/N_A is observed at a large value of time and if the decay of total current of A is observed as a function of time. From the decay of A the value for α_{BA} is obtained from Equation (100). Knowing α_{BA}, a value of α_{AB} can be obtained from Equation (98). Experimentally, there is one large deficiency in this reasoning. When the ratio of N_B/N_A is measured, the data usually will have to be corrected for an unknown mass discrimination factor in the ion sampling process. If this correction cannot be accurately made, large errors can be associated with reaction rates determined by the indiscriminate use of Equations (98) and (100).

Techniques were sought which would be independent of mass discrimination. Let us define

$$K_{EM} = \frac{N_{BM}}{N_{AM}} = \psi \frac{N_B}{N_A} = \psi K_E \qquad (101)$$

where K_{EM} is the experimentally measured ratio, N_{BM} and N_{AM} are the experimentally measured ion currents, and ψ is the mass discrimination factor. If α_{AB} and α_{BA} have different N (number density) dependency (α_{BA} is 3-body; α_{AB} is 2-body), then by taking data in some appropriate

pressure region the condition that $\alpha_{AB} >> \alpha_{BA}$ could be satisfied. Using this assumption and considering the effects of mass discrimination, the ratio of Equations (96) and (97) yields

$$\frac{N_{BM}}{N_{AM}} = \psi \frac{\alpha_{BA}}{\alpha_{AB}} [1-\exp(-\alpha_{AB}t)]. \tag{102}$$

From Equation (101), it is known that

$$\frac{K_{EM}}{\psi} = \frac{\alpha_{BA}}{\alpha_{AB}} . \tag{103}$$

Substitution of (103) into (102) removes the effect of mass discrimination and yields, after rearranging terms

$$-\alpha_{AB}t = \ln\left[1 - \frac{1}{K_{EM}} \frac{N_{BM}}{N_{AM}}\right] . \tag{104}$$

Therefore, the backward reaction frequency can be determined from observing the rate of rise of the ratio N_{BM}/N_{AM} as a function of time and by observing K_{EM}. This value of α_{AB} is independent of mass discrimination. An estimate of α_{BA} which depends on mass discrimination can be obtained from K_{EM}. However, the consistency of the estimate can be checked by observing the depletion of species A as a function of time.

There is an experimental situation which will allow determination of α_{BA} independent of mass discrimination. If data can be obtained

where the statement $\alpha_{BA}N_A \gg \alpha_{AB}N_B$ is valid, then it is trivially true that

$$\frac{N_A}{C} = \exp[-\alpha_{BA}t]. \tag{105}$$

Thus, the forward reaction frequency can be obtained by observing the decrease in the ion current of species A. Note, that the assumption can be written as $N_A/N_B \gg \alpha_{AB}/\alpha_{BA}$. At equilibrium $N_A/N_B = \alpha_{AB}/\alpha_{BA}$. Therefore, the observations must be made long before equilibrium occurs.

Several techniques have been developed in this section for determination of the rates of a forward-backward reaction scheme based on the total ion current. However, as mentioned previously, the ion current is sampled on axis in the present experiment and the total current is not measured. The sampled current will be affected by the difference in drift velocity and diffusion coefficients of the two species. The sampled ion current is directly proportional to the integral of Equations (70) and (73) with respect to time. Therefore, the ratio of the integral of Equation (73) to the integral of Equation (70) is the analytic ratio of the sampled ion currents. A comparison of such a ratio with a ratio determined from Equations (96) and (97) would give a measure of the deviation caused by the difference in diffusion coefficients and drift velocities. The ratios from Equations (70) and (73) are referred to as being derived from complex analysis and the ratios from (96) and (97), from simplified analysis. Another difference in the two ratios is that the complex ratio is sampled at fixed z whereas the

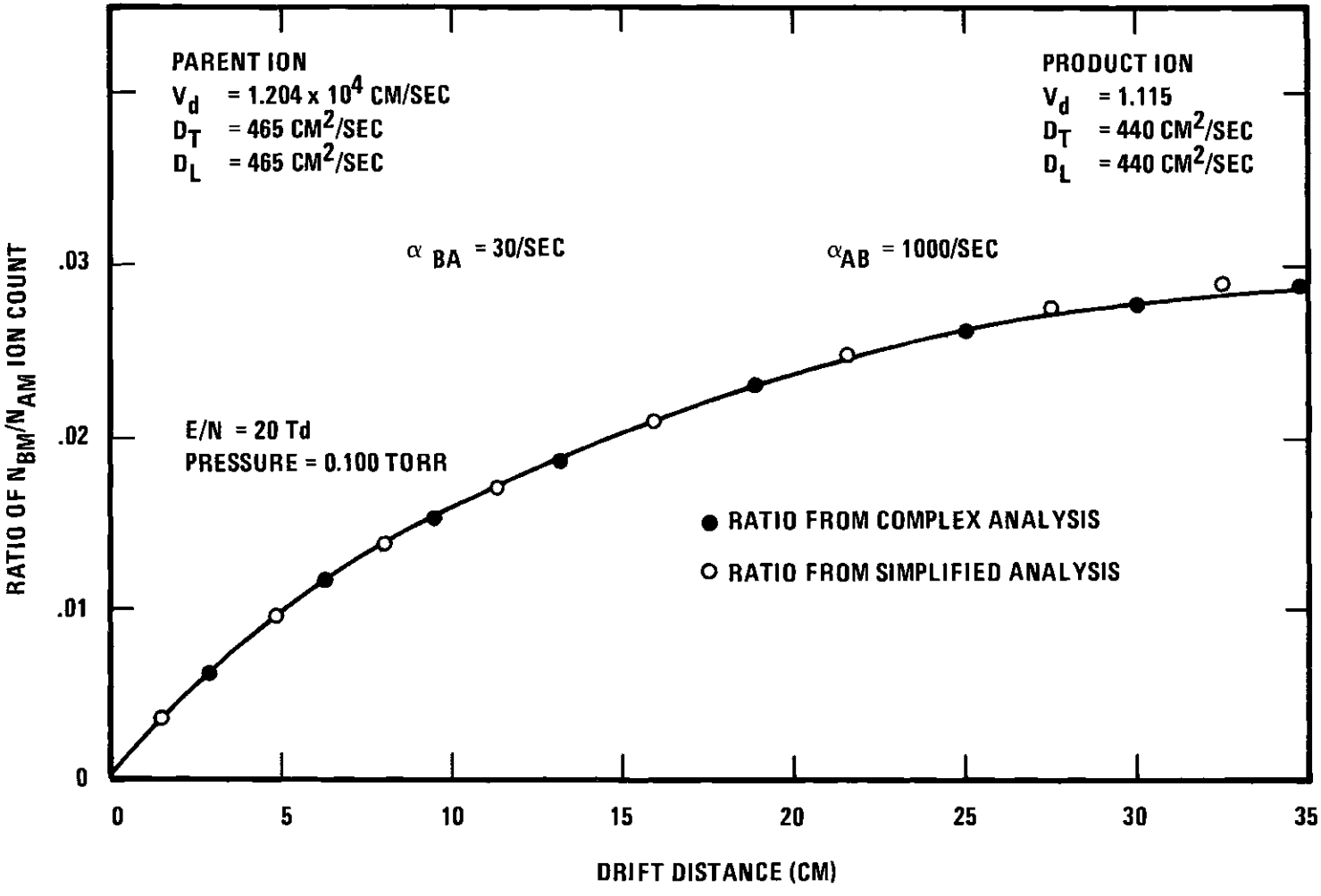

Figure 12. Comparison of the Analytic Ratios of the Product Ion Current to the Parent Ion Current

simplified analysis is sampled at fixed t. The simplified ratios in the figure were generated with $t = z/v_{dA}$. The agreement between the two sets of ratios is seen to be quite good. This agreement results from the drift velocities being so similar. These are drift velocities typical for O_2^+ and O_4^+. Therefore, it seems that Equations (103), (104), and (105) could be used in the investigation of Reaction (18).

CHAPTER IV

MOBILITIES

Production of Oxygen Ions

The electron impact ion source has already been described in Chapter II. In this section the ions produced in the source will be considered. The ions produced directly by electron impact are true primary ions. In addition, under some conditions of the experiment, ions formed by secondary processes are produced almost solely in the ion source. These ions will be designated source-produced to distinguish them from the primary ions. However, for the considerations of this research there is no significant difference between source-produced and true primary ions.

Until a few years ago, little importance was attached to the mode of formation of the ions. It was considered sufficient merely to mass analyze the ions of beam and swarm experiments to describe the collision properties of the ions. The inadequacy of this procedure has been demonstrated in a number of beam and swarm experiments wherein the collisional properties of ions of a given chemical type are observed to depend upon the nature and mode of operation of the ion source. In the case of an electron bombardment ion source, many beam and swarm experiments[63,64] have indicated that the rates of the reactions being investigated are extremely sensitive to the energy of the ionizing electrons. Therefore, the full description of a collision requires not only that

the identity of the participants be known, but also their state of excitation be determined. Unfortunately, the present experiment cannot determine the ionic excitation state, and the possibility of various degrees of excitation of the ions will have to be considered.

O_2^+

The initial formation of O_2^+ is by simple ionization:

$$O_2 + e \rightarrow O_2^+ + 2e. \tag{106}$$

This process has a threshold at about 12.2 eV.[65] O_2^+ is also formed in a charge transfer reaction involving O^+ [see Equation (22)]. This reaction occurs so rapidly that, in the present experiment, O_2^+ formed in this manner can be considered source-produced for the mobility measurements of O_2^+. O_2^+ is also formed by dissociation of O_4^+, but O_2^+ ions produced in this manner are not primary ions, nor can they ever be considered source-produced under the conditions of this research.

Turner et al.[66] learned in a novel experiment that electron bombardment at energies (25 to 100 eV) typically used in the present ion source produced 22 to 33 per cent of the ions in the first electronically excited state of O_2^+ (the metastable $a^4\pi_u$ state). The possibility of excited states necessitates examining the O_2^+ measurements of the present experiment as a function of electron energy.

O_4^+

The formation of O_4^+ ions in pure oxygen gas has been studied by Curran[67] at pressures up to 0.4 Torr in a differentially pumped high

pressure mass spectrometer ion source using controlled electron-energy beam techniques. The O_4^+ ion appearance potential at 16.9 eV and its cubic pressure dependence were consistent with the three-body process

$$O_2^+(A^2\pi_u) + 2O_2 \rightarrow O_4^+ + O_2. \qquad (107)$$

(The $A^2\pi_u$ state is the second electronically excited state of O_2^+.) Upper vibrational levels of the first electronically excited state of O_2^+ could also be involved.

In a flowing afterglow experiment performed by Bohme et al.,[68] O_2^+ ions were generated by reacting He^+ ions with oxygen gas. Electronically excited O_2^+ ions decayed by radiation or collisional quenching before the point of neutral-gas addition further downstream. Therefore, the O_4^+ observed in the afterglow apparatus arose from the ground state O_2^+.

The ion source of the present experiment can be used to obtain crude appearance potential data. Application of a 3 volt bias (relative to the filament) to the control grid prevents the creation of ions. The data were taken with a 2 volt bias on the control grid to give improved resolution of the electron energy. However, because electrons of low kinetic energy are produced in collisions of fast electrons with gas molecules, the resolution is not very good. The applied accelerating voltage does represent the maximum energy an electron can have, and because we are interested in the appearance potential of an ion, the present technique should produce useful data.

Figure 13 is a plot of ion currents of O_2^+, O_4^+, and O^+ versus the maximum energy that an electron can receive from the applied accelerating voltage. The maximum electron energy scale is shifted so that the appearance potential of O_2^+ lies at 12.2 eV. This requirement necessitated the addition of 1.7 volts to the absolute voltage reading. These results indicate that O_4^+ can be formed from the O_2^+ ground state.

If the experiment had used a technique which provided good electron energy resolution, one might expect that as the electron energy becomes sufficient to excite higher levels of O_2^+, one could detect an increase in the ratio of O_4^+ to O_2^+ ion current. The ratio of O_4^+ to O_2^+ ion current was constant from threshold to the last measurement at 19.8 eV in the present experiment. However, because the energy spread of the ionizing electrons is large, the present experiment may not be able to detect a break in the ratio.

The data of the present experiment demonstrate that some of the O_4^+ ions are being produced along the entire length of the drift tube. If all the O_4^+ ions were being created by the process Curran observed, the O_4^+ ions would all be source-produced because the O_2^+ ions involved in this reaction have to be in the second or higher electronic states which have radiative lifetimes of less than 10^{-6} seconds.[69] In the present experiment, the possibility of the presence of O_4^+ produced by the process Curran observed could not be denied but neither could it be verified.

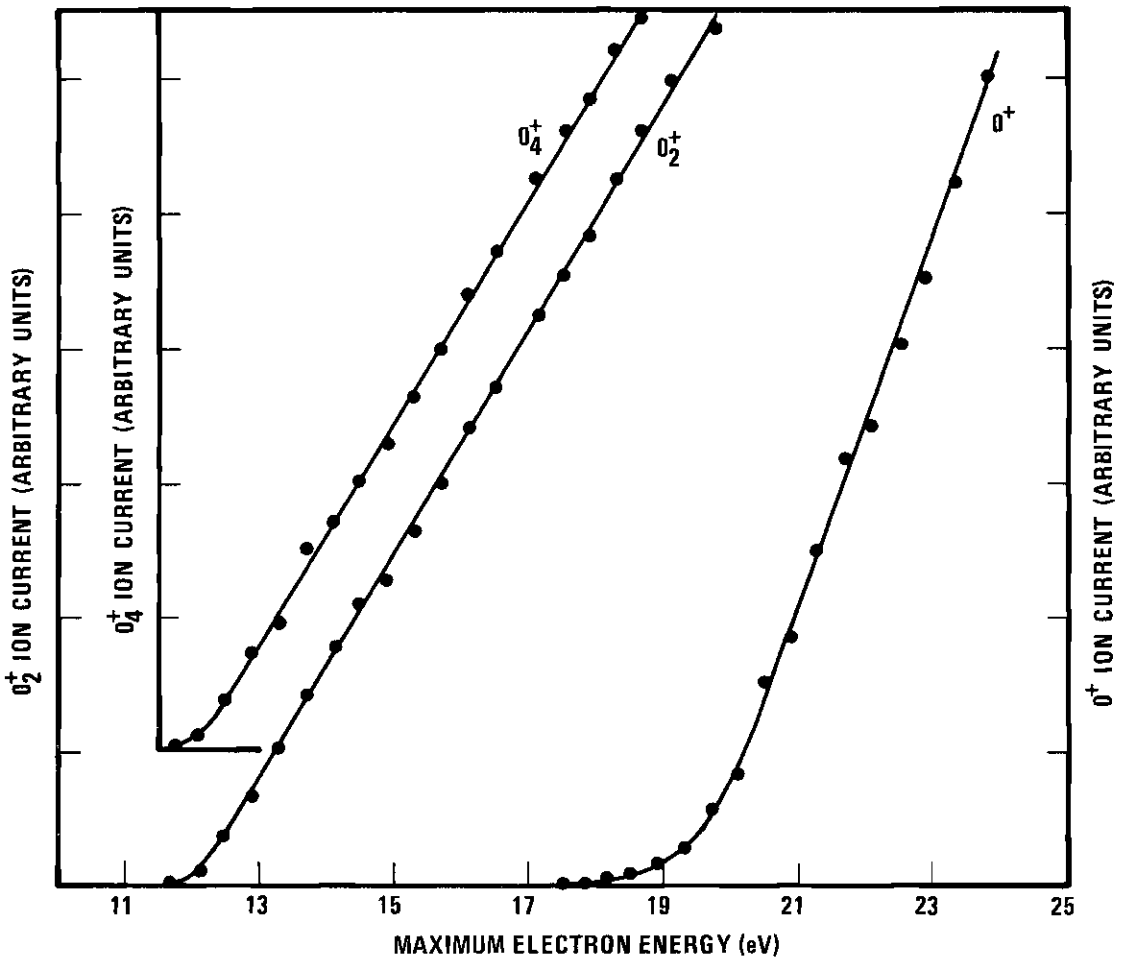

Figure 13. Electron Energy Dependence of O_2^+, O_4^+ and O^+ Ion Current

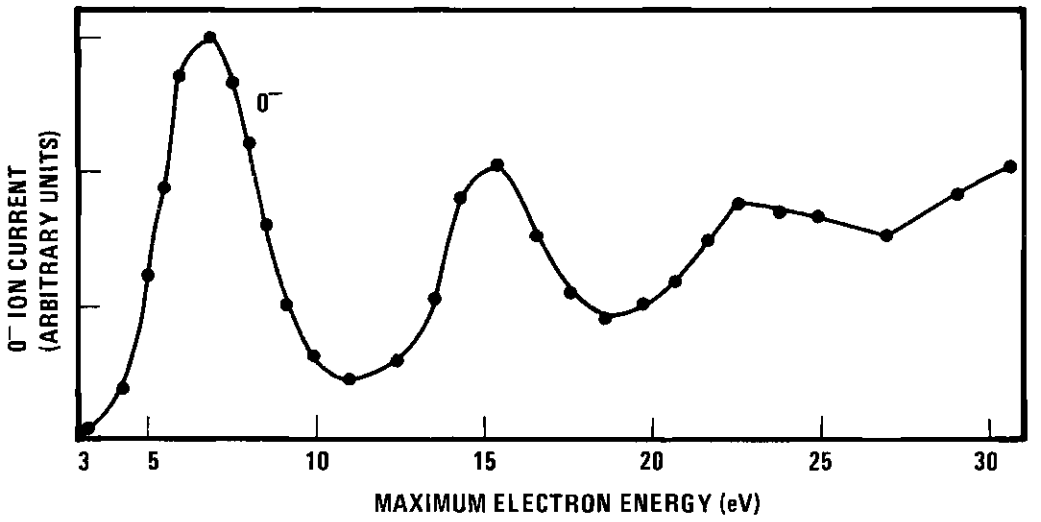

Figure 14. Electron Energy Dependence of O^- Ion Current

O^+

O^+ is formed by two processes in the present experiment. O^+ is produced by dissociative ionization

$$e + O_2 \rightarrow O^+ + O + 2e \qquad (108)$$

and by the ion pair formation process

$$e + O_2 \rightarrow O^- + O^+ + e. \qquad (109)$$

Process (109) has a threshold at 17.3 eV[70] and Process (108) has a threshold at 18.9 eV.[70]

An experiment similar to the one mentioned in the discussion of O_4^+ was performed for O^+. These data are plotted in Figure 13. The appearance potentials obtained from the graph are in fair agreement with the previously mentioned values. These agreements verify the correctness of the energy shift used in plotting these results.

O^-

O^- is formed by a two-body dissociative attachment process[71]

$$e + O_2 \rightarrow O^- + O \qquad (110)$$

and by the ion-pair formation process[70]

$$e + O_2 \rightarrow O^- + O^+ + e. \qquad (111)$$

Figure 14 is a plot of O^- ion appearance potential data which were obtained in a manner similar to the O_2^+ appearance potential data. The maximum electron energy scale has been shifted so that the maximum of the first peak occurs at 6.7 eV, where according to the experimental data of Schulz[72] a maximum occurs for Reaction (110). The presence of the additional peaks above 10 eV can probably be explained by the presence of free electrons of low kinetic energy which are produced in collisions of fast electrons with gas molecules or walls of the source. The O^- ion currents produced by accelerating voltages above 30 eV are not shown here. The ion current rises in a straight line between 30 and 80 eV to a value which is three times its value at 30 eV. This phenomena might be explained in the following manner. Ionization of O_2 is possible at these values of electron energy and increases the flux of low energy electrons. Process (111) occurs above 17 eV and makes certain contributions to the ion current. Varney[32] has hypothesized that this phenomenon may be caused by the electrons exciting O_2 by collision, and that these excited molecules may have had a higher attachment probability.

Excited states for negative ions are rare because the forces binding the extra electron are short range, so that excitation would result in the nuclear Coulomb force being so strongly screened that the extra electron would no longer be stably bound. A few negative ion excited states have been found, but none is known for O^-.

O_2^-

The most likely mechanism for the formation of O_2^- is by three-body attachment

$$e + 2O_2 \rightarrow O_2^- + O_2. \qquad (112)$$

This process would occur entirely in the ion source, and all the resulting ions can be considered source-produced. O_2^- can also be formed by charge exchange of O^- with O_2 at E/N greater than 60 Td. O_2^- ions formed by this process will not usually be considered source-produced in the present experiment. O_2^- is also produced in the dissociation of O_4^-. Such O_2^- ions are never considered source-produced ions in this experiment.

O_3^-

O_3^- is created through the association of O^- and O_2 [see Reaction (16)]. This reaction will in general lead to creation of O_3^- as the swarm drifts.

O_4^-

O_4^- is produced by the association of O_2^- and O_2 in a three-body process. Because O_4^- rapidly dissociates to form O_2^-, an equilibrium situation occurs which makes it impossible ever to consider O_4^- as a source-produced ion.

CO_3^- and CO_4^-

These are impurity ions which appear in the present experiment as the result of Reactions (23) and (25). All mass-analyzed

experiments[29,40,34] performed at pressures high enough to produce appreciable O_3^- and O_4^- detect these impurities. Because the Reactions (24) and (26) which involve O^- and O_2^- are three-body, their contribution to the impurity intensity would be negligible.

Several sources have been postulated for the CO_2. The oil vapors from the diffusion pumps have been considered as a likely source of CO_2. The necessity of sampling the ions through a pin hole and of differentially pumping the analysis region might allow some oil vapors into the drift region. However, the oil vapors probably are not a major source of CO_2 because McKnight,[34] who uses mercury diffusion pumps, also detects these impurities. The possibility that the CO_2 is admitted with the O_2 is disallowed because the intensity of the impurities is a function of the time that the gas has been left in the drift region. McKnight has been able to reduce these impurities to a negligible amount by connecting a trapped forepump directly to his drift region, so that a high gas throughput could be obtained. On the basis of this observation and similar experiences in the present investigation, it is hypothesized that the CO_2 is coming from the stainless steel walls of the vacuum system. The impurity ions are not usually considered source-produced ions in this research.

Method of Data Analysis

Drift velocities were obtained from the experimental arrival time spectra by using the mean arrival time $\bar{t}$ of the spectra and the known drift distance z, as discussed by Moseley.[73] In order to

eliminate end effects and the diffusion error, a differencing technique was used, so that the drift velocity could be calculated by the equation

$$v_d = \frac{z_i - z_j}{\bar{t}_i - \bar{t}_j} . \qquad (113)$$

When more than two drift distances were used, a straight line of best fit (in the least squares sense) was constructed through the $(z_i, \bar{t}_i)$ points and the slope of this line used to determine v_d. The mobility K was then calculated using

$$K = v_d/E. \qquad (114)$$

This mobility was reduced to standard conditions of temperature and pressure using Equation (7), and the data are presented as the reduced mobility versus E/N. From these data a zero-field reduced mobility is determined.

This procedure has been justified analytically by Moseley[73] under the assumptions of (1) a delta-function input pulse of ions, and (2) no reactions occurring in the drift region which lead to the creation of the ion species under consideration. The first of these assumptions is closely approximated in this experiment; the second assumption can be fulfilled to a good approximation for most of the ions which are secondary ions (in particular O_3^-, CO_3^-, CO_4^-) by making measurements at high enough pressures to insure that the reactions which create these ions go to completion before the swarm has drifted the shortest

distance used. For the primary ions O^-, O_2^-, and O_2^+ slight problems are encountered, but true drift velocities can be obtained. In order to keep the correction for the depleting reactions small, data are obtained at low pressures for the primary ions. O_2^- and O_2^+ also pose a difficult problem because they can be formed by the dissociation of O_4^- and O_4^+, respectively. However, if mobility measurements of O_2^- and O_2^+ are made at low pressures, errors due to dissociation should be extremely small because little O_4^- and O_4^+ will be formed.

Obtaining satisfactory O_2^- data at high E/N is made difficult because of the reaction of O^- with O_2 to form O_2^- [see Equation (17)]. This reaction results in a leading foot appearing on the O_2^- time spectra. However, deletion of the leading foot prior to calculation of $\bar{t}$ makes any error in the mobility of O_2^- small.

It is impossible to adjust experimental parameters so that condition 2 is satisfied for O_4^+ and O_4^- ions detected in this experiment. O_4^+ and O_2^+ are in chemical equilibrium; thus any detected O_4^+ ion will have spent part of its drift as O_2^+. Similar remarks can be made for O_4^- and O_2^-. However, the O_4^+ and O_4^- time spectra will be analyzed as if they did satisfy condition 2. This procedure leads to an error that is later assessed. The analysis of O_4^- mobility data is further complicated by its reaction with CO_2.

Experimental Procedures

Preparation of the System

In order to achieve the low base pressure desired and thus minimize impurities in the drift region, the system is baked at an average

temperature of about 250°C for 18 to 24 hours. Cooling requires several days because many of the rather massive internal components must cool mainly by radiation. The base pressure at the end of such a bake cycle is about 2×10^{-9} Torr as read by Bayard-Alpert ionization gauges located at the top of the drift tube, at the bottom of the outer vacuum chamber and in the analysis region. The pressure in the drift tube with the isolation valve (see Figure 1) closed does not rise above 7×10^{-8} Torr.

With the isolation valve closed, the drift tube is pressurized with the sample gas by manually opening the servo-operated valve until the desired pressure is reached. Control of the servo-valve is then transferred to the capacitance manometer-automatic pressure controller system, which maintains the desired pressure. The heating current to the electron filament, which is left on continuously at a low value, is turned up and the temperature of the filament is allowed to stabilize. (Leaving the current on decreases the time necessary for stabilization.) The desired electric field is established by applying a corresponding potential to the resistor string which supplies the drift field electrodes.

Ion Source Parameters

The ion source may be operated in several different modes. If the front plate electrical shutter is left open and the electron beam is allowed to cross the ionization gap continuously, a dc mode of operation is obtained. Another mode is to operate the electron beam dc but pulse the shutter. This mode is not used in practice because the shutter,

while quite efficient, does let through a small fraction of the ions impinging on it when it is closed. Thus, a small constant background of ions is observed in this mode. A third mode of operation is to pulse the electron beam and, at some later time, pulse the front plate shutter. Operation in this manner allows best control over the ion swarm entering the drift tube. In addition, this mode of operation permits the technique of holding the swarm in the source for a time to allow a reaction to go essentially to completion before gating the swarm into the drift tube. Still another mode of operation is to pulse the electron beam but leave the shutter open at all times. Since, for a given number of ions created in the source, fewer ions will enter the drift region when the shutter is pulsed than when it is simply left open, it is occasionally desirable to operate in this manner, particularly at very low E/N.

The typical mode of operation is that of pulsing both the electron beam and the front plate shutter. The electron pulse width is typically 4.0 microseconds. The front plate shutter pulse width is 2.0 microseconds. The timing of the front plate shutter is adjusted so that, for a given pulse width, a maximum number of ions of the species under consideration exits the source. This time will correspond to the 0.5 cm distance from the center of the electron beam to the front plate divided by the drift velocity of the ion. The timing of the front plate pulse can be adjusted within reasonably wide limits (± 50 per cent) about this optimum time while still allowing a useable number of ions to exit the source. The timing of the shutter can also be adjusted

to discriminate against one ion species in favor of another, if their drift velocities are different.

The three grids in the alkali-source are shown in Figure 5. The first grid draws the ions away from the filament, and normally is adjusted to be 20 to 45 volts negative with respect to the filament. The second grid is positive with respect to the first and is adjusted so as to barely keep the alkali ions from passing it, that is, to "bias off" the ion current, so that the application to it of a negative pulse of about one microsecond in duration allows a short burst of alkali ions to pass through the third grid which is at the potential of the repeller and to enter the main part of the ion source. There they thermalize and are gated into the drift region by the front plate shutter.

Analysis Region Parameters

Since it has been ascertained in Chapter II that application of a small attractive potential to the skimmer does not result in any dissociation in the differential pumping region for any of the ions under consideration here, a potential of 30 to 40 volts was usually applied. This procedure increased the ion intensity at the detector by about a factor of 10. The potential of the focussing grid between the skimmer and quadrupole was adjusted for maximum detected intensity. Typically it was set at about +30 volts. The ions were then decelerated to about 3 eV before entering the quadrupole, in order to obtain good resolution in the spectrometer.

The quadrupole mass spectrometer was set on the e/m value corresponding to the ion species desired and usually remained on this

setting for several hours while other parameters were varied.

The high voltage to the electron multiplier and the input attenuator of the time analyzer were adjusted to permit counting of most of the ion signal pulses while excluding noise pulses. This was generally quite easy to do, due to the large signal pulses obtained from the electron multiplier. Usually the noise level amounted to less than three or four counts per channel during the accumulation of a spectrum with several thousand counts in its peak channel.

Data Accumulation Procedure

After the preceding adjustments had been made, data accumulation could begin. The normal operating procedure was to remain at a fixed pressure and investigate the E/N variation of v_d for a particular ion species by varying the electric field. For a particular E/N the drift distances (usually three) were chosen with regard to the considerations discussed earlier. During each of the counting periods for the three chosen ion source positions, three temperatures were measured from the chromel-alumel drift tube thermocouples. Pertinent information about the run, such as the pressure, field, drift distances, ion source parameters, time analyzer parameters, and the temperatures were recorded for later transfer to punched cards for the computer. Other observations, often qualitative, were recorded on a comment sheet. When the counting period ended, the spectrum was punched onto paper tape which could be read by the computer. The process of obtaining data from three positions to yield one mobility value at a particular E/N required from a minimum of 20 minutes up to about two hours, depending on the ion intensity at the field and pressure used.

When the desired range of E/N had been covered for the ion under consideration, the spectrometer was set on another ion if such data at this pressure were desired. After data on all desired ions were obtained at this pressure, the pressure was changed and the process repeated.

After each day of data accumulation, the punched paper tapes and the punched cards containing the run information were read into the computer and the data analyzed. The computer program which determines the mobility is similar to the one discussed in detail by Albritton.[74] The present program is written in Fortran V to run on the Univac 1108. All of the mobility and drift velocity data and the information associated with an experimental data run are stored permanently on magnetic tape and printed as computer output. Figure 15 shows a typical computer output sheet. Detailed explanation of the headings of the computer output are given by Miller[75] and Moseley.[76]

Experimental Results

The experimental mobility results will be presented in this section. These results, as well as the drift velocity values, are given in tabular form in Appendix I.

Figure 16 shows the mobility data for O_2^+ ions in oxygen. The symbols are coded according to the pressure at which the data were taken. Note that most of the O_2^+ data were taken at low pressure (0.025 to 0.209 Torr) in order to reduce the frequency for conversion of O_2^+ into O_4^+ (and hence reduce conversion of O_4^+ back to O_2^+) to a negligible value. This necessity to work in the low pressure regions determined the low E/N

DATA NUMBER	DATE	IONIC MASS	DRIFT POTENTIAL	DRIFT FIELD	PRESSURE (MICRONS)	PULSE WIDTH	EMITTED CURRENT
218	6 3 69	39	25.650	.586	418.10	4.00	.0

POSITION	CHANNEL WIDTH	NUMBER DELAYS	NUMBER OF TRIGGERS	PEAK HEIGHT	PEAK LOSS	NOISE/ CHANNEL	NOISE/ SECOND	CORRECTED DRIFT TIME(MICROSEC)
5	64.00	0	29629	510	.004	3.5	1.85	10047.626
4	64.00	0	23435	511	.005	3.0	1.99	8048.854
3	32.00	0	66456	1027	.008	4.5	2.09	6043.560

POSITION	DISTANCE	DRIFT TIME	VELOCITY	DEVIATION	MOBILITY
5 4	6.2573	1998.7719	.3131	.19	2.6871
4 3	6.2537	2005.2940	.3119	-.19	2.6768

ANALYSIS TIME (MICROSECONDS)	TEMP (DEG K)	E/P-0 (V/CM TORR)	E/N (TD)	DRIFT VELOCITY ((10)4 CM/SEC)	RED. MOBILITY ((CM)2/V-SEC)	EINSTEIN DIFF COEFF ((CM)2/SEC	NUMBER DENSITY ((10)15/(CM)3)	ND ((10)17/SEC-CM)
42.39	298.56	1.53	4.34	.312	2.682	137.2	13.52	18.560
PERCENT ERROR=	.2			.1	.3			

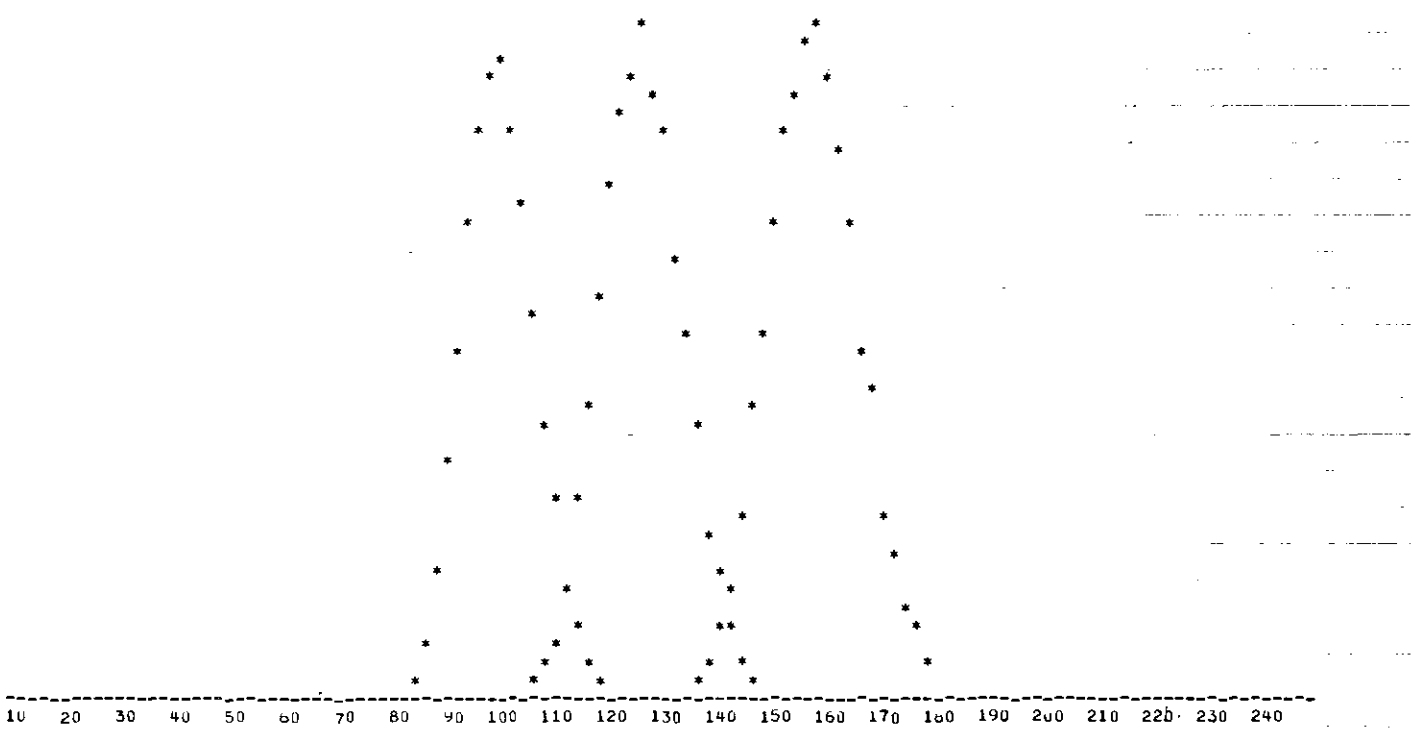

Figure 15. Typical Computer Output Giving Results of Data Analysis for K^+ in O_2

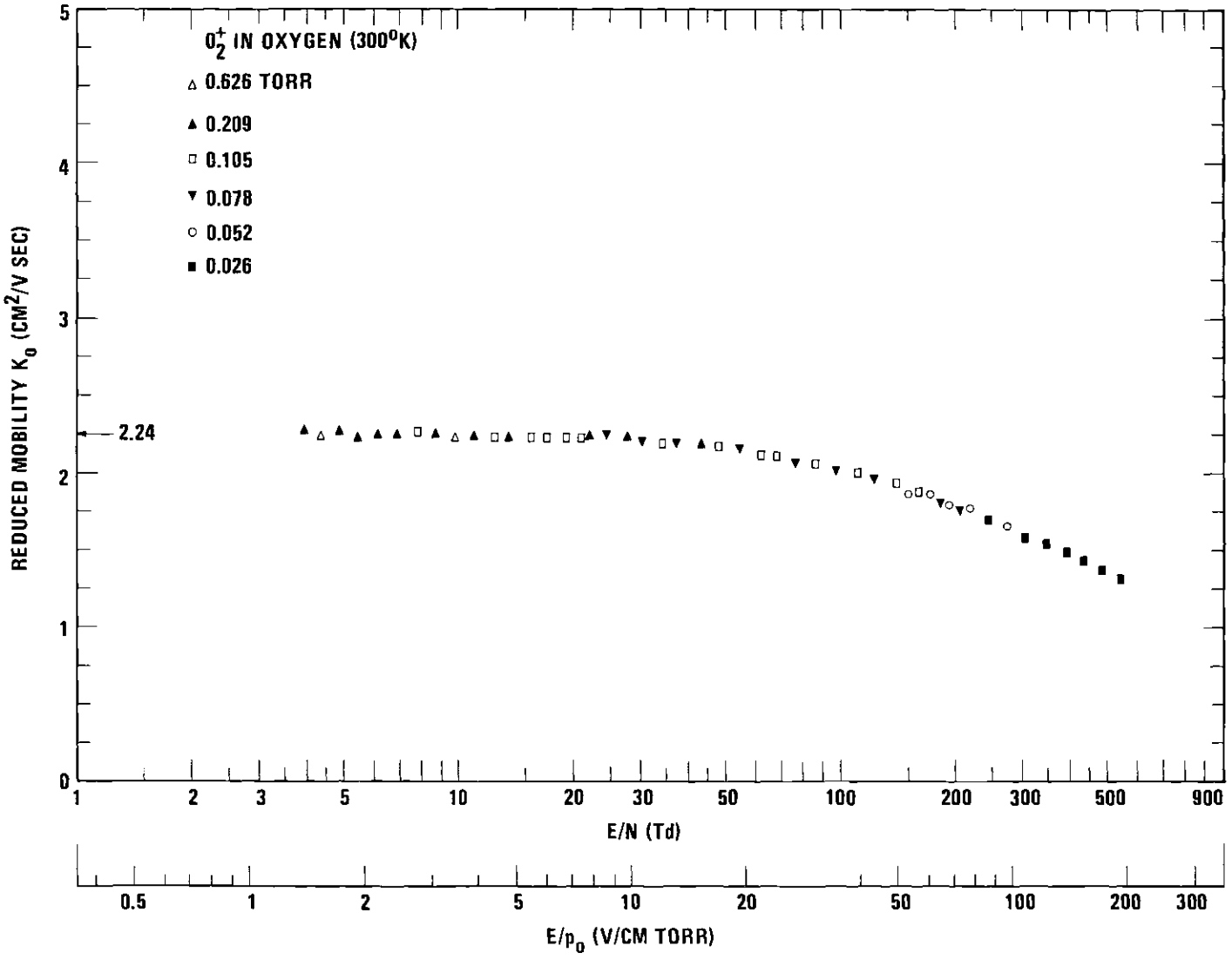

Figure 16. Mobility Results for O_2^+ in Oxygen

limit on the O_2^+ data. The zero-field reduced mobility for O_2^+ obtained from the data below an E/N of 20 Td is 2.24 cm^2/V sec. The mobility is almost constant below an E/N of 20 Td and decreases steadily toward higher E/N, reaching a value of 1.35 cm^2/V sec at an E/N of 539 Td. No pressure dependence is observed in this data.

Figure 17 shows the mobility results for O^- and O_2^-. The O^- data were taken at pressures less than 0.261 Torr in order to minimize the effects of the O^- participation in reactions forming O_3^- and O_2^-. The pressure range for the O_2^- data was dictated at low E/N by the reaction to form O_4^- and at high E/N by the appearance of O_2^- which was not source-produced. The zero-field reduced mobility obtained from the data below an E/N of 20 Td for O_2^- is 2.16 cm^2/V sec. Above an E/N of 20 Td, the mobility slowly decreases, reaching a value of 1.95 at an E/N of 140 Td. The zero-field reduced mobility for O^- is 3.20 cm^2/V sec, obtained from the data below an E/N of 16 Td. The mobility then increases rapidly to a value of 4.82 at an E/N of 109 Td and declines thereafter. No evidence of a pressure dependence is revealed by the O_2^- or the O^- data.

Figure 18 presents the mobility data for O_3^-. The data were taken at pressures greater than 1.045 Torr in order to insure that the ion detected had spent 100 per cent of its drift time after the shortest drift distance used as O_3^-. The data were taken immediately after the system was pressurized so that the effect of O_3^- reaction to form CO_3^- would be minimized. The reduced mobility appears to be constant below an E/N of 10 Td, and a zero-field reduced mobility of 2.55 cm^2/V sec is

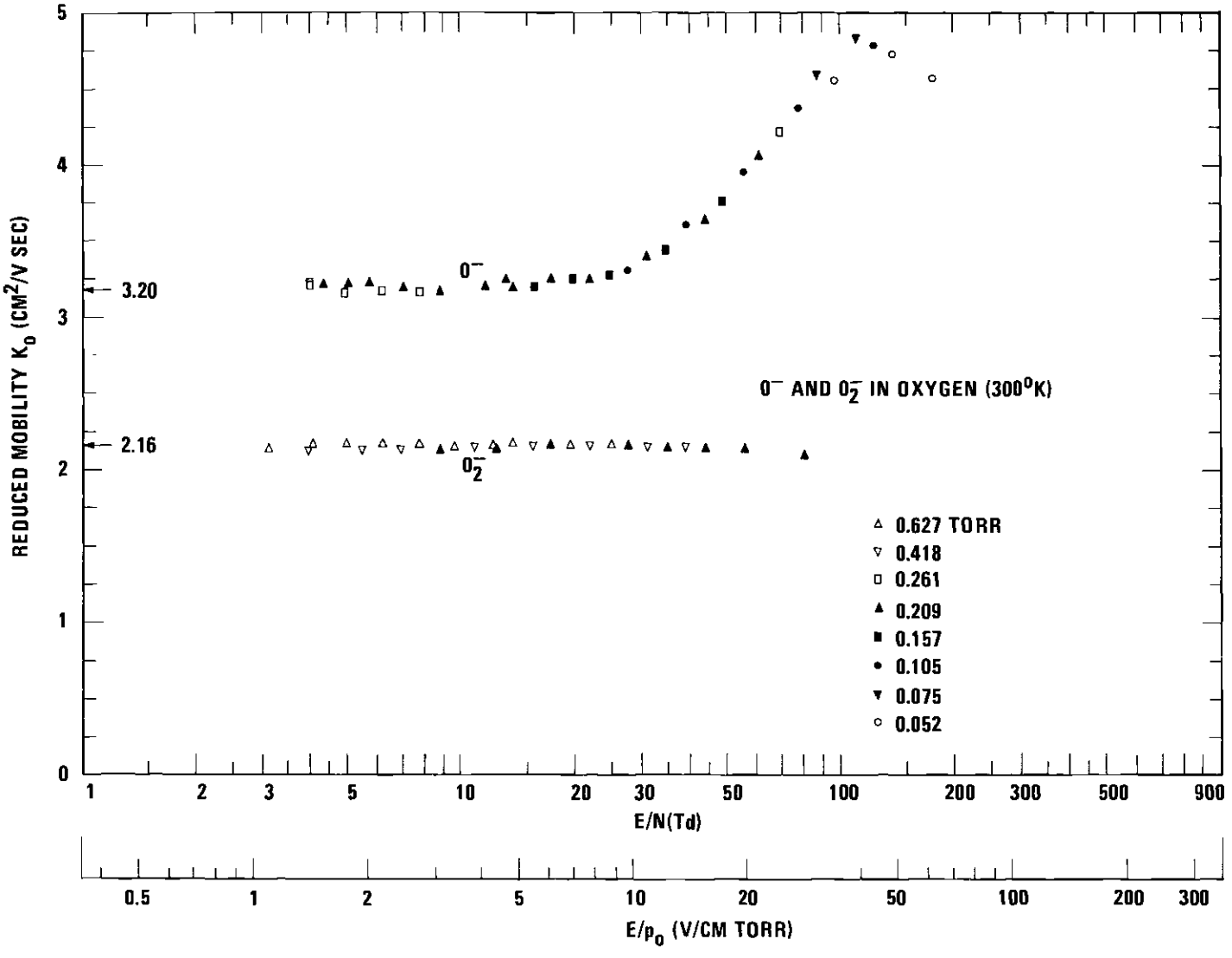

Figure 17. Mobility Results for O^- and O_2^- in Oxygen

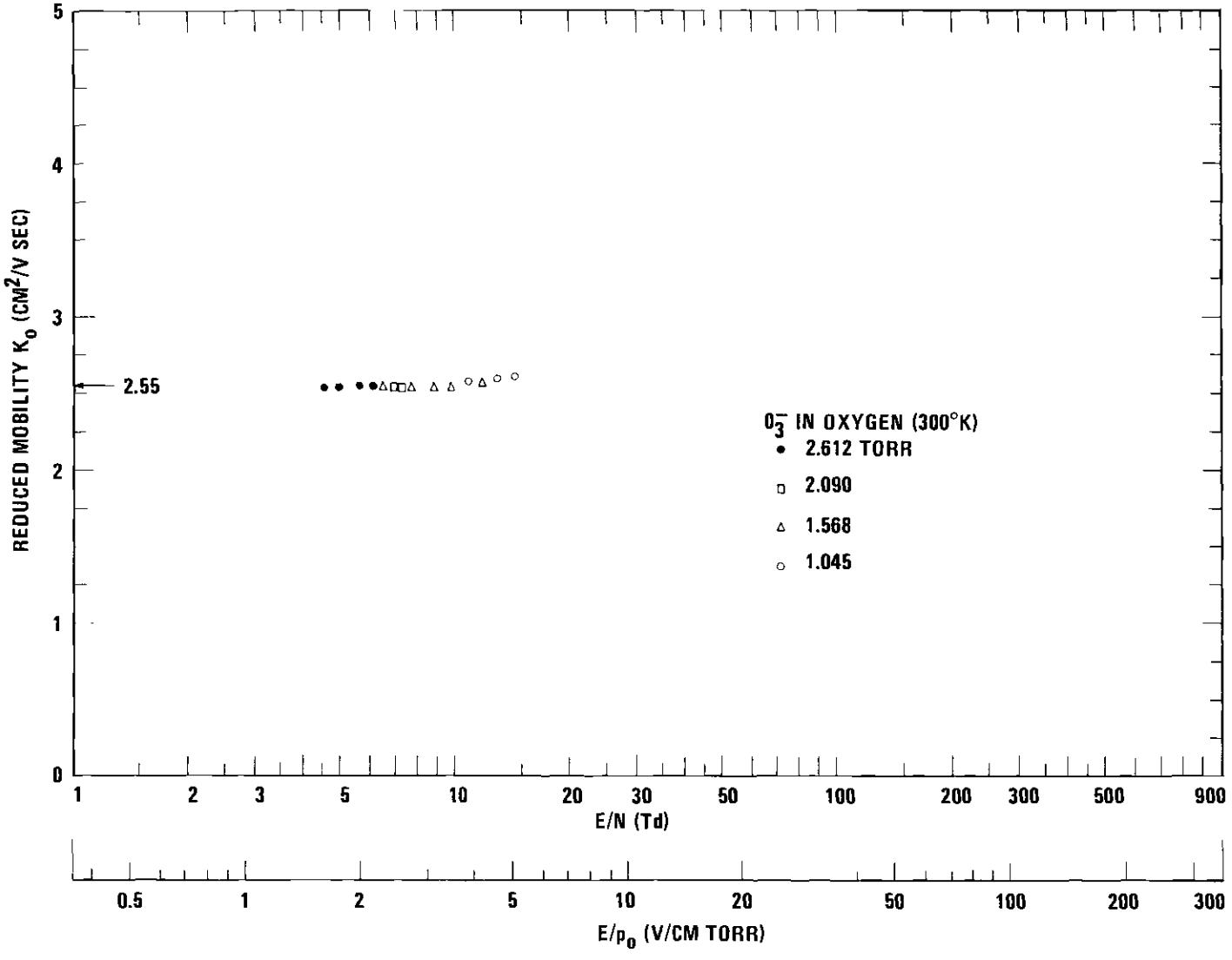

Figure 18. Mobility Results for O_3^- in Oxygen

obtained from the data. The required high pressure limited the data for O_3^- to E/N values less than 15 Td.

Appendix I contains mobility values for O_4^+ and O_4^-. O_4^+ is involved in a backward-forward reaction scheme with O_2^+, and it is impossible to get to pressures high enough to insure that the ions are spending essentially 100 per cent of their time as O_4^+ ions. At pressures where sufficient O_4^+ ions are present to perform a pulsed experiment (greater than 0.8 Torr), equilibrium results between O_2^+ and O_4^+ long before the ions travel the shortest drift distance used in mobility analysis. Therefore the ion detected as O_4^+ will have spent some of its drift time as O_2^+. In fact, the same apparent mobility value was obtained from either the O_2^+ or the O_4^+ spectrum. The percentage of its time that the ion spends as O_4^+ depends on the ratio of the reaction frequencies. The larger the forward reaction frequency is in comparison to the backward, the more time the ion spends as O_4^+. Therefore to obtain a good value for the mobility of O_4^+, the data should be taken at as high a pressure as possible. Our upper limit on pressure for O_4^+ data is imposed by the inability of the source to produce sufficient ions to perform the experiment above 6.27 Torr. Data were taken over the pressure range of 3.13 to 6.27 Torr. The ratio of the O_4^+ detected intensity to the O_2^+ intensity was about 3/2 at 3.13 Torr and 3/1 at 6 Torr. Any pressure dependence of the mobility values was less than the scatter in the data. The zero-field mobility is estimated to be 2.16 cm^2/V sec for O_4^+.

Similar reasoning holds for O_4^- except the high pressure limit is determined by the inability of the ion source magnetic field to prevent electrons from entering the drift region. This occurs above at 4.18 Torr. Again the scatter in the data masks any pressure dependence of the mobility. The zero-field mobility for O_4^- is estimated to be 2.14 cm^2/V sec.

Mobilities were also determined for CO_3^- and CO_4^- and are shown in Figure 19. The data had to be taken at pressures above 2.09 Torr in order that sufficient O_3^- and O_4^- would be produced. These data were taken several hours after the drift tube had been valved off from the pumps and filled with oxygen at the desired pressure. The data were taken at drift positions which correspond to long drift distances in order that the reactions could go to completion. Zero-field reduced mobility values of 2.50 and 2.45 cm^2/V sec were determined for CO_3^- and CO_4^-, respectively.

The potassium mobility results are shown in Figure 20. Data were obtained over the pressure range from 0.052 to 6.270 Torr. The reduced mobility is constant below an E/N of about 10 Td and a zero-field reduced mobility of 2.68 cm^2/V sec is obtained. Above an E/N of 10 Td the mobility increases slowly to a value of 2.78 at an E/N of 38 Td, then increases rapidly to a value of 3.48 at an E/N of 153 Td and declines for still greater E/N.

Error Analysis

Determination of the drift velocity from a pair of experimental spectra requires that the difference in the drift distances,

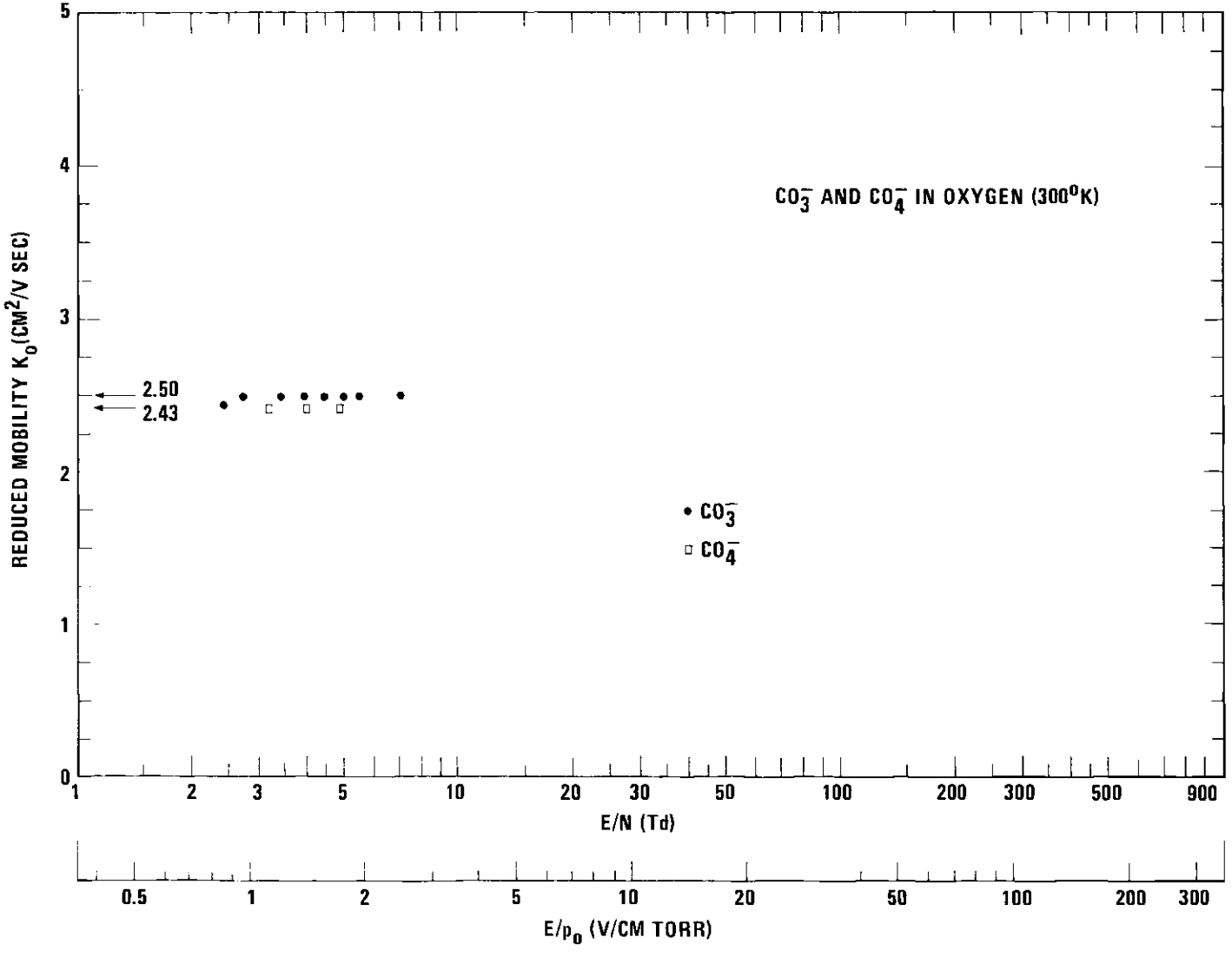

Figure 19. Mobility Results for CO_3^- and CO_4^- in Oxygen

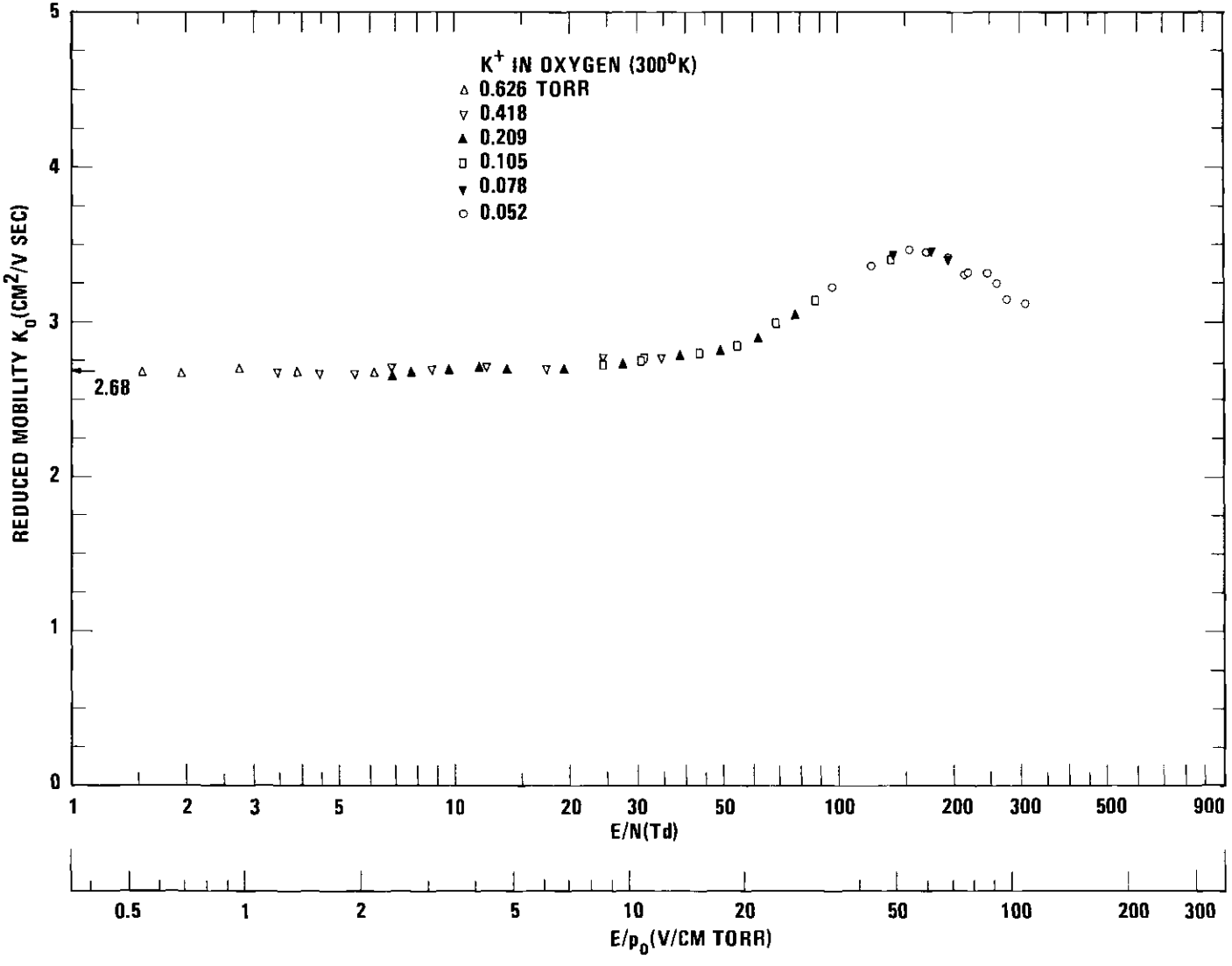

Figure 20. Mobility Results for K^+ in Oxygen

$\Delta z = z_i - z_j$ and the difference in the mean arrival times, $\Delta\bar{t} = \bar{t}_i - \bar{t}_j$ be measured. Conversion of this drift velocity into a reduced mobility requires knowledge of the electric field strength E, the pressure p, and the temperature T. The reduced mobility can be expressed in terms of these experimental quantities by

$$K_o = (\Delta z/E\Delta\bar{t})(p/760)(273.16/T). \qquad (115)$$

Each of the quantities in Equation (115) will be discussed in turn.

Distance

The absolute measurements of the drift distances are accurate to ± 0.005 cm and the ion source can be positioned at any of these distances with a reproducibility of ± 0.003 cm. Hence, for the shortest Δz normally used, 6.25 cm, the maximum systematic error is ± 0.16 per cent and the maximum random error is ± 0.10 per cent.

Electric Field

The possible error in the electric field arises mainly from the possible error in the drift potential V applied across the electrode resistor string and the drift length z_i. For a drift length of 6.25 cm, the random error is ± 0.05 per cent and the systematic error is ± 0.08 per cent. The error in the drift potential V is associated with the systematic ± 0.1 per cent possible error in the resistors of the voltage divider. Since the errors in z_i and V are independent, the two systematic errors are combined by taking the square root of the sum of their squares, resulting in a possible systematic error in E of ± 0.13 per cent. The possible random error is ± 0.05 per cent.

Temperature

The temperature for a given mobility point is obtained from the average of nine thermocouple readings, one reading of each of the three drift tube thermocouples for each of the three drift distances. This average value is believed to represent the true gas temperature to ± 0.5 per cent. In addition, ion source heating effects can cause a temperature gradient of up to about 4.0°K in the drift tube. Therefore, another ± 0.5 per cent uncertainty is added, leading to a possible error in T of ± 1.0 per cent.

Pressure

Random error in the pressure arises from the zero drift of the capacitance manometer. Over the periods of time between pumping out the drift tube and checking this zero, the drift is always less than $\pm 2 \times 10^{-4}$ Torr. At 0.1 Torr this represents a possible error of ± 0.5 per cent. For pressures below 0.1 Torr care is taken to check the zero drift more often and the same ± 0.5 per cent error limit holds. A systematic error of ± 2.0 per cent is assigned.

Time

Systematic errors in the measurement of $\bar{t}$ due to diffusion and reaction were discussed by Moseley.[77] It was concluded there that, for the diffusion error, differenced mean arrival times $\Delta\bar{t}$ should yield drift velocities differing from the true drift velocities by no more than ± 0.1 per cent. The error to the mobility values due to the presence of a reaction depends on the reaction frequency, α, if the ionic species being measured is involved only in a depletion type

reaction. For O^- an error of ± 0.2 per cent was assigned. O_2^+ and O_2^- are complicated by the dissociation of O_4^+ and O_4^-, respectively. However, data for O_2^+ and O_2^- are taken at pressures low enough that an error of ± 0.1 per cent is realistic. The high E/N data of O_2^- are further complicated by a foot that arises on the time spectra at E/N above about 60 Td. The error depends on the source position, the difference in O^- and O_2^- drift velocities, and the reaction rate. An additional error of ± 0.2 per cent is assigned to the mobility values of O_2^- above an E/N of 60 Td. The O_3^- data are affected by the reaction with the impurity. Little is known about the reaction frequency, but it is believed the error due to reaction is less than ± 0.2 per cent. The O_4^+ mobility data are greatly affected by the O_4^+ reaction scheme with O_2^+. Similarly, O_4^- mobility data are affected by O_2^-. Because O_4^+ spends about 30 to 40 per cent of its drift time as O_2^+ at pressures where O_4^+ mobility values were determined, the error will depend on the difference in their mobilities. The pressure dependence of the drift velocities should give an indication of the error. However, the observed pressure dependence is less than the random scatter in the data. The scatter is 2 per cent; therefore an error of ± 1.0 per cent is assigned due to the reaction. O_4^- is affected by the same errors as O_4^+. In addition the situation is complicated by the reaction with the impurity. A reaction error of ± 1.5 per cent is assigned to O_4^-. The data for CO_3^- and CO_4^- are not affected by reaction errors.

A measure of the random experimental error is obtained by examining the differences between the mean arrival times for each of

the three positions and the least squares fit straight line. The standard deviation of these differences is given in the data tabulation in Appendix I. For the oxygen data, the standard deviation for only a few points exceed 1 per cent. Thus, a ± 1.0 per cent random error limit seems appropriate.

Since the random errors are independent of the systematic errors, the square root of the sum of the squares of the possible random and systematic errors will yield a bound on the error of our mobility results. The per cent error in the mobility values for each ion is as follows: O_2^+, 3.9; O_4^+, 4.4; O^-, 3.7; O_2^-, 3.9; O_4^-, 4.6; CO_3^-, 3.6; CO_4^-, 3.6; K^+, 3.6.

Experimental Checks on Possible Systematic Errors

Although random error from some unknown source would manifest itself as scatter in the data, a relatively large systematic error could remain undetected. Several additional sources of possible systematic errors are discussed here.

Mutual repulsion or space charge effects could distort the ion swarm and possibly give rise to a situation where the analysis in Appendix IV is not applicable. However, the fact that the experimental spectra have a shape which can be fitted with low error by the analytic expression is an indication that the mobilities of this experiment are not influenced to a great extent by mutual repulsion. The fact that the drift velocities do not vary systematically with position is also a check on systematic error.

Variation of the potential between the drift tube exit aperture and the skimmer, over the limits discussed earlier, showed no influence on the measured drift velocities, nor was any dissociation observed.

It has been mentioned earlier that a check on possible systematic errors is possible by a comparison of the potassium mobility data with the high accuracy results of other experiments which do not employ mass analysis and which consequently can operate at high pressures. This has been possible for the ions previously investigated with this apparatus. However, for oxygen, no high precision results are yet available to check with our data. When they do become available, corrections to the present data can be easily made. The potassium data also give a check on the linearity of the pressure gauge. Low E/N data were taken over the pressure range of 0.2 to 6.3 Torr and displayed only a random error of less than 1 per cent. On this basis, a very low error would be assigned to the pressure due to non-linearities of the gauge.

Comparisons with Existing Experimental Data

In this section, the oxygen mobility data obtained in the present experiment will be compared with existing experimental data. A general discussion of these previous experiments has been given in Chapter I.

Figure 21 gives a comparison of the O_2^+ mobility data of the present research with the results of other experiments. Eiber[22] used a crude mass analysis of the ions. The other investigators had no mass analysis. The agreement with all the investigators is quite good at values of E/N greater than 70 Td. The data of Samson *et al.*[27] are

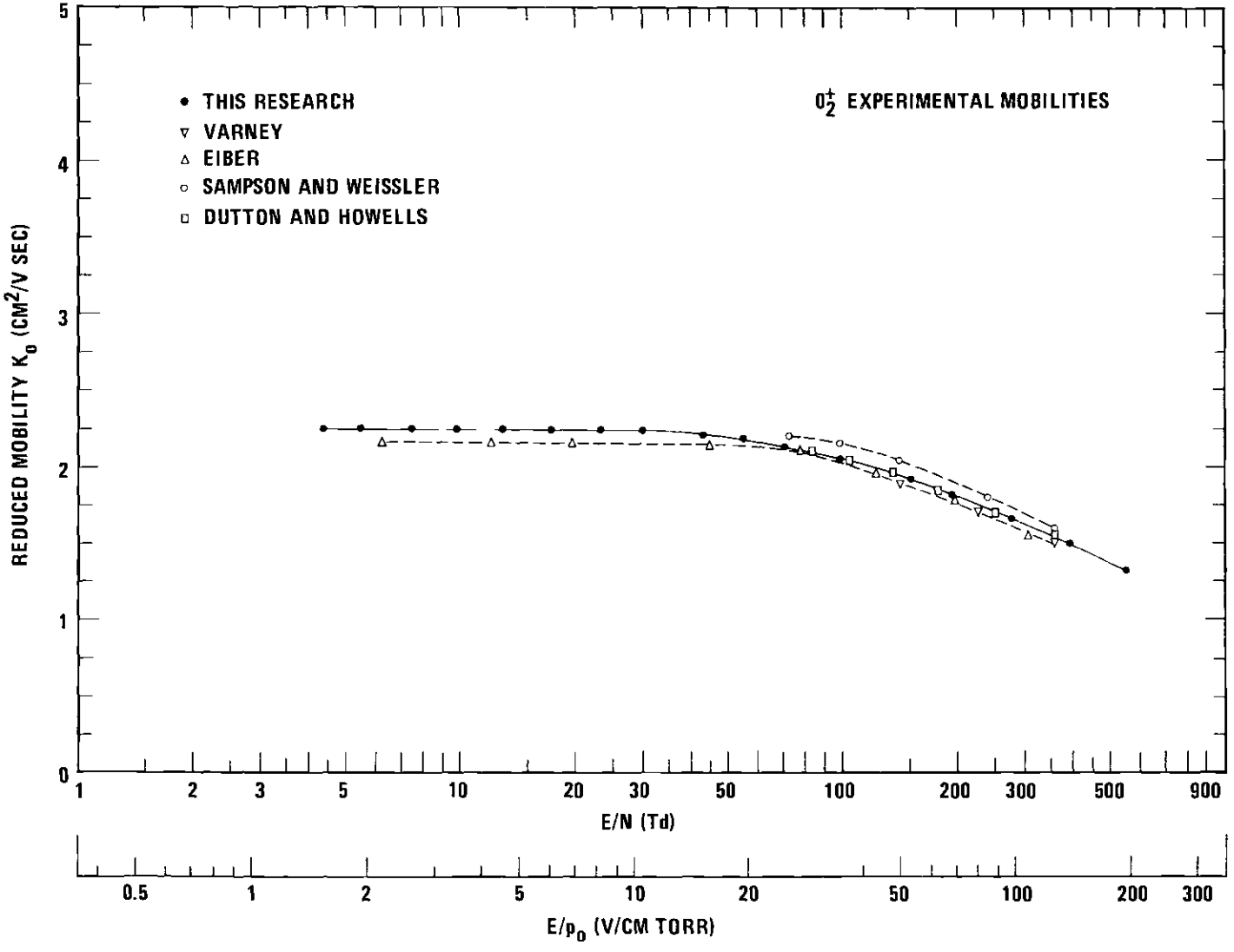

Figure 21. Comparison of O_2^+ Mobility Data with the Results of Other Experiments

slightly higher than the present data, but are well within the combined experimental errors. The present data agree well with the recent high E/N data of Fleming and Rees[31] which are not plotted here. Varney's[32] most recent unpublished results are about 8 per cent above those of the present research.

At E/N less than 30 Td the present result for O_2^+ is 5 per cent above the low E/N data of Eiber. However, Eiber's measurements were made at pressures of 10 to 340 Torr. At these pressures, a detected O_2^+ ion would have spent most of its drift time as O_4^+. Therefore, Eiber's low E/N mobility data are more appropriately assigned to O_4^+. The data of Eiber give a zero-field reduced mobility of 2.15 cm^2/V sec, which is in good agreement with the O_4^+ mobility value of the present research.

There are no mass analyzed O_4^+ mobility data available. Fleming and Rees[31] and Dutton and Howells[30] deduced the presence of a second positive ion species in oxygen from the pressure dependence of their drift velocities. Fleming and Rees found a value of 2.20 cm^2/V sec for the zero-field mobility of O_4^+ which was slightly above their O_2^+ data. Dutton and Howells obtained a value of 2.15 cm^2/V sec for O_4^+ which was also slightly higher than their O_2^+ results. The present data indicate that the O_4^+ mobility at low E/N (less than 7 Td) is less than the O_2^+ mobility. The present results may not be in conflict with the above experiments because the regions of E/N do not overlap.

Figure 22 shows comparisons between the O^- mobility data and the data of other experiments. The agreement with the present O^- data

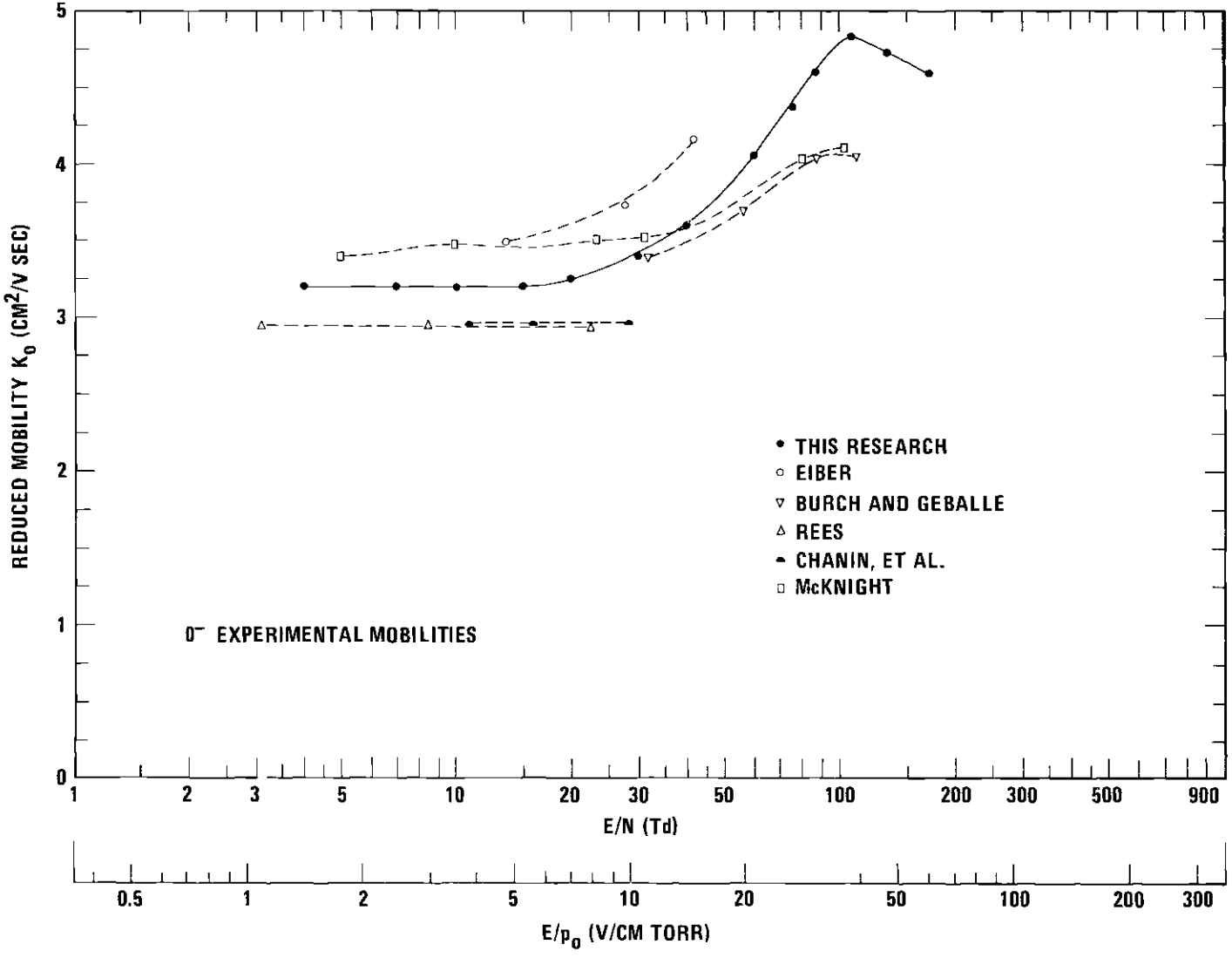

Figure 22. Comparison of O^- Mobility Data with the Results of Other Experiments

is fair. McKnight[34] obtained results which are about 7 per cent above the present low E/N results, but the scatter of his data overlaps the present data. His data are the only published values which were obtained with high resolution mass analysis. The data of Eiber are about 10 per cent above the present results. The data of Burch and Geballe[17] are in good agreement at their lowest E/N of 40 Td. However, the disagreement increases as E/N increases and is about 20 per cent at an E/N of 100 Td. The data of Chanin et al.[21] and those of Rees[24] are about 7 per cent below those of the present experiment, but at the pressures and the drift distances used in each of those investigations, all the O^- ions should have been converted to O_3^-. Their data probably refer to an impurity or to another negative oxygen ion which is affected by large experimental errors.

The results of several investigators are not shown in Figure 22, but comparisons are made with them. Varney's[32] recent unpublished O^- mass analyzed data are almost 100 per cent above those of this research. The data of Nielsen and Bradbury[9] which were labeled O_2^- are in fair agreement with the O^- data of this research and probably should be assigned to O^- rather than O_2^-. Schafer and Beaty[29] reported mass analyzed mobility data for O^- which are in fair agreement with the results of this research.

The comparison of the O_2^- mobility data of the present experiment with the results of other experiments is shown in Figure 23. Agreement is good with all investigators except Rees. The data of Rees[24] were taken at pressures high enough that the detected ions should be spending

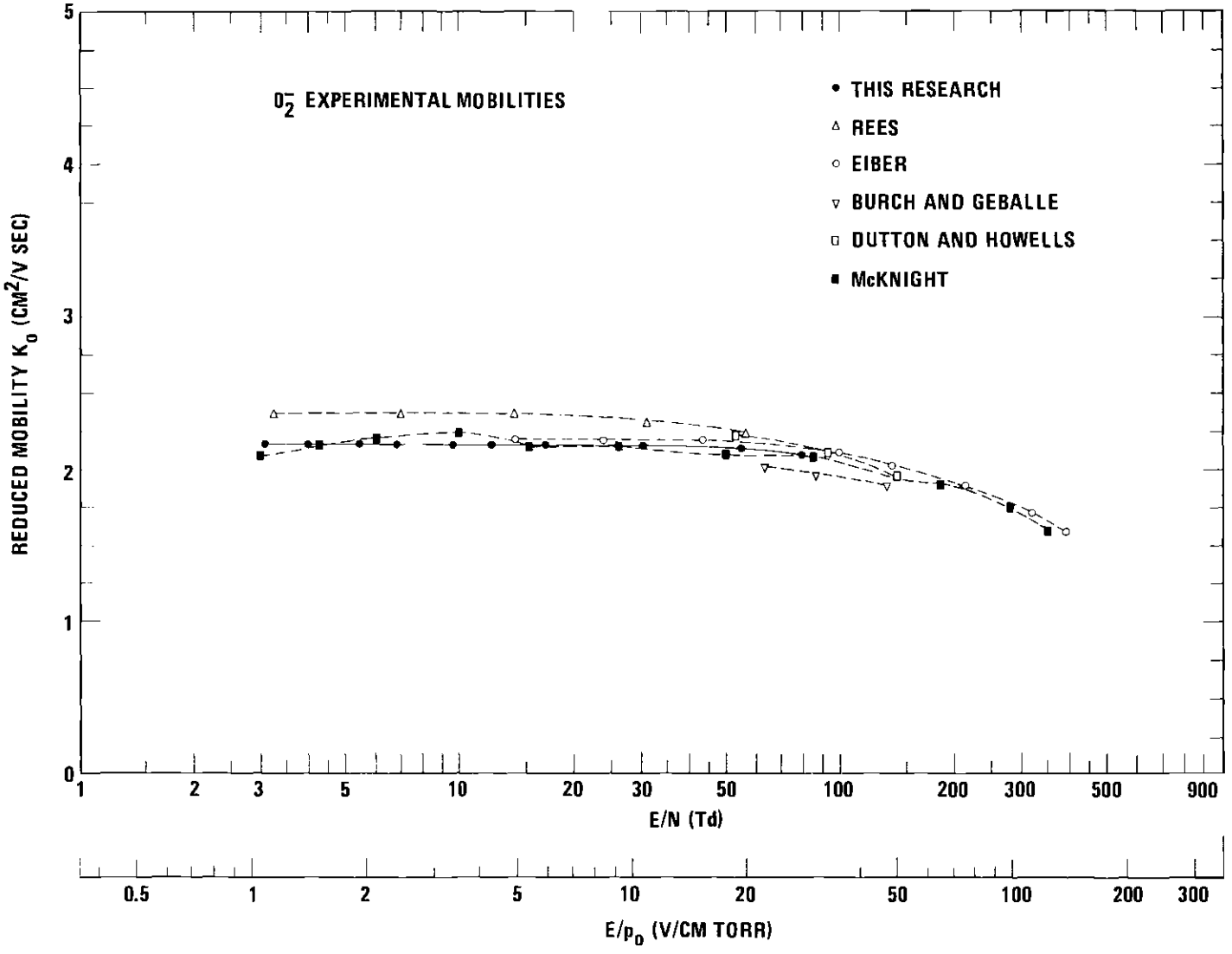

Figure 23. Comparison of O_2^- Mobility Data with the Results of Other Experiments

most of their time as O_4^-. Also his data may be affected by the presence of CO_2 which converts O_4^- to CO_4^-. The results of two mass analyzed experiments are not shown. Varney's[32] data are about 12 per cent above those of the present research. The unpublished data of Schafter and Beaty[29] are in good agreement.

Figure 24 shows a comparison of the O_3^- mobility data with those of other experiments. Unfortunately the present O_3^- data extend over only the E/N range of 4.6 to 14.7 Td. Our data are in good agreement with the low E/N data of Eiber,[22] McKnight,[34] and Rees.[24] Data of Chanin et al.[21] which were labeled O_2^- are about 8 per cent above the O_3^- data of the present experiment. Comparisons are also made with the data of several investigators not shown in Figure 24. The data of McDaniel and Crane[18] which were labeled as O_3^- are in fair agreement with the present O_3^- data. The results of Voshall et al.[25] which were labeled O_2^- are also in fair agreement. On the basis of the agreement of the present O_3^- data with the data of Doehring,[11] it can be deduced that his data could be assigned to O_3^-. The unpublished data of Schafer and Beaty[29] are in good agreement.

McKnight[34] and Schafter and Beaty[29] in mass analyzed experiments found that O_4^- had a mobility very similar to O_2^- which is in agreement with our conclusions. Rees[24] obtained data for an ion which had a zero-field mobility of 2.18. He labeled the ion an impurity, but it may have been O_4^-. Some of Eiber's[22] O_2^- mobility data were taken at pressures where the ion would have spent most of its time as O_4^-. These data are within the scatter of his data taken at lower pressures where

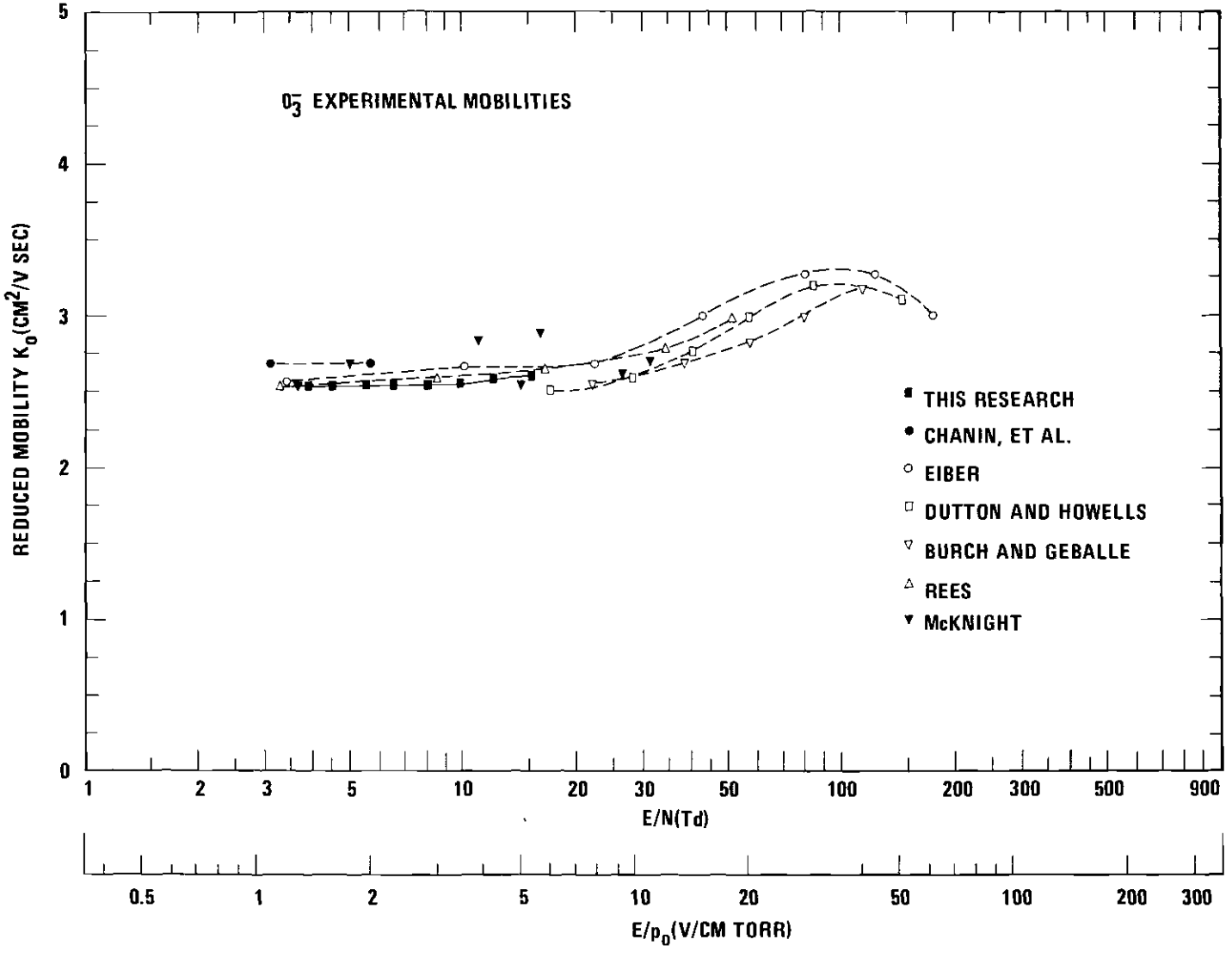

Figure 24. Comparison of O_3^- Mobility Data with the Results of Other Experiments

the ion would have spent most of its time as O_2^-. Therefore, the data of Eiber are also in agreement with the results of the present experiment.

CHAPTER V

LONGITUDINAL DIFFUSION COEFFICIENTS

Method

In Chapter I, during the discussion of Figure 4, it was stated that the shape and width of a time profile were determined by the longitudinal diffusion coefficient, D_L. For the case where there is a depletion reaction, Moseley[78] showed that the shape of the time profile of the parent species is insensitive to the values of the reaction frequency and the transverse diffusion coefficient. He showed that D_T can be varied from 0.01 D_L to 10 D_L, and that the reaction frequency, α, could be varied from zero up to 10^6 sec^{-1} without appreciably distorting the shape of the time spectra. The variation of D_T and α does have a significant effect on the overall intensity of the spectra. However, when the analytical spectra corresponding to various values of D_T and α are normalized to agree at their points of maximum intensity, the resulting profiles are virtually identical. Therefore even when only estimates of the transverse diffusion coefficient and the reaction frequency may be available, D_L can be determined from the shapes of the experimental profiles.

The technique used to determine D_L was to adjust D_L in the analytical expression for the flux, Equation (129), until the analytical profile and the experimental data best correspond when normalized to agree at their points of maximum intensity. This analysis is applied

to the same data used to determine mobilities, which were discussed in Chapter IV.

The computer program used by previous investigators in this laboratory performed a least squares fit of the flux, Φ, to an experimental spectrum by varying D_L. This procedure occasionally provided a poor fit which was caused by forcing the two curves to agree at their peak values. During the present research a better fitting technique has been incorporated into the analysis. Initially, the theoretical spectrum and the experimental data are again normalized to agree at their peak intensity values. Because the theoretical spectrum contains no analysis time error, the peak of the experimental spectrum is shifted so as to be aligned in time with the peak of the theoretical spectrum. (These same steps were also followed in the previous investigations.) However, instead of a least squares fit, a least cubes fit of the theoretical spectrum to an experimental spectrum is now performed by varying D_L. If the difference between the two spectra on one side of the peak is of opposite sign as compared to the difference on the other side of the peak, a shift in the spectra should bring about a better fit. The experimental spectrum is shifted one channel at a time until the differences are either of the same sign or a shift produces no improvement.

In fitting the expression for Φ, v_d is taken to be known from the previous mobility measurements, as described in Chapter IV, α is taken to be zero, and D_T is assigned to have its Einstein value.

Figure 25 shows the results of a least cubes fit for K^+ ions in oxygen. All parameters listed on the figure were given as input to the computer program. The agreement between the experimental spectrum and the resulting analytical spectrum can be seen to be quite good.

Experimental Procedures

The computer determines a longitudinal diffusion coefficient for every experimental spectrum which is accepted for mobility analysis. However, not all of these D_L values are acceptable. Because the differencing technique used in the analysis of mobilities cannot be applied in the determination of an appropriate value of D_L for each spectrum, the spectra used for determining acceptable values of D_L must meet more stringent conditions than those acceptable for use in mobility determinations. The following are additional restrictions placed on the spectra:

(1) The use of the Tyndall shutter to gate the ions into the drift region at a precisely known time under precisely determined conditions is a necessity.

(2) The initial density in the swarm should be low, so that no detectable space charge broadening of the swarm occurs.

(3) The ions composing an experimental spectrum must have all been formed in the ion source. The condition that a reaction go to completion before the swarm has drifted the shortest drift distance used is not sufficient for the determination of D_L.

Since the data generally included three different drift distances for each pressure and E/N, comparisons such as those shown in Figure 25

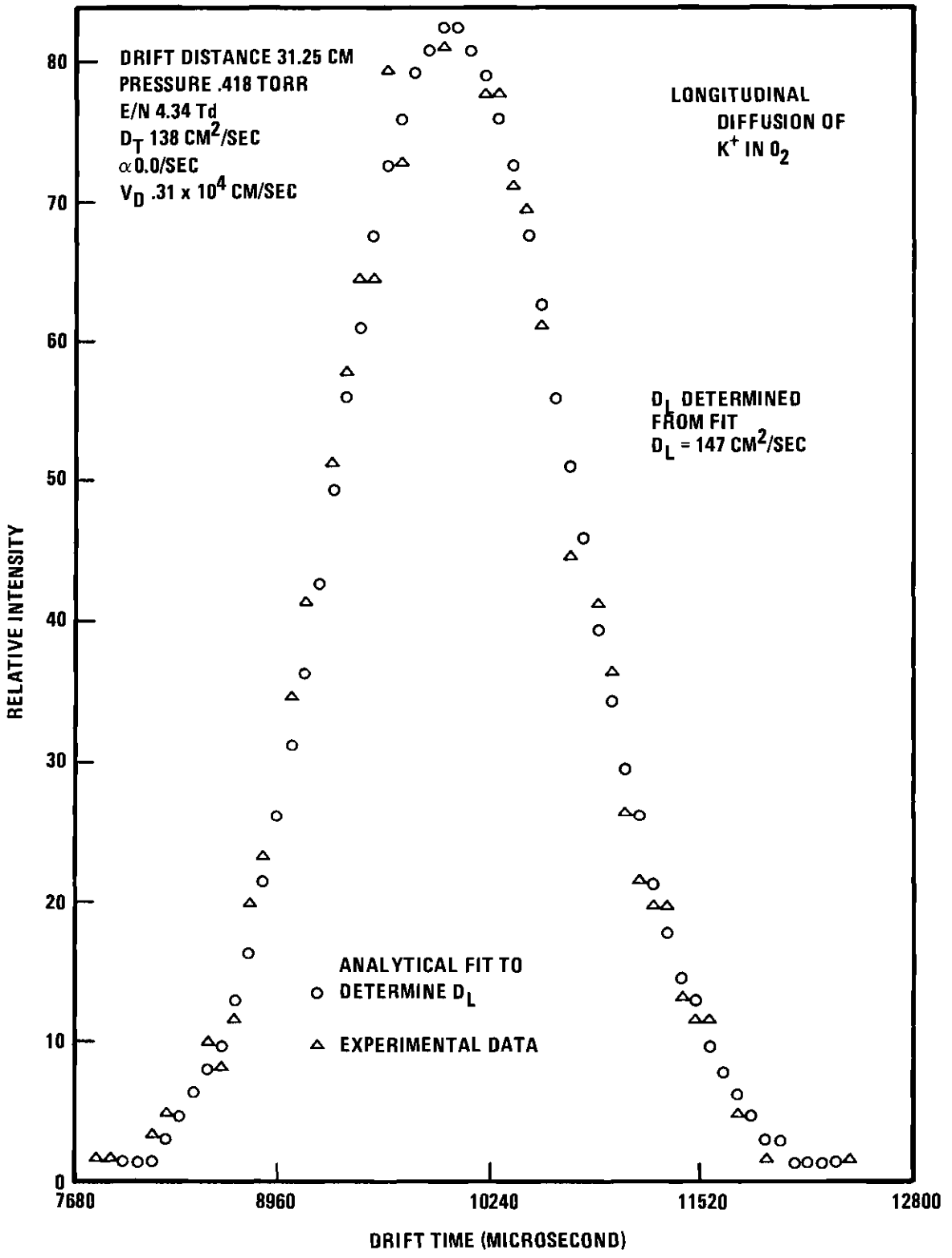

Figure 25. Example of Least Cubes Fit of the Analytical Profile to the Experimental Spectra to Determine D_L

were made for each distance. The resulting three values of D_L were then averaged to determine the longitudinal diffusion coefficient. For a set of data which met the conditions discussed above, these three values of D_L would generally not differ by more than ± 7 to 8 per cent.

The spectra of both O_2^+ and O_2^- do not rigorously satisfy the requirements that the ions composing an experimental spectrum must have been formed only in the ion source. O_2^+ is also created from the O^+ charge exchange and the dissociation of O_4^+. However, as mentioned in Chapter I, the charge exchange reaction has such a large rate that the reaction does go essentially to completion inside the source at the pressures and E/N at which the D_L data were taken. The formation of O_2^+ by dissociation of O_4^+ can be minimized by taking data at pressures where the rate of the reaction which initially creates the O_4^+ is small. Thus O_2^+ spectra suitable for D_L analysis could be obtained over restricted ranges of the experimental parameters.

O_2^- is created at all E/N by the dissociation of O_4^-. This distortion can be minimized by acquiring data at pressures where the rate of the reaction which initially creates the O_4^- is small. At E/N above 50 Td, O_2^- is also formed from O^-. This reaction is manifested by a foot appearing on the early side of the main peak in the O_2^- spectra. However, as shown in Figure 26, the source-produced O_2^- can easily be distinguished from the O_2^- which results from the reaction involving O^-. Values of D_L for O_2^- can be determined by fitting only that part of the experimental spectrum which can be attributed to source-produced O_2^-.

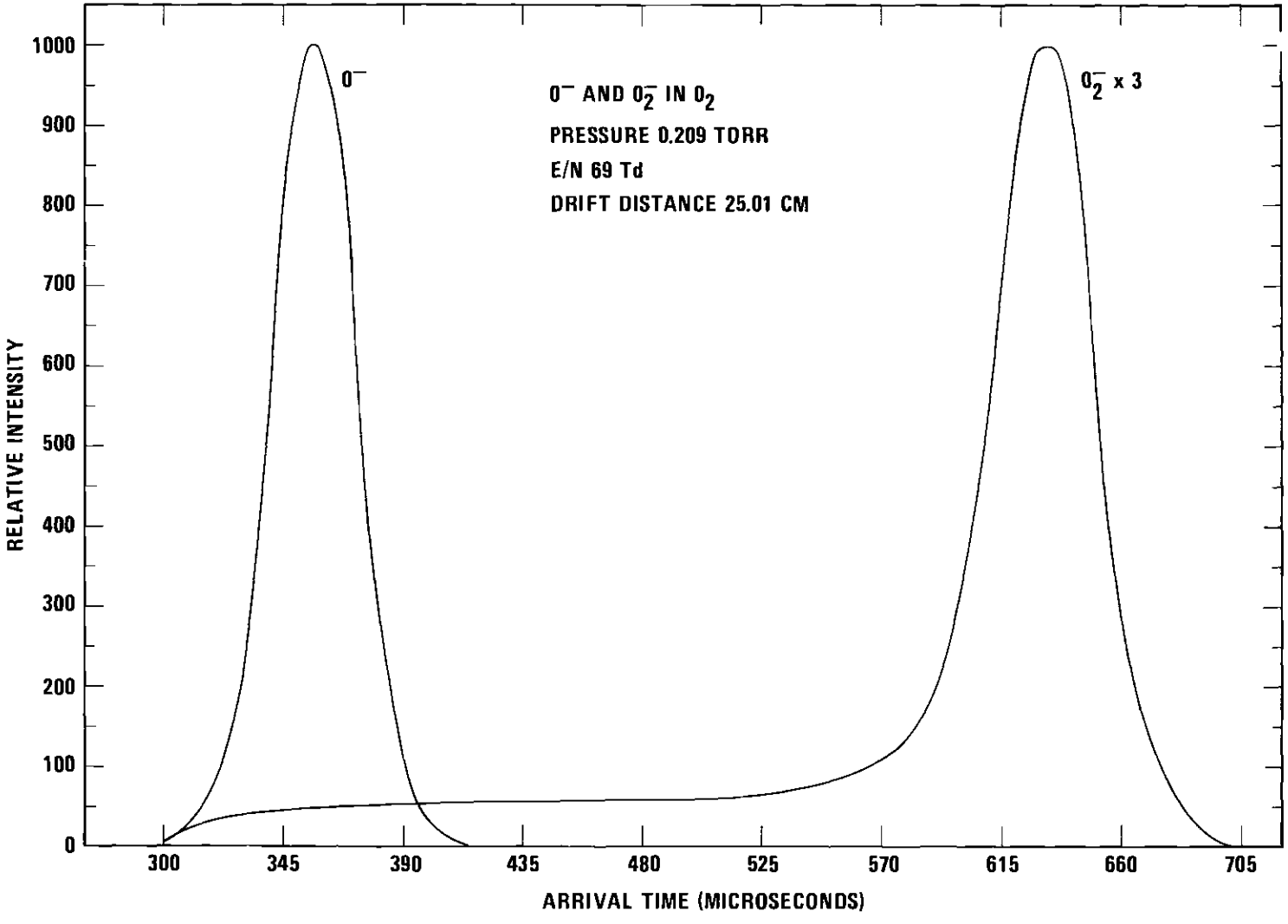

Figure 26. Comparison of O^- and O_2^- Arrival Time Spectra Showing the Effect of the Formation of O_2^- by O^-

Experimental Results

Longitudinal diffusion coefficients were determined for O_2^+, K^+, O_2^-, and O^- ions in O_2 over a wide range of drift distances and E/N values. The results for O_2^+ and K^+ are shown in Figure 27. Figure 28 shows the results for O^- and O_2^- ions. Since $D_L \propto 1/N$, the results are expressed as the value of ND_L versus E/N. Note that for all four ions D_L appears to approach some limiting value at low E/N, and is relatively constant below an E/N of 20 Td.

The values of ND_L predicted from the zero-field mobilities by the Einstein relation are as follows: O_2^+, 15.6 x 10^{17}/cm sec; K^+, 18.6; O_2^-, 14.9; O^-, 22.1. The low field values of ND_L determined from fitting the experimental data with an analytic expression are as follows: O_2^+, 18.6 x 10^{17}/cm sec; K^+, 20.3; O_2^-, 14.2; O^-, 20.2. The experimental ND_L values differ from the Einstein ND_L by the following amounts: O_2^+, 16 per cent high; K^+ 8 per cent high; O_2^-, 5 per cent low; O^-, 8 per cent low. This agreement is reasonably good for values of D_L which are determined by a curve fitting method. In the earlier nitrogen research of this laboratory,[79] it was found that the curve-fitting ND_L values differed from the Einstein ND_L values by 30 per cent for K^+ in N_2, 13 per cent for N^+, and 19 per cent for N_2^+.

The Einstein values of ND_L would be expected to lie within the scatter of the experimentally determined values of ND_L. Experimental reasons were sought to explain why this was not the case. Space charge was thought to be the best candidate for the source of error and an extensive investigation of the effects of various experimental

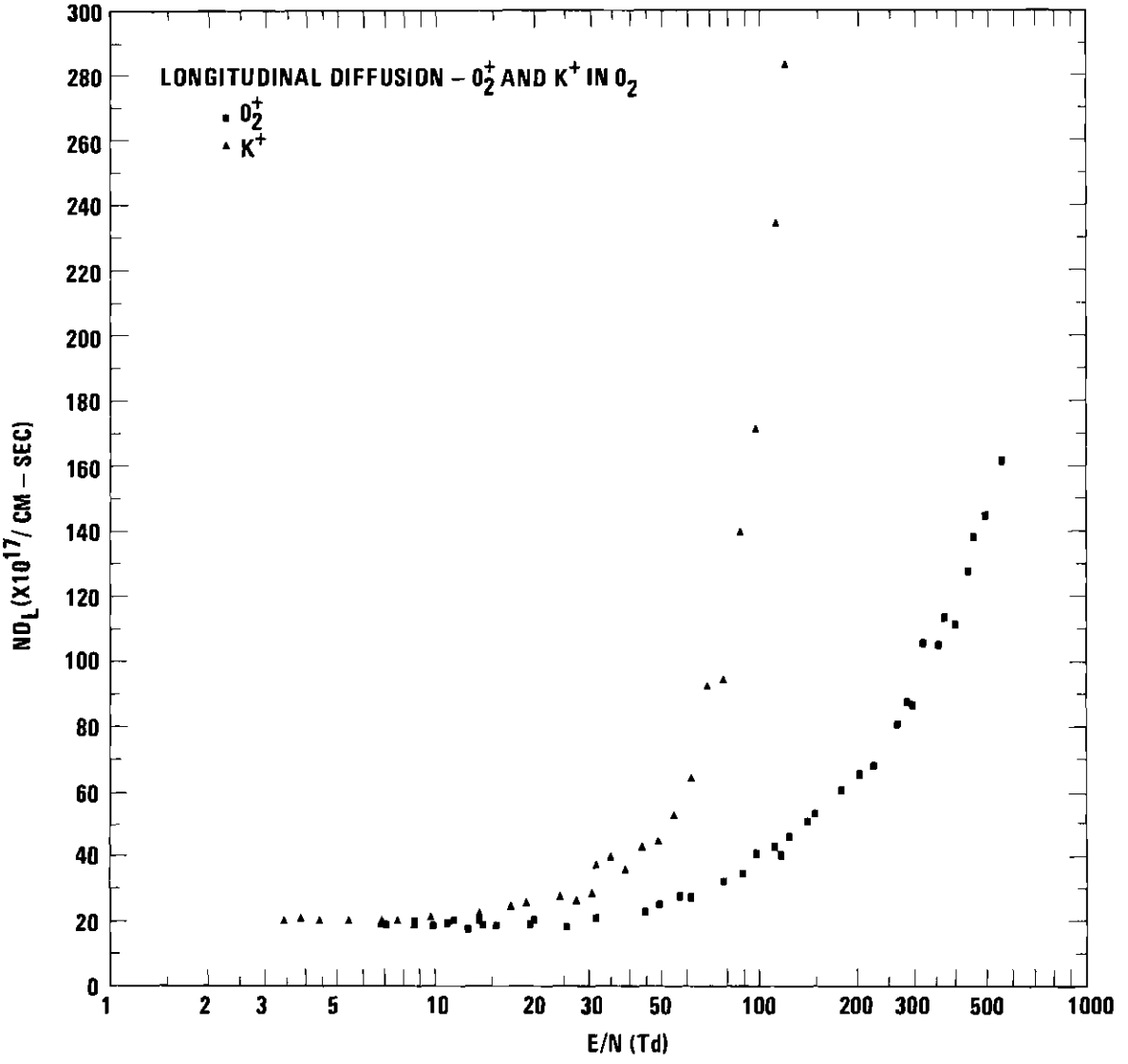

Figure 27. Longitudinal Diffusion Coefficients for O_2^+ and K^+ Ions in Oxygen

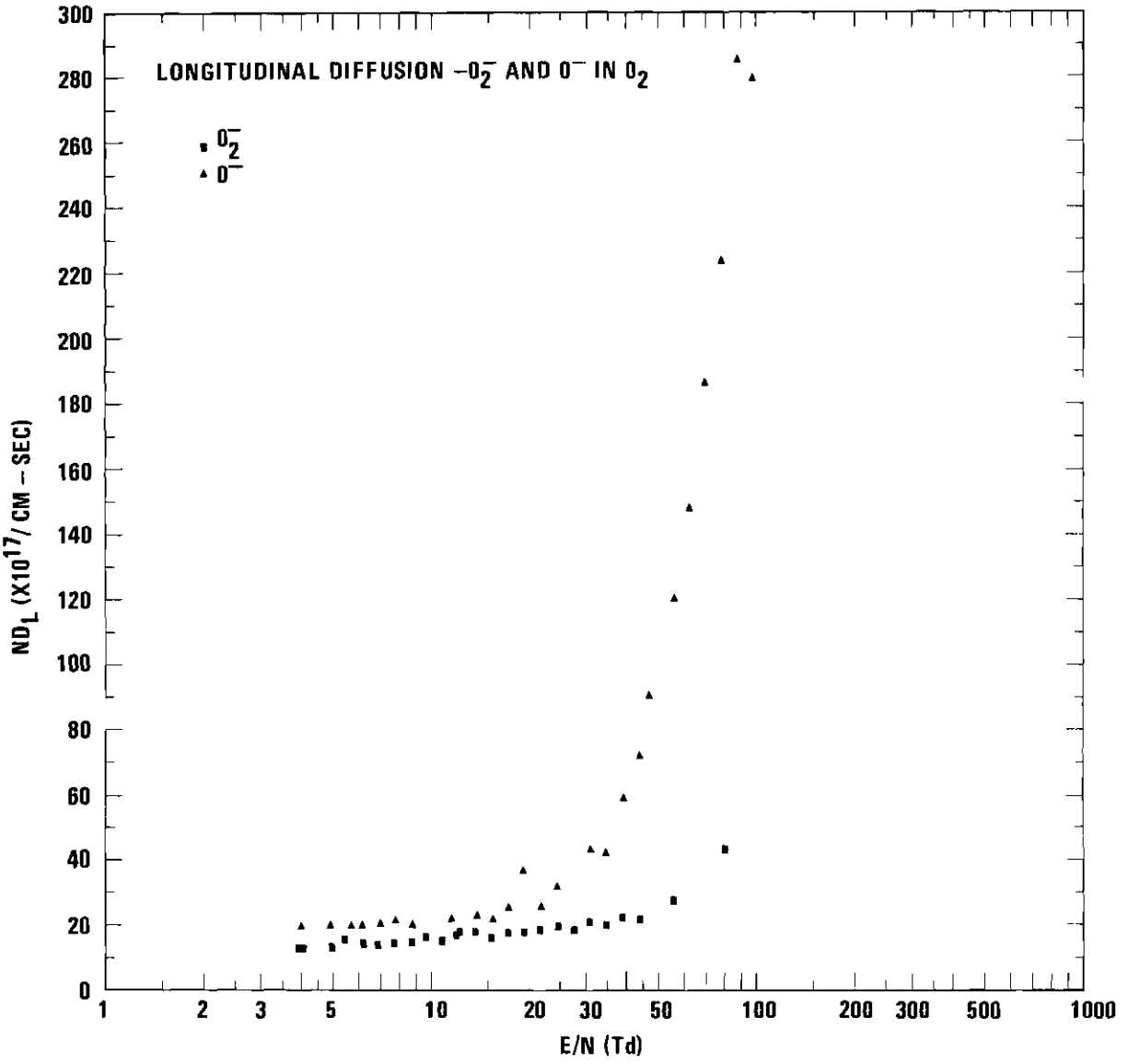

Figure 28. Longitudinal Diffusion Coefficients for O^- and O_2^- Ions in Oxygen

parameters on the spectra was undertaken. The following discussion is a description of one of the investigations.

One of the parameters investigated was the magnitude of the ion current. With all parameters at their usual values including the ion count rate, an experimental spectrum was generated. Then a change was made in the electron filament current so that the ion count rate was ten times the normal count rate. The corresponding spectrum had a value of D_L 30 per cent above the D_L value corresponding to the normal ion count rate. However, when the count rate was reduced to 1/2, 1/5, or 1/10 the normal count rate, their corresponding spectra had values of D_L which were the same as that for the normal count rate. These values of D_L were still about 13 per cent above the Einstein value for D_L. Because the present experiment is always performed with the normal count rate or less, space charge due to excessive ion current does not seem to be the problem.

Systematic investigations of the effects of the pulsewidth to the Tyndall grid, pulse amplitude to the Tyndall grid, filament accelerating voltage, skimmer voltage, control grid pulse width and amplitude, and drift distances demonstrated that the present experiment was being performed under conditions which produced time spectra with values of D_L in best agreement with the Einstein values of D_L. However, these values were consistently higher than Einstein values for positive ions and lower for negative ions. No reasons were found for this disagreement between the Einstein value and the experimental value or why the negative ions are lower and the positive ions are higher. The

lower values for the negative ions are confusing because all the distortions seen in this experiment tend to make the experimentally determined values of D_L higher than the Einstein values for D_L.

If Figures 27 and 28 are examined at E/N above 30 Td, it is noted that as E/N increases, D_L increases in each case, but it increases much more rapidly for O^- and K^+ than it does for O_2^+ and O_2^-. This weaker dependence on E/N for the O_2^+ and O_2^- values of D_L might be attributed to the fact that resonant charge transfer is an important part of the total scattering interaction for these ions in O_2. An analogous effect was seen for N_2^+ in N_2 by Moseley.[80]

No longitudinal diffusion coefficient results are presented for O_3^-, O_4^-, and O_4^+. Most of the data taken for these ions violate the condition of the ions being entirely source produced. The high pressure data for O_3^- which fulfilled this condition were all at low E/N and D_L values determined from them were in fair agreement with the Einstein value.

Error Analysis

The possible error in the determination of D_L arises from four sources: the error in determining the drift velocity, the error in determining the "best" fit, the possible error in pressure, and the error which causes the low E/N experimental value of D_L not to agree with the Einstein value of D_L.

Moseley[81] showed that the possible error due to v_d is 1.2 per cent. An estimate of the error in determining the best fit can be made

by investigating the difference between values of D_L obtained by fitting the several spectra (usually three), taken at different drift distances but otherwise under the same conditions. No set of appropriately taken spectra was found to give values of D_L which varied by more than 10 per cent. Over 90 per cent of the runs had variations less than 8 per cent. Hence, a possible error of ± 8 per cent is assigned to values of D_L due to the possible error in obtaining a best analytical fit.

The pressure error does not enter until ND_L is calculated or a particular value of E/N is associated with a value of D_L. The possible error in N is shown in Chapter IV to be ± 2.7 per cent.

The error which causes the low E/N experimental values of D_L not to agree with the Einstein values is difficult to assess, as this disagreement is caused by unknown factors. An estimate of its magnitude could be taken to be the deviation of the low E/N experimental value from the Einstein value. Since the high E/N data were taken under conditions similar to the low E/N data (except for the magnitude of the electric field), it is felt that this estimated error also represents a reasonable upper limit to the error at high E/N. The error is -16 per cent for O_2^+; -8 per cent for K^+; +5 per cent for O_2^-; and +8 per cent for O^-.

Totaling these possible errors, it is found that the error bounds which should be placed on D_L for O_2^+ are (+12, -28) per cent; for K^+, (+12, -20); for O_2^-, (+17, -12); and for O^-, (+20, -12). These error bounds mean, for example, that the experimental values of D_L for O_2^+

shown in Figure 27 and tabulated in Appendix II are believed to be no more than 12 per cent below the true values or 28 per cent above the true values.

As has been stated in Chapter I, there are no published results with which the values of D_L obtained in this research can be compared.

CHAPTER VI

ION-MOLECULE REACTIONS

In this chapter the measurements of the reaction rate coefficients for the ion-molecule reactions

$$O^- + 2O_2 \rightarrow O_3^- + O_2, \tag{16}$$

$$O^- + O_2 \rightarrow O_2^- + O \tag{17}$$

and

$$O_2^+ + 2O_2 \rightleftarrows O_4^+ + O_2 \tag{18}$$

will be described.

Method

Three measurement techniques were used in the present investigation of Reactions (16), (17), and (18). These techniques will be referred to as parent ion attenuation, product ion curve fitting, and forward-backward and will be discussed in the following sections.

Parent Ion Attenuation

This method has been discussed in detail by Miller[82] and Moseley[83] and will be only outlined here. The method is applicable to the determination of a depletion reaction rate. The parent ion must be

produced in the source and cannot be produced in the drift region. The parent ion must be depleting to only one product ion species.

The method consists of a comparison of the experimental attenuation, with increasing drift distance, of the intensity of the integrated ion current on axis, $I'(z_j)$, with the analytical expression for the integrated intensity on the axis, $I(z)$, calculated for corresponding E/N and pressure conditions. The analytical expression for the integrated ion current on axis is defined by

$$I(z) = \int_0^\infty \Phi(o,z,t)dt \tag{116}$$

and is calculated in Appendix V. That calculation yields the following expression

$$I(z) = \frac{As\ \exp(zv_d/2D_L)}{4D_L^{1/2}} \left\{ \left[2D_L^{1/2} + \frac{v_d}{(\alpha + v_d^2/4D_L)^{1/2}} \right] \exp\left[\frac{-z}{D_L^{1/2}} \left(\frac{v_d^2}{4D_L} + \alpha \right)^{1/2} \right] \right.$$

$$\left. - \left[\frac{z}{(z^2/4D_L + r_o^2/4D_T)^{1/2}} + \frac{v_d}{(\alpha + v_d^2/4D_L)^{1/2}} \right] \times \right. \tag{117}$$

$$\left. \exp\left[-2 \left(\frac{z^2}{4D_L} + \frac{r_o^2}{4D_T} \right)^{1/2} \left(\frac{v_d^2}{4D_L} + \alpha \right)^{1/2} \right] \right\}.$$

The comparable experimental quantity is the total number of detected ions composing each of the experimental spectra at the various drift distances,

$$I'(z) = \sum_i n_i \tag{118}$$

where the summation is over the channels of the time analyzer and n_i is the number of counts in the ith channel. All variables in Equation (117) are assumed known except for D_L, D_T, and α. It has been shown that the D_L dependence of I(z) is weak.[84] The requirement that D_T be known divides the determination of α into two regions.

In the low E/N region D_T can be calculated from the Einstein relation and α is the only parameter which must be determined from the attenuation of the parent ion.

At high E/N use is made of the N dependence of α and D_T. D_T is $\propto 1/N$ and $\alpha \propto N$ or N^2. For small N, the effect of D_T on I(z) is much greater than the effect of α; for large N the situation is reversed. A determination of a first approximation of a high E/N D_T value can be made by assuming that it has its low E/N value. Then the first approximation for D_T can be used with high pressure experimental data to obtain a first approximation for α at high E/N. The first approximation for α can then be used with low pressure experimental data to obtain a second approximation for D_T which in turn can be used to determine a second approximation for α from the high pressure data, and so on until stationary values of D_T and α are obtained.

Product Ion Curve Fitting

As shown by Equation (84), the slope of the log of the product ion current versus drift time is related to the reaction frequency and transverse diffusion coefficients of the ionic species participating in the reaction. This technique is valid only for source produced parent ions which are not formed in the drift region. The product ion can only be created from the parent ion and cannot itself undergo reactions. All parameters in the analytical expression for the slope of the log of the product ion current are assumed known except for D_T and α. The requirement that D_T be known divides the determination of α into two regions.

In the low E/N region where D_T is related to the mobility by the Einstein relation, the transverse diffusion makes no contribution to the slope. Therefore α can be determined uniquely from the slope.

At high E/N use is made of the N-dependence of α and D_T. By assuming that D_T has its Einstein value, a first approximation can be obtained for α by using the slope of the log of the product ion current. Then the slope of another spectrum at the same E/N but at a different pressure is examined. The first approximation for α from the first spectrum is assumed and a first approximation for D_T is determined from the slope of the second spectrum. The first approximation for D_T is now assumed for the first spectrum and a second approximation for α is calculated which is consistent with the slope of the first spectrum and this value of α is used to determine a second approximation for D_T from the second spectrum, and so on until stationary values of D_T and α are obtained.

The product ion curve fitting method has two disadvantages in comparison to the parent ion depletion method. The drift velocities of the parent and product ion must be sufficiently different that a suitable slope can be determined from the spectrum. Furthermore, the product ion cannot undergo reactions to form another species.

However, the product ion curve fitting technique does have one major advantage. To apply the parent ion depletion method, the source output must be maintained constant over long periods of time. This is not the case for the curve fitting technique.

Forward-Backward

The ratio of the product ion to the parent ion total integrated intensity on axis is examined as a function of drift distance. Some of the data are taken under conditions where $\alpha_{AB} >> \alpha_{BA}$. Equation (99) shows that these data will enable one to calculate a value of α_{AB} that is independent of mass discrimination effects. Knowing this value an estimate of α_{BA} which is dependent on mass discrimination can be obtained from the equilibrium value. Consistency checks can be made by examining the depletion of the parent ion intensity to determine if it is consistent with the values of α_{AB} and α_{BA}. Because the drift velocities of O_2^+ and O_4^+ are very similar, O_2^+ spectra which show the effects of dissociation cannot be observed.

Experimental Procedure

The experimental procedures for the three methods discussed in the last section are different and will be discussed separately here.

Parent Ion Attenuation

The experimental procedures for this case were basically the same as those used to obtain mobility data. Four differences are important. First, detailed spectra are not required, only the total number of ions composing each spectrum. Therefore, for most of the data, only this total count was recorded. However, the spectrum was always observed visually as a check on possible data-taking errors. Second, in order to obtain a good comparison with $I(z)$, $I'(z_j)$ was evaluated at six or seven drift distances. Third, the source output must be maintained constant, during the series of runs making up a set. In order to judge the stability of the source, each set of runs for the several drift distances were repeated three times. Any data which exhibited substantial variations in count rate for the several times a given drift distance was repeated were not used in the determination of α. Finally, the same total counting time or, equivalently, the same number of ion source pulses were used for every drift distance under a given set of conditions.

Product Ion Curve Fitting

These experimental procedures are very similar to those used to obtain mobility data. Two differences are important. Because the details of the spectra are very important, the maximum count per channel is increased from 2^{11} to 2^{14}. In order to make the time separation between the parent ion and product ion large only the far back ion source positions are used.

Forward-Backward

For the present research two techniques were used in the investigation of a forward-backward reaction scheme. The experimental procedures for obtaining the ratios of O_4^+/O_2^+ on axis integrated current are as follows. Because the ratios are to be measured in the pressure region where $\alpha_{AB} > \alpha_{BA}$, the ratio experiment must be performed at low pressure (less than 0.2 Torr). This requirement means that O_4^+ will not be present in high enough concentration to do a pulsed experiment. Therefore a d.c. experiment was performed. Since we are only interested in the integrated intensity on axis, a d.c. or pulsed experiment gives the same results. A scaler was now used instead of the multichannel analyzer. The counting rate was set at a level that will make mutual repulsion a negligible effect. The mass spectrometer was set so that O_4^+ was passed and the scaler counted for two minutes. Two minute counting periods were picked so that the statistics of the O_4^+ intensity would be good. Then the mass spectrometer was switched to pass O_2^+ and its intensity was recorded by the scaler. This procedure was repeated three or four times at each position. The source had to be stable only during the data taking at one position. Data were taken at seven source positions.

Because the estimate of the forward reaction rate α_{BA} is affected by mass discrimination, a consistency check may be made by examining the O_2^+ intensity as a function of drift distance. The experimental procedures for this technique are the same as described for parent ion attenuation.

Experimental Results

The experimental results will be discussed in three sections. The reaction being discussed will be the heading.

$O^- + 2O_2 \rightarrow O_3^- + O_2$

Both the parent ion attenuation and the product ion curve fit were used to measure the rate of this reaction. Figure 29 shows an example of the comparison between I(z) and $I'(z_j)$ for O^- at an E/N of 1.2 Td. The values of v_d, D_L and D_T used to calculate I(z) are indicated on the figures, and are obtained from the results discussed in Chapter IV. The various values of $k = \alpha/N^2$ are also indicated. The assumption of a three-body reaction is verified by the fact that k is constant over a pressure range of 0.313 to 0.836 Torr. The reaction rates measured by the parent ion attenuation technique are shown plotted versus E/N in Figure 32. Figure 30 shows a curve fit of the O_3^- ion spectrum. Because these data were taken at low E/N, no correction has to be made to the slope due to diffusion. Reaction rates obtained from the slope of the log of the O_3^- current are plotted in Figure 32. Comparison of the reaction rates obtained by the two techniques shows that the product ion curve fit values are consistently low. This is caused by the reaction of O_3^- with CO_2 to form CO_3^-. Examination of Equation (86) shows that such a reaction would reduce the slope of the log of the O_3^- current. CO_3^- was detected during the taking of all the O_3^- spectra. The presence of CO_3^- has no effect on the attenuation of O^-. Because the concentration of CO_2 depends on the time the drift tube has been valved off from the diffusion pumps, all the O_3^- spectra were

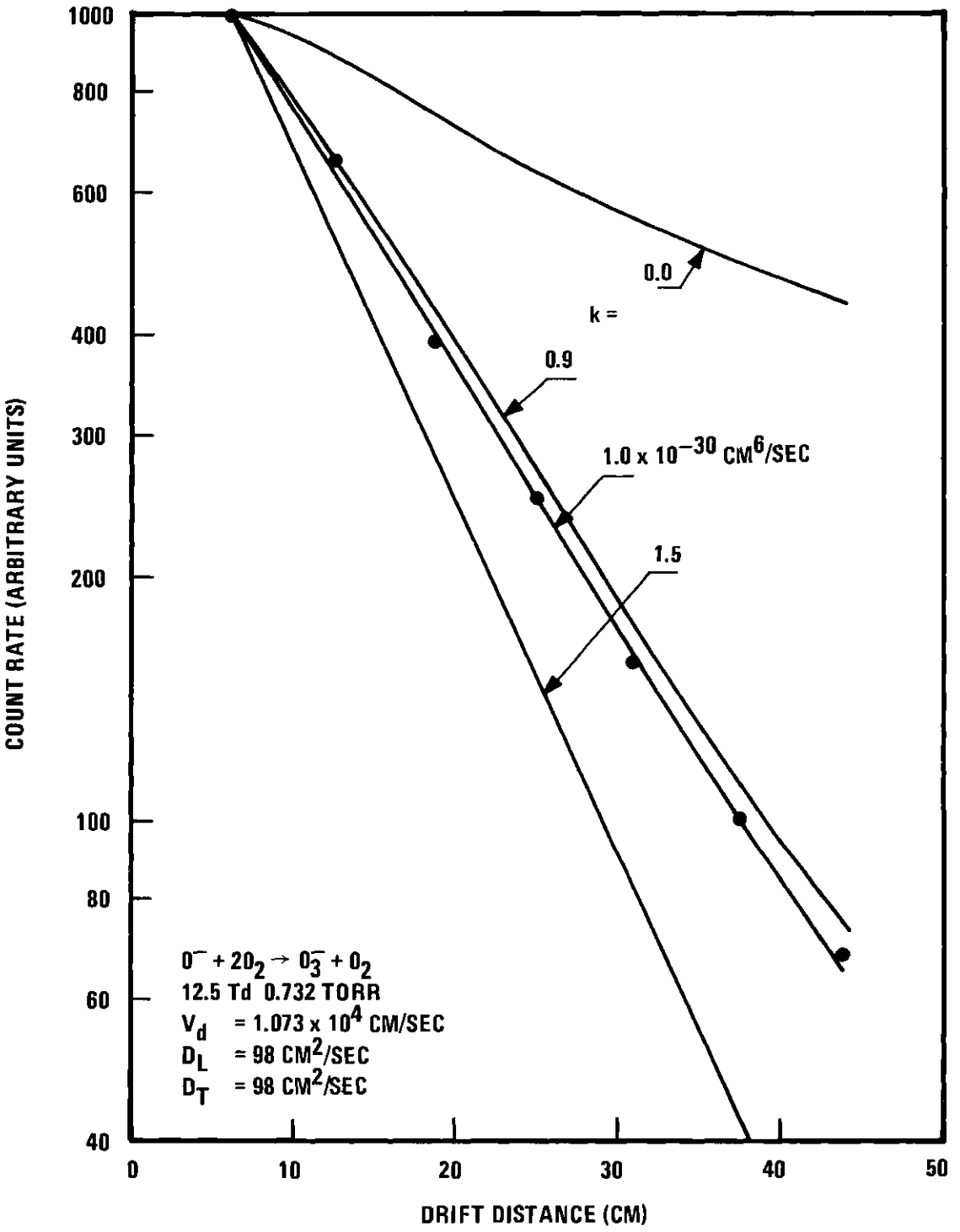

Figure 29. Typical Attenuation Data for O^- in O_2 at an E/N of 12 Td

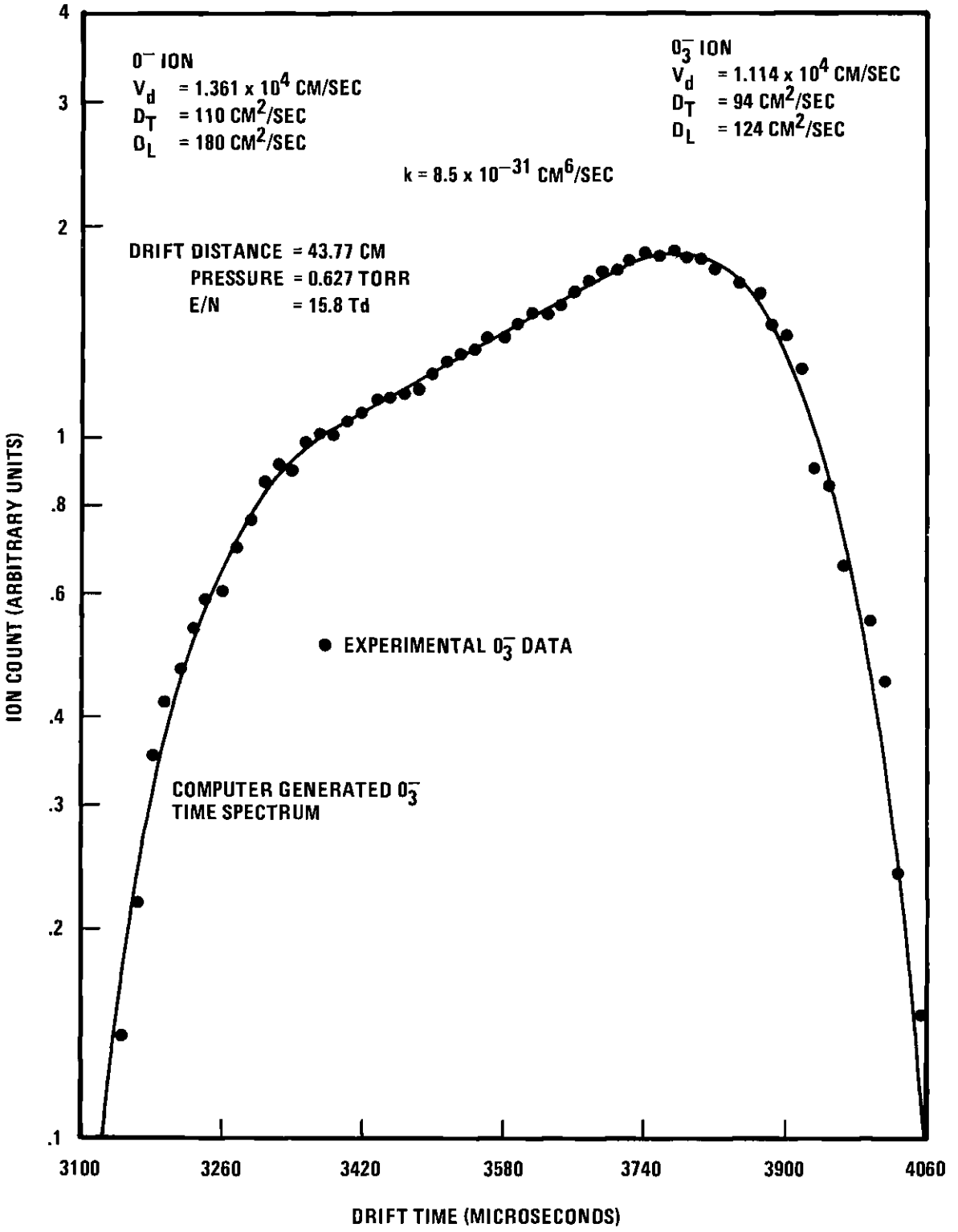

Figure 30. Comparison of an Experimental Time Spectrum with the Corresponding Analytical Profile for O_3^- in O_2

taken immediately after the 2-inch isolation valve had been closed and the system pressurized. A few O_3^- spectra were taken after the valve had been closed two hours. The slope of the log of the O_3^- count rate from such spectra indicated a reaction rate as low as 3×10^{-31} cm^6/sec. Data of this type are not plotted in Figure 32. The O^- attenuation data are the only data used in obtaining a value for the reaction rate. Those data give a value of 1.0×10^{-30} cm^6/sec. The reaction rates were obtained from an E/N of 6 to 29 Td. These reaction rates are tabulated in Appendix III.

$O^- + O_2 \rightarrow O_2^- + O_2$

Rates for this reaction were measured by the product ion curve fit technique. Figure 31 shows a curve fit of the O_2^- ion spectrum. As shown on the figure there are two sources of O_2^-. There are the O_2^- created in the source and there are the O_2^- created by reaction in the drift tube. A fit of the source produced O_2^- spectrum was made by using the analysis described in the determination of D_L values in Chapter V. Only the last half of the peak was fitted in this manner. (D_L was changed in Equation (129) until a good fit was obtained. The experimental data and the analytic spectrum were normalized to agree at their points of maximum intensity.)

The fit of the reaction produced O_2^- is found by finding the right combination of D_T for O^- and k which gives the slope indicated in the figure. D_T for O_2^- is assumed not to change much from its low E/N value because of charge exchange. This was found to be the case for N_2^+ in nitrogen.[80] The experimental data ascribed to reaction created

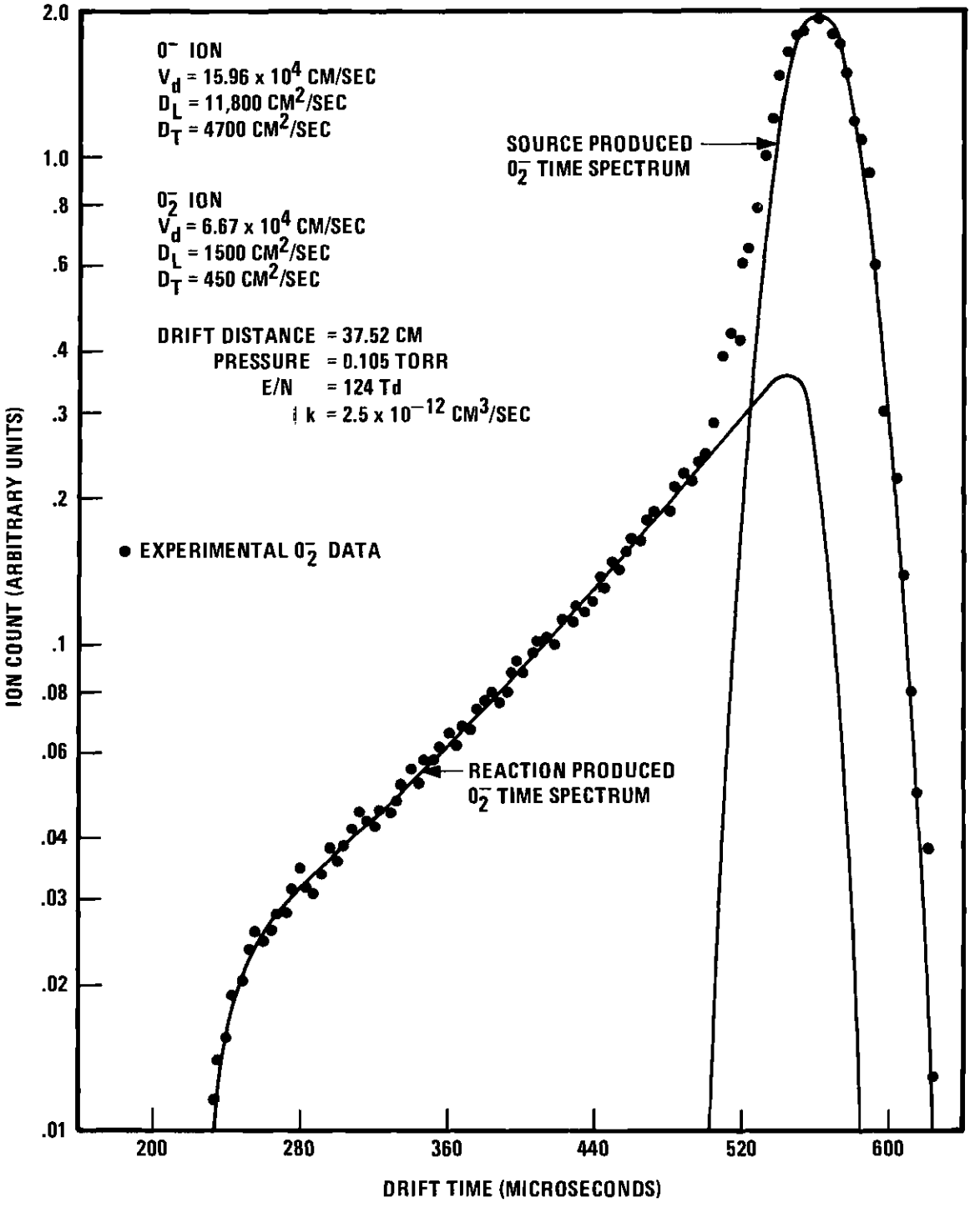

Figure 31. Comparison of an Experimental Time Spectrum with the Corresponding Analytical Profile O_2^- in O_2

O_2^- are normalized to agree with the analytical data at time $z(v_{d1}+v_{d2})/2v_{d1}v_{d2}$ where v_{d1} and v_{d2} are the drift velocities of O^- and O_2^-, respectively. The data used to generate the analytic spectra are indicated on the figure.

Such O_2^- time profiles were taken at 0.105 and 0.209 Torr and over an E/N range of 62 to 140 Td. Figure 33 shows a plot of the reaction rate versus E/N. The reaction rate increases from 2.5×10^{-14} cm^3/sec at an E/N of 62 Td to 3.4×10^{-12} at an E/N of 140 Td. These reaction rates are tabulated in Appendix III.

Figure 33 shows that at an E/N of 60 Td O_2^- ions are produced in sufficient quantities by Reaction (17) that a rate constant can be determined by the present experiment. The energy of the O^- ion at this E/N calculated on the basis of the Wannier expression[41] is 0.3 eV. However, the difference in electron affinity between O^- and O_2^- would indicate that O^- ion would need 1.0 eV kinetic energy to make the reaction go. This discrepancy could be caused by the fact that the Wannier expression estimates the mean energy of some unknown energy distribution. Therefore, it could well be that the energy distribution with a mean energy of 0.3 eV could have sufficient ions with energy of 1.0 eV to enable a rate to be measured by the present experiment.

$$O_2^+ + 2O_2 \rightleftarrows O_4^+ + O_2$$

The investigation of this forward-backward reaction scheme encountered an experimental difficulty which made it possible to obtain only order of magnitude estimates of the reaction rates involved. The difficulty encountered was that of temperature variation. O_4^+ has a binding energy of 0.4 eV.[37] A three or four degree variation from room

temperature causes the reverse reaction rate to change by a factor of three. Gradients of two to four degrees existed in the drift tube during the taking of most of the ratio data. The mean temperature of the drift tube typically increased by four or five degrees during the data taking. As a result, the ratio data were not very reproducible. An average was taken but the scatter about the mean was quite large. The O_2^+ ion intensity data as a function of drift position did not show noticeable variation. This is caused by diffusion dominating the attenuation of the O_2^- ion intensity rather than the reaction rates. The reaction rates that are found to be consistent with the mean of the ratio data and with the O_2^+ ion intensity attenuation are 7.5×10^{-30} cm^6/sec for the forward reaction rate and 5.0×10^{-14} cm^3/sec for the backward rate.

Better ratio data could possibly be obtained by using the thoriated-iridium filament which requires much less power than the $BaZO_3$ filament.

Error Analysis

$O^- + 2O_2 \rightarrow O_3^- + O_2$

For the parent attenuation data possible systematic errors can arise from two sources: the possible error in the drift velocity of O^- used to calculate the I(z) curves and the error induced by using a value of D_T calculated from the Einstein relation, rather than an experimentally measured value of D_T. The mobility error bound of ± 3.7 per cent determined in Chapter IV will be taken to represent the contribution to the error due to an error in the mobility. All of the reaction rates measured in this manner were taken at relatively low

E/N (29 Td or less). Therefore appreciable deviation from the Einstein diffusion value is not expected. A ± 2.0 per cent error is assigned due to possible error in D_T.

The random error in k can be estimated by examining the comparisons of I(z) and $I'(z_j)$ from which the values of k were determined. It was found that a random error bound of ± 12 per cent would include all the $I'(z_j)$ data. However, most of the data are better than that. The square root of the sum of the squares of the independent random and systematic possible errors yields an error of 14 per cent for the rate of the depletion of O^- to O_3^-.

No account was taken of the possibility of O^- depleting also to O_2^- because at the E/N at which these measurements were made this reaction was not present.

No error will be calculated for the O_3^- curve fit data because of the presence of the reaction of O_3^- with CO_2.

$\underline{O^- + O_2 \rightarrow O_2^- + O}$

There are four sources of systematic error for this reaction rate: the difference in drift velocities, the D_T value of O^-, the assumption that D_T for O_2^- does not appreciably deviate from the Einstein value, and the E/N value associated with k.

Although the total error assigned to a drift velocity is about ± 4 per cent, the drift velocities in relation to each other have a smaller error. A relative error of ± 2 per cent will be assigned to the drift velocities. This relative error causes an error of 6 per cent in the difference in drift velocities. The error caused by an error in

the D_T value of O^- is very dependent on the reaction frequency. Therefore because the reaction rate is E/N dependent so is the error. Even though the effects of diffusion are greater at high E/N, the reaction rate is increasing much faster than diffusion and hence the error is largest at low E/N. An error of ± 5 per cent is assigned at an E/N of 140 Td and an error of ± 15 per cent at an E/N of 62 Td. The assumption that D_T for O_2^- does not appreciably deviate from the Einstein value is taken into account for the most part in the discussion of the error due to D_T for O^-. As shown in Equation (81), the effect of diffusion depends on the difference in D_T values for O_2^- and O^-. Therefore any error caused by this assumption is considered in the error due to D_T for O^-. Because the reaction rate is very E/N dependent, an error in pressure could cause a large error in the reaction rate associated with that E/N. Here again the error is E/N dependent. If we assume an error of ± 2 per cent in the pressure, then at an E/N of 140 Td the error in the reaction rate is ± 6 per cent; at an E/N of 62 Td the error is ± 36 per cent.

The random error was estimated by examining the scatter of the experimental data about the analytic fit. A random error bound of ± 8 per cent includes most of the experimental data. The square root of the sum of the squares of the independent random and systematic possible errors yields an error of ± 19 per cent at an E/N of 140 Td and an error of ± 58 per cent at an E/N of 62 Td.

Because the reaction frequency for the conversion of O^- to O_3^- is negligible compared to the conversion of O^- to O_2^-, that reaction was not considered as a source of error.

Comparisons with Existing Experimental Data

Figure 32 shows a comparison of the reaction rate for conversion of O^- to O_3^-. The agreement is reasonably good with McKnight.[34] The Morruzzi and Phelps[40] data are an order of magnitude lower than the data of the present experiment. The data of the present experiment are in good agreement with the unpublished results of Woo[43] and Beaty[26].

Figure 33 is a comparison of the reaction rate for conversion of O^- to O_2^-. The agreement among all investigators is quite good.

The only other available reaction rates for the O_2^+ to O_4^+ forward-backward reaction scheme are those of Durden et al.[42] They obtained a value of 2.8×10^{-30} cm^6/sec for the forward reaction and 2.8×10^{-13} cm^6/sec for the backward reaction. The agreement with the data of the present research is not good, but because of the high scatter in the present research this is not unexpected.

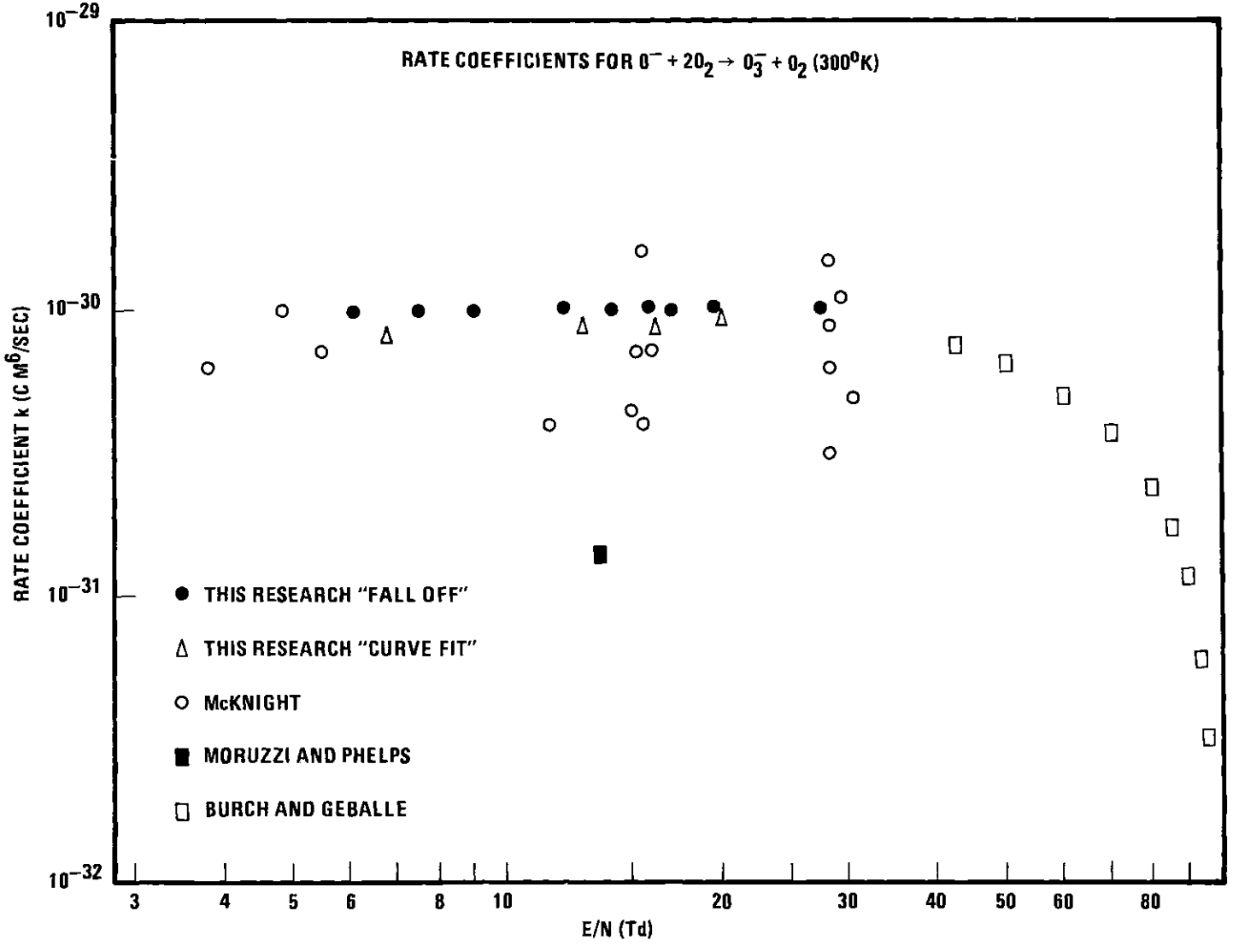

Figure 32. Comparison of the Reaction Rate Coefficients for the Conversion of O^- to O_3^- with the Results of Other Experiments

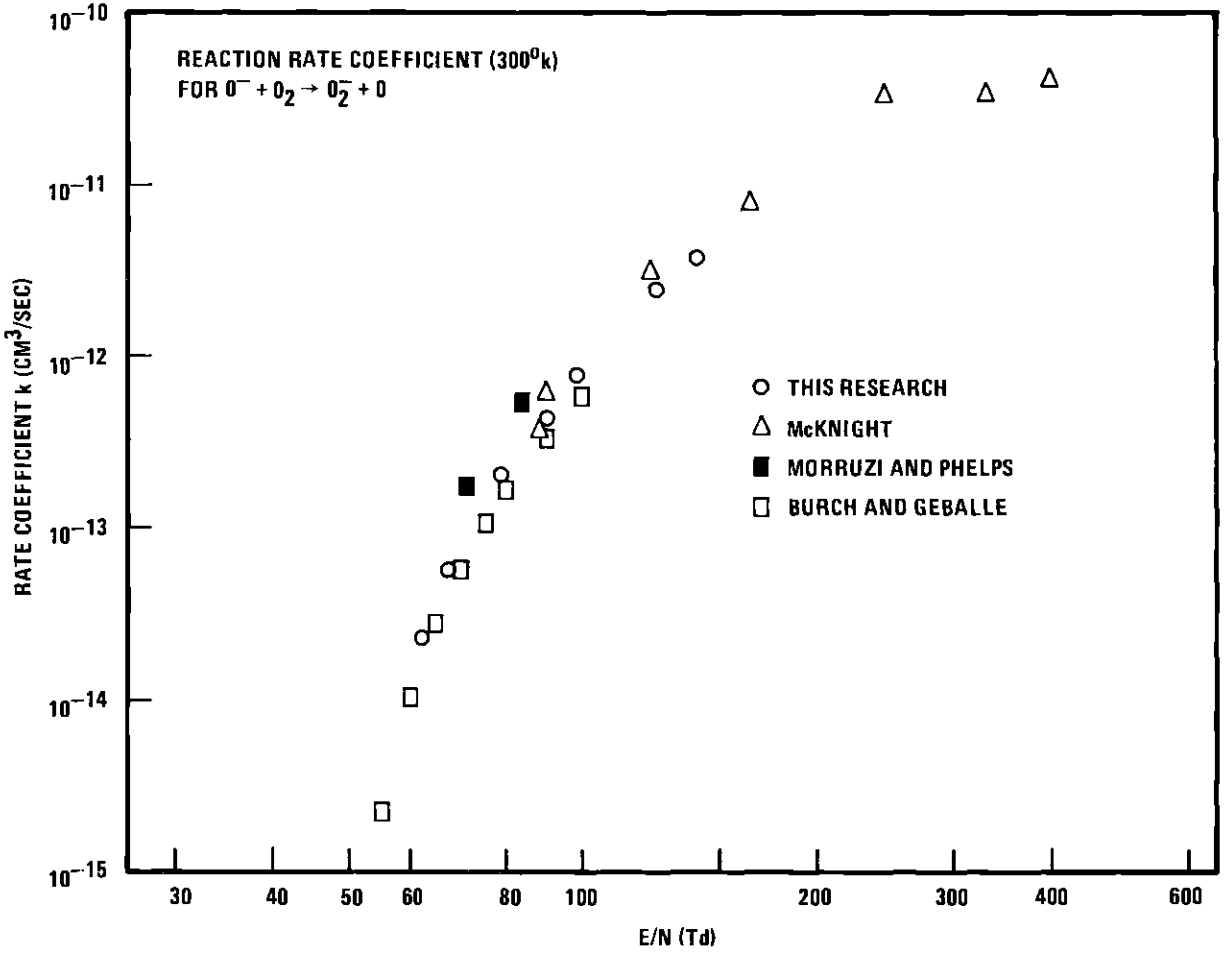

Figure 33. Comparison of the Reaction Rate Coefficients for the Conversion of O^- to O_2^- with the Results of Other Experiments

CHAPTER VII

CONCLUSIONS

Mobilities

The mobility of O_2^+ was obtained on the E/N range from 7 to 550 x 10^{-17} V cm^2 and over a pressure range of 0.20 to 0.03 Torr. The zero-field reduced mobility for O_2^+ was determined to be 2.24 ± .09 cm^2/V sec. The mobility of O^- was obtained on the E/N range from 4 to 175 x 10^{-17} V cm^2 and over a pressure range of 0.26 to 0.05 Torr. The zero-field reduced mobility for O^- was shown to be 3.20 ± .13 cm^2/V sec. The mobility of O_2^- was measured on the E/N range from 3 to 140 x 10^{-17} V cm^2 and over a pressure range of 0.63 to 0.10 Torr. The zero-field reduced mobility for O_2^- was determined to be 2.16 ± .09 cm^2/V sec. The mobility of O_3^- was obtained on the E/N range from 4 to 15 x 10^{-17} V cm^2 and over a pressure range of 1.05 to 2.61 Torr. The zero-field reduced mobility for O_3^- was shown to be 2.55 ± .10 cm^2/V sec. The mobilities of O_4^+ and O_4^- were measured on the E/N range from 2 to 5 x 10^{-17} V cm^2 and over a pressure range of 3.13 to 6.27 Torr. The zero-field reduced mobility for O_4^+ was shown to be close to that for O_2^+; the mobility of O_4^- was determined to be similar to that for O_2^-. The mobility of K^+ was obtained on the E/N range from 3 to 300 x 10^{-17} V cm^2 and over a pressure range of 6.27 to 0.05 Torr. The zero-field reduced mobility for K^+ was determined to be 2.68 ± .11 cm^2/V sec.

Longitudinal Diffusion Coefficients

Longitudinal diffusion coefficients were measured for O_2^+, O^-, O_2^- and K^+ in O_2 on the E/N range from 3 to 500 x 10^{-17} V cm^2 and over a pressure range of 0.26 to 0.03 Torr. All coefficients at low E/N were within 16 per cent of the values predicted from the mobilities by the Einstein relation. At higher E/N the coefficients increased, in some cases quite rapidly, as E/N was increased. D_L increases much more rapidly for O^- and K^+ than it does for O_2^+ and O_2^-. This weaker dependence on E/N might be attributed to the fact that resonant charge transfer is an important part of the total scattering interaction for these ions in O_2.

Ion-Molecule Reactions

The rate constant for the reaction

$$O^- + 2O_2 \rightarrow O_3^- + O_2 \qquad (16)$$

was measured on the E/N range from 6 to 29 x 10^{-17} V cm^2 and at pressures from 0.31 to 0.84 Torr. The rate coefficient was found to be 1.0 ± 0.2 x 10^{-30} cm^6/sec over the entire E/N range. The data clearly indicate that this reaction is three-body over the E/N and pressure range of these measurements. The reaction

$$O^- + O_2 \rightarrow O_2^- + O \qquad (17)$$

was observed with a rate that increased sharply with E/N. This is as

might be expected of an endothermic reaction. The reaction is endothermic because the electron affinity of O^- is about 1 eV greater than that for O_2^-. The rate coefficient was found to increase from 2.5 ± 1.5 x 10^{-14} cm^3/sec at E/N of 62 x 10^{-17} V cm^2 to a value of 3.4 ± 1.0 x 10^{-12} cm^3/sec at E/N of 140 x 10^{-17} V cm^2. Order of magnitude rate coefficients for the reaction

$$O_2^+ + 2O_2 \longrightarrow O_4^+ + O_2 \qquad (18)$$

and

$$O_4^+ + O_2 \longrightarrow O_2^+ + 2O_2 \qquad (18)$$

were estimated, at thermal energies, to be 7.5 x 10^{-30} cm^6/sec and 5.0 x 10^{-14} cm^3/sec, respectively.

Impurity Ions

Impurity ions which could not be eliminated were seen at pressures greater than 0.6 Torr and over all E/N. The impurity ions were identified as CO_3^- and CO_4^-, CO_3^- being much more intense. Mobilities were determined for both CO_3^- and CO_4^- at pressures on the range from 2.6 to 3.1 Torr and on the E/N range of 2.5 to 7.0 x 10^{-17} V cm^2. CO_3^- and CO_4^- had zero-field mobilities of 2.50 ± .10 and 2.45 ± .10 cm^2/V sec, respectively. The CO_3^- appears to arise primarily from a reaction involving O_3^-, and CO_4^- from a reaction involving O_4^-. The impurity molecule which reacts with the negative oxygen ions to form these impurity

ions is thought to be CO_2. The source of CO_2 is unknown, but is speculated to be the stainless steel walls of the drift tube.

APPENDIX I

TABULATION OF THE DRIFT VELOCITY AND MOBILITY RESULTS

The following pages list the results of the mobility determinations described in Chapter IV. The drift velocity and mobility results appear in order of increasing E/N for each ion species. E/N is in townsends (Td). The reduced mobility is simply the value of the ratio v_d/E, reduced according to Equation (7) to 760 Torr at 0°C. The standard deviation is the standard deviation in percentage of the experimental points from the least squares fit straight line. The drift velocity is obtained from the least squares fit straight line except when only two positions were used. Then a simple difference was employed. The units are 10^4 cm/sec. Pressure is in Torr. Run number refers to an identification number assigned to each set of (usually) three experimental spectra. The positions are the ion source drift positions used (see Chapter IV).

O_2^+ in O_2

E/N (Td)	Reduced Mobility (cm^2/Vsec)	Standard Deviation (Per Cent)	Drift Velocity (10^4cm/sec)	Pressure (Torr)	Run Number	Positions
3.91	2.253	1.5	0.240	0.261	125	321
4.88	2.250	1.5	0.300	0.209	121	321
5.47	2.220	0.5	0.327	0.209	120	321
6.13	2.258	1.0	0.372	0.209	119	321
6.85	2.265	0.4	0.417	0.209	30	321
6.87	2.208	0.6	0.408	0.157	114	321
7.74	2.264	1.1	0.473	0.157	113	321
8.63	2.255	0.9	0.523	0.209	31	321
8.66	2.261	0.8	0.529	0.157	112	321
9.71	2.258	1.0	0.590	0.157	111	321
9.79	2.234	1.0	0.594	0.627	165	421
10.88	2.325	0.5	0.653	0.209	32	321
10.89	2.245	0.9	0.657	0.157	110	321
10.94	2.267	1.5	0.667	0.105	106	321
11.42	2.232	0.8	0.685	0.209	202	543
12.18	2.264	0.3	0.743	0.078	98	321
12.24	2.261	1.0	0.744	0.105	105	321
12.44	2.247	0.8	0.752	0.157	164	321
12.90	2.262	0.1	0.772	0.732	155	531
13.56	2.234	0.9	0.814	0.209	117	321
13.63	2.206	0.5	0.808	0.105	69	321
12.64	2.262	0.9	0.883	0.078	99	321
13.68	2.228	0.6	0.820	0.157	109	321
13.70	2.204	0.7	0.811	0.209	33	321
13.72	2.242	0.4	0.834	0.105	42	321
14.04	2.196	1.2	0.827	0.105	166	531
15.36	2.217	0.6	0.915	0.314	66	321
15.37	2.201	0.4	0.909	0.157	108	432
15.45	2.267	0.6	0.936	0.105	43	321
15.41	2.246	0.8	0.930	0.105	104	321
15.49	2.200	0.4	0.916	0.157	162	321
17.18	2.227	0.3	1.028	0.105	70	321
17.27	2.160	1.3	1.003	0.209	34	321
17.28	2.225	1.0	1.033	0.105	103	321
18.96	2.228	0.7	1.135	0.105	143	321
18.96	2.248	0.4	1.151	0.105	144	321
19.35	2.210	0.6	1.150	0.105	102	321
19.39	2.247	0.7	1.171	0.105	44	321
19.60	2.222	0.6	1.170	0.157	163	421
20.14	2.192	0.7	1.186	0.105	167	653
21.56	2.226	0.3	1.290	0.105	129	321
21.58	2.233	0.2	1.295	0.105	130	321

O_2^+ in O_2 (Continued)

E/N (Td)	Reduced Mobility (cm^2/V sec)	Standard Deviation (Per Cent)	Drift Velocity (10^4 cm/sec)	Pressure (Torr)	Run Number	Positions
21.67	2.240	0.9	1.304	0.105	71	321
21.71	2.220	0.4	1.295	0.314	67	321
21.76	2.252	0.8	1.317	0.209	35	321
21.99	2.258	1.0	1.334	0.105	150	321
22.16	2.224	0.5	1.384	0.105	128	321
22.19	2.234	0.6	1.392	0.105	129	321
24.31	2.205	0.9	1.440	0.105	147	321
24.36	2.231	1.0	1.461	0.105	148	321
24.38	2.211	0.3	1.449	0.105	101	321
24.41	2.251	0.2	1.477	0.078	134	321
24.43	2.243	0.7	1.472	0.105	45	321
24.87	2.222	0.3	1.467	0.052	185	532
25.52	2.196	0.8	1.486	0.105	168	653
27.26	2.180	0.6	1.597	0.105	72	321
27.31	2.231	0.6	1.638	0.078	133	321
27.41	2.246	0.8	1.655	0.209	36	321
30.76	2.206	0.7	1.823	0.078	135	432
31.40	2.226	1.0	1.878	0.078	176	531
34.25	2.189	1.0	1.996	0.105	74	321
34.32	2.183	0.3	2.013	0.105	73	654
34.48	2.262	0.6	2.092	0.105	152	432
34.56	2.198	0.6	2.041	0.209	37	321
37.26	2.233	0.8	2.236	0.078	142	321
37.31	2.229	1.0	2.235	0.078	136	321
37.31	2.220	0.2	2.226	0.078	137	321
38.62	2.182	0.3	2.264	0.078	91	432
38.71	2.207	0.8	2.295	0.105	46	321
43.16	2.222	0.4	2.577	0.052	11	321
43.54	2.191	0.4	2.256	0.209	38	321
44.48	2.177	0.9	2.566	0.078	177	653
44.93	2.215	0.8	2.699	0.078	178	321
48.52	2.184	0.5	2.848	0.105	8	321
48.77	2.188	0.6	2.868	0.105	47	321
49.04	2.154	0.8	2.798	0.105	170	654
54.55	2.156	0.3	3.161	0.078	92	543
56.99	2.137	0.9	3.269	0.078	179	431
61.81	2.103	0.5	3.493	0.105	171	654
68.49	2.111	0.6	3.885	0.105	77	543
68.68	2.114	0.2	3.903	0.105	48	321
76.40	2.131	0.1	4.375	0.052	52	321
76.93	2.065	1.0	4.270	0.078	93	654
77.89	2.072	0.6	4.336	0.105	172	654

O_2^+ in O_2 (Continued)

E/N (Td)	Reduced Mobility (cm^2/Vsec)	Standard Deviation (Per Cent)	Drift Velocity (10^4 cm/sec)	Pressure (Torr)	Run Number	Positions
86.13	2.072	0.7	4.794	0.105	6	321
86.24	2.072	0.4	4.800	0.105	78	543
86.40	2.061	0.6	4.785	0.105	49	321
88.73	2.026	0.5	4.830	0.078	180	654
96.45	2.033	0.1	5.268	0.078	94	653
97.57	2.010	0.7	5.270	0.105	173	654
108.60	2.000	0.3	5.836	0.105	79	543
111.1?	2.006	1.0	5.990	0.078	181	654
116.90	1.953	0.7	6.135	0.052	186	654
120.99	2.003	0.1	6.511	0.052	53	321
121.49	1.959	0.3	6.393	0.078	95	654
123.02	1.928	0.4	6.374	0.105	174	654
136.69	1.926	0.?	7.073	0.105	80	654
137.01	1.924	0.5	7.084	0.105	51	321
137.36	1.943	1.0	7.170	0.105	132	321
140.63	1.894	0.8	7.157	0.078	182	654
148.17	1.843	0.8	7.338	0.052	187	654
152.95	1.869	0.2	7.682	0.078	96	654
153.39	1.925	0.6	7.933	0.052	15	321
155.57	1.897	0.9	7.931	0.105	175	654
170.87	1.854	0.4	8.510	0.052	54	321
178.80	1.802	0.9	8.657	0.078	183	654
191.75	1.841	0.9	9.488	0.052	55	321
192.61	1.789	0.?	9.159	0.078	97	654
197.05	1.795	0.4	9.311	0.052	17	321
201.42	1.759	0.9	9.521	0.078	184	654
215.17	1.763	0.7	10.196	0.052	56	321
216.02	1.774	0.8	10.300	0.026	21	321
216.67	1.736	0.4	10.105	0.052	18	321
223.14	1.684	0.9	10.095	0.052	188	654
241.45	1.697	0.6	11.007	0.052	57	321
242.69	1.672	0.9	10.901	0.026	87	654
243.15	1.685	0.3	11.008	0.052	19	321
250.95	1.671	1.2	11.266	0.052	189	654
262.09	1.639	1.0	11.545	0.037	192	654
268.89	1.645	0.3	11.882	0.026	82	543
270.48	1.646	0.1	11.965	0.026	59	543
270.86	1.640	0.2	11.937	0.052	58	321
271.93	1.645	0.9	12.089	0.026	23	321
272.85	1.641	0.6	12.032	0.052	20	321
282.12	1.591	0.9	12.057	0.052	190	654
295.17	1.566	0.8	12.417	0.037	193	654

O_2^+ in O_2 (Continued)

E/N (Td)	Reduced Mobility (cm^2/v sec)	Standard Deviation (Per Cent)	Drift Velocity (10^4cm/sec)	Pressure (Torr)	Run Number	Positions
303.71	1.482	0.4	12.098	0.026	60	543
317.43	1.533	0.9	13.073	0.052	191	654
339.58	1.522	0.5	13.390	0.026	84	654
342.29	1.539	0.7	14.156	0.026	25	321
350.68	1.484	0.9	13.983	0.037	195	654
367.15	1.497	0.5	14.764	0.026	197	654
382.34	1.478	0.9	15.181	0.026	62	543
384.07	1.475	1.0	15.226	0.026	26	321
393.60	1.418	0.8	14.999	0.037	195	654
427.61	1.413	0.6	16.241	0.026	85	654
428.87	1.439	0.2	16.578	0.025	63	543
434.78	1.417	0.5	16.550	0.026	198	654
443.87	1.393	0.7	16.610	0.037	196	654
483.68	1.336	1.0	17.359	0.026	86	543
488.44	1.352	0.9	17.743	0.026	199	654
539.97	1.354	0.7	19.649	0.026	65	543
549.17	1.299	1.0	19.166	0.026	200	654

O_4^+ in O_2

E/N (Td)	Reduced Mobility (cm^2/Vsec)	Standard Deviation (Per Cent)	Drift Velocity (10^4cm/sec)	Pressure (Torr)	Run Number	Positions
2.56	2.160	0.8	0.161	6.270	425	321
2.61	2.131	0.7	0.154	6.270	424	321
2.76	2.184	0.9	0.164	5.225	427	321
3.39	2.137	0.9	0.220	5.225	429	321
4.60	2.155	0.6	0.266	3.135	418	432
5.25	2.111	0.7	0.298	3.135	419	432
6.87	2.151	0.6	0.395	3.135	416	432
7.79	2.15[illegible]	0.9	0.450	3.135	417	432

K^+ in O_2

E/N (Td)	Reduced Mobility (cm^2/Vsec)	Standard Deviation (Per Cent)	Drift Velocity (10^4cm/sec)	Pressure (Torr)	Run Number	Positions
1.53	2.686	0.1	0.110	0.626	246	321
1.94	2.672	0.1	0.139	0.626	247	321
2.59	2.706	0.4	0.190	5.270	426	432
2.74	2.697	0.8	0.199	0.626	248	321
3.05	2.680	0.4	0.218	3.135	390	432
3.10	2.709	0.4	0.226	4.180	422	432
3.31	2.713	0.9	0.243	5.225	430	432
3.40	2.674	0.6	0.246	3.135	391	543
3.43	2.685	0.1	0.248	0.418	217	432
3.44	2.726	0.8	0.252	4.180	423	432
3.46	2.673	0.4	0.263	3.135	392	543
3.67	2.719	0.5	0.268	3.135	379	543
3.89	2.684	0.4	0.280	0.626	249	432
4.11	2.705	0.6	0.301	3.135	380	543
4.43	2.682	0.3	0.312	0.418	218	543
5.45	2.680	0.4	0.392	0.418	219	543
5.50	2.699	0.5	0.399	2.090	378	543
6.15	2.678	0.9	0.442	0.626	250	543
6.42	2.685	0.5	0.463	1.045	374	432
6.85	2.682	0.5	0.493	0.209	209	543
6.88	2.689	0.3	0.497	0.418	220	654
7.69	2.687	0.3	0.555	0.209	208	543
7.78	2.695	0.5	0.564	1.045	375	432
8.67	2.701	0.5	0.629	0.418	221	654
8.71	2.701	0.5	0.630	1.045	376	432
9.67	2.699	0.8	0.701	0.209	207	543
11.59	2.718	0.4	0.846	0.209	206	321
12.24	2.721	0.4	0.895	0.418	222	654
13.67	2.694	0.5	0.990	0.209	210	543
17.32	2.715	0.3	1.264	0.418	223	654
19.32	2.704	0.3	1.404	0.209	211	543
24.35	2.744	0.7	1.795	0.105	231	654
24.48	2.737	0.8	1.811	0.418	224	654
27.32	2.727	0.5	2.002	0.209	212	543
30.63	2.755	0.2	2.267	0.105	232	654
31.35	2.770	0.9	2.331	0.105	204	543
34.55	2.772	0.4	2.573	0.418	225	654
38.58	2.787	0.3	2.889	0.209	213	654
43.28	2.811	0.5	3.268	0.105	233	654
48.61	2.823	0.4	3.687	0.209	214	654
54.47	2.866	0.8	4.194	0.105	234	654
61.21	2.914	0.5	4.792	0.209	215	654
69.57	3.105	0.6	5.555	0.105	235	654

K^+ in O_2 (Continued)

E/N (Td)	Reduced Mobility (cm^2/Vsec)	Standard Deviation (Per Cent)	Drift Velocity (10^4cm/sec)	Pressure (Torr)	Run Number	Positions
77.06	3.059	0.3	6.33	0.209	216	654
86.37	3.152	0.4	7.314	0.105	236	654
96.62	3.243	0.7	8.418	0.052	239	654
121.61	3.377	1.0	11.034	0.052	240	654
136.77	3.425	0.6	12.588	0.105	238	654
137.80	3.449	0.3	12.772	0.078	335	543
153.13	3.479	0.7	14.315	0.052	241	654
169.97	3.464	0.8	15.234	0.052	304	654
173.37	3.454	0.4	16.088	0.078	336	654
194.46	3.425	0.4	17.894	0.078	337	654
194.58	3.440	0.9	17.969	0.052	338	654
217.68	3.327	0.8	22.431	0.052	301	654
244.68	3.310	0.5	26.739	0.052	303	654
258.31	3.267	0.4	29.922	0.052	304	654
274.35	3.168	0.7	23.357	0.052	340	654
308.06	3.138	1.0	25.997	0.052	341	654

O^- in O_2

E/N (Td)	Reduced Mobility ($cm^2/Vsec$)	Standard Deviation (Per Cent)	Drift Velocity (10^4 cm/sec)	Pressure (Torr)	Run Number	Positions
3.97	3.205	0.8	0.342	0.261	322	543
3.98	3.225	1.0	0.352	0.261	292	543
4.34	3.219	0.9	0.376	0.313	294	321
4.91	3.165	0.9	0.416	0.261	321	543
5.01	3.214	0.9	0.436	0.313	293	321
5.70	3.225	0.5	0.494	0.209	318	543
6.14	3.111	0.8	0.523	0.261	320	543
7.04	3.188	0.6	0.603	0.209	317	543
7.73	3.178	0.6	0.658	0.261	319	543
8.73	3.167	0.8	0.743	0.209	316	543
11.54	3.201	0.8	0.992	0.209	315	543
13.73	3.184	0.4	1.174	0.209	314	543
15.49	3.206	0.9	1.234	0.157	268	321
17.33	3.297	0.7	1.527	0.209	263	432
19.56	3.292	1.0	1.736	0.157	269	542
21.86	3.306	0.7	1.942	0.209	264	543
24.37	3.310	0.7	2.168	0.157	270	321
27.50	3.362	0.7	2.336	0.105	274	321
30.94	3.394	0.7	2.822	0.209	265	543
34.42	3.431	0.7	3.172	0.157	271	432
38.96	3.612	1.0	3.782	0.105	276	432
43.67	3.632	0.5	4.261	0.209	266	654
48.68	3.764	0.4	4.924	0.157	217	432
55.70	3.964	1.4	5.879	0.105	277	532
61.70	4.069	0.6	6.746	0.209	267	654
68.97	4.223	0.8	5.827	0.157	273	432
77.30	4.376	0.4	9.090	0.105	278	432
86.69	4.592	0.5	10.697	0.078	279	652
96.72	4.555	0.8	11.837	0.052	283	432
109.27	4.819	0.8	14.149	0.078	280	432
122.64	4.783	1.2	15.762	0.105	275	654
137.65	4.725	0.9	17.476	0.052	284	432
174.85	4.578	0.9	21.265	0.052	285	543

O_2^- in O_2

E/N (Td)	Reduced Mobility (cm^2/Vsec)	Standard Deviation (Per Cent)	Drift Velocity (10^4cm/sec)	Pressure (Torr)	Run Number	Positions
3.10	2.177	0.8	0.177	0.627	346	432
3.94	2.131	0.4	0.226	0.523	334	432
4.03	2.163	0.6	0.234	0.627	349	432
4.96	2.173	0.7	0.290	0.627	348	543
5.47	2.131	0.8	0.313	0.523	333	432
6.20	2.174	0.6	0.362	0.627	347	432
6.85	2.164	0.5	0.393	0.522	332	432
7.70	2.173	0.9	0.450	0.418	305	321
8.70	2.166	0.6	0.499	0.522	342	543
9.66	2.154	0.7	0.559	0.627	350	654
10.84	2.165	0.4	0.634	0.418	306	432
12.01	2.172	0.3	0.701	0.627	298	543
12.32	2.163	0.8	0.716	0.522	343	543
13.66	2.181	0.6	0.801	0.627	351	654
15.41	2.169	0.6	0.898	0.418	307	432
17.44	2.174	0.8	1.019	0.522	344	654
19.35	2.162	0.9	1.124	0.627	352	654
21.82	2.164	0.6	1.269	0.418	308	543
24.68	2.176	0.8	1.443	0.522	345	654
27.43	2.162	0.9	1.594	0.209	353	653
30.80	2.159	0.7	1.787	0.418	309	654
34.82	2.152	0.5	2.013	0.209	354	543
38.97	2.159	0.4	2.260	0.418	310	654
43.99	2.144	0.6	2.534	0.209	355	543
55.58	2.145	0.6	3.204	0.209	356	654
79.46	2.119	0.9	4.525	0.209	358	654
87.17	2.098	0.6	4.918	0.104	462	654
98.34	2.021	0.9	5.338	0.104	463	654
124.16	2.002	0.7	6.672	0.004	464	654
140.49	1.954	0.4	7.361	0.104	465	654

O_3^- in O_2

E/N (Td)	Reduced Mobility (cm^2/Vsec)	Standard Deviation (Per Cent)	Drift Velocity (10^4cm/sec)	Pressure (Torr)	Run Number	Positions
4.56	2.529	0.3	0.310	2.612	449	543
5.11	2.541	0.2	0.349	2.612	450	543
5.69	2.557	0.3	0.391	2.612	453	543
6.24	2.561	0.6	0.432	2.612	454	543
6.40	2.533	0.2	0.436	1.568	442	543
6.80	2.550	0.5	0.466	2.090	433	543
7.01	2.551	0.2	0.481	1.568	443	543
7.26	2.542	0.3	0.496	2.090	434	543
7.31	2.533	0.4	0.497	1.568	441	654
7.72	2.555	0.3	0.530	2.090	435	543
7.93	2.562	0.4	0.546	1.568	444	654
8.85	2.563	0.3	0.609	1.568	445	654
9.78	2.565	0.8	0.674	1.568	446	654
10.71	2.608	0.4	0.751	1.568	447	654
10.76	2.614	0.8	0.756	1.568	440	654
10.95	2.632	0.7	0.780	1.045	436	654
11.34	2.629	0.9	0.811	1.568	439	654
11.64	2.621	0.8	0.812	1.568	448	654
12.79	2.624	0.5	0.922	1.045	437	654
14.65	2.634	0.9	0.921	1.045	438	654

O_4^- in O_2

E/N (Td)	Reduced Mobility (cm^2/Vsec)	Standard Deviation (Per Cent)	Drift Velocity (10^4cm/sec)	Pressure (Torr)	Run Number	Positions
3.10	2.141	0.9	0.203	4.180	473	543
3.44	2.152	0.3	0.242	4.180	474	543
4.26	2.116	0.6	0.256	3.135	476	543
4.60	2.162	0.5	0.272	3.135	475	543

CO_3^- in O_2

E/N (Td)	Reduced Mobility ($cm^2/Vsec$)	Standard Deviation (Per Cent)	Drift Velocity ($10^4 cm/sec$)	Pressure (Torr)	Run Number	Positions
2.44	2.420	0.9	0.159	3.135	368	432
2.75	2.493	0.5	0.184	3.135	369	432
3.49	2.492	0.5	0.233	3.135	370	432
3.97	2.500	0.6	0.267	3.135	371	432
4.48	2.518	0.1	0.305	2.090	383	543
4.49	2.510	0.2	0.304	3.135	372	543
5.09	2.511	0.1	0.342	3.135	373	543
5.11	2.502	0.2	0.344	2.612	451	543
5.67	2.516	0.2	0.384	2.612	452	543
7.10	2.492	0.4	0.475	2.090	382	654

CO_4^- in O_2

E/N (Td)	Reduced Mobility (cm^2/Vsec)	Standard Deviation (Per Cent)	Drift Velocity (10^4cm/sec)	Pressure (Torr)	Run Number	Positions
3.23	2.427	0.7	0.210	3.135	405	543
4.03	2.420	0.8	0.262	3.135	406	543
4.86	2.450	0.6	0.330	3.135	407	543

APPENDIX II

TABULATION OF THE LONGITUDINAL DIFFUSION COEFFICIENT RESULTS

The following pages list the results of the longitudinal diffusion coefficient determinations described in Chapter V. The results appear in order of increasing E/N for each ion species. The column headings, E/N, Pressure, Run Number, and Positions, have the same meaning as in Appendix I. ND_L gives the gas density normalization required if diffusion coefficients obtained at various pressures are to be compared, in units of 10^{18}/cm sec. The standard deviation is the standard deviation in percentage that gives the per cent by which the D_L values for the three positions differed from the average. D_L is the longitudinal diffusion coefficient as determined by the least cubes fit to Equation (126). The value is the average of the values obtained from the three drift positions.

O_2^+ in O_2

E/N (Td)	ND_L ($\times 10^{18}$/cm sec)	Standard Deviation (Per Cent)	D_L (cm^2/sec)	Pressure (Torr)	Run Number	Positions
7.07	1.84	9.1	274	0.209	201	431
8.66	1.98	6.7	394	0.157	112	321
9.89	1.86	2.8	93	0.418	165	321
10.89	1.85	6.4	376	0.157	110	321
11.43	2.00	7.6	298	0.209	202	543
12.62	1.74	2.6	266	0.209	169	543
13.69	1.86	6.0	407	0.157	109	321
14.04	1.92	9.2	583	0.105	166	321
15.50	1.87	2.1	372	0.157	162	421
19.60	1.88	5.6	376	0.157	163	421
20.14	1.94	3.7	614	0.105	167	653
25.52	1.85	4.2	575	0.105	168	654
31.40	2.15	5.6	868	0.078	176	531
44.48	2.30	7.8	931	0.078	177	653
49.04	2.52	1.0	751	0.105	170	654
56.93	2.78	10.0	1147	0.078	179	421
61.81	2.75	4.4	822	0.105	171	654
77.89	3.22	5.4	961	0.105	172	654
88.73	3.44	6.6	1394	0.078	180	654
97.57	4.07	2.3	1213	0.105	173	654
111.13	4.27	2.7	1724	0.078	181	654
116.90	4.45	3.6	2437	0.052	186	654
123.02	4.58	2.6	1366	0.105	174	654
140.63	5.10	3.7	2067	0.078	182	654
148.17	5.37	4.4	3258	0.052	187	654
178.80	6.11	3.3	2501	0.078	183	654
201.42	6.54	1.9	2691	0.078	184	654
223.54	6.83	2.1	4158	0.052	188	654
262.09	8.10	6.3	6983	0.037	192	654
282.12	8.77	3.9	5364	0.052	190	654
295.17	8.68	8.3	7487	0.037	193	654
317.43	10.55	4.1	6471	0.052	191	654
350.69	10.50	5.0	7913	0.037	194	654
367.15	11.35	3.1	13506	0.026	197	654
393.60	11.14	1.4	9618	0.037	195	654
434.78	12.78	2.8	15215	0.026	198	654
443.87	13.80	3.6	11981	0.037	196	654
488.44	14.47	2.0	17243	0.026	199	654
549.17	16.16	1.2	19137	0.026	200	654

K^+ in O_2

E/N (Td)	ND_L ($\times 10^{18}$/cm sec)	Standard Deviation (Per Cent)	D_L (cm^2/sec)	Pressure (Torr)	Run Number	Positions
3.43	2.00	5.2	148	0.418	217	421
3.89	2.07	5.0	102	0.626	249	432
4.43	2.01	3.9	148	0.418	218	543
5.45	2.02	4.6	149	0.418	219	543
6.85	2.03	4.6	300	0.209	209	543
6.88	1.98	3.9	146	0.418	220	654
7.69	2.04	2.9	300	0.209	208	543
8.67	1.97	7.6	146	0.418	221	654
9.67	2.10	2.6	310	0.209	207	543
13.67	2.24	3.5	330	0.209	210	543
17.32	2.45	8.6	181	0.418	223	654
19.32	2.52	4.6	371	0.209	211	543
24.35	2.73	5.7	806	0.105	231	654
27.32	2.61	7.7	385	0.209	212	543
30.63	2.84	4.6	839	0.105	232	654
31.35	3.72	2.4	1126	0.105	204	543
34.55	3.94	4.4	292	0.418	225	654
38.58	3.57	8.0	528	0.209	213	654
43.28	4.26	5.2	1258	0.105	233	654
48.61	4.44	3.2	656	0.209	214	654
54.47	5.31	4.2	1570	0.105	234	654
61.21	6.43	5.7	952	0.209	215	654
68.57	9.25	3.1	2735	0.105	235	654
77.06	9.95	3.1	1472	0.209	216	654
86.37	13.97	5.0	4131	0.105	236	654
96.62	17.17	3.8	10127	0.052	239	654
121.61	23.41	4.6	13805	0.052	240	654
136.77	32.12	5.8	9494	0.105	238	654
137.80	29.31	2.7	11241	0.078	335	543
153.13	32.83	4.0	19365	0.052	241	654
169.97	35.56	5.3	21154	0.052	304	654
173.37	38.81	3.0	15403	0.078	336	654
194.46	40.30	1.8	16016	0.078	337	654
217.94	41.31	2.2	24365	0.052	339	654
244.68	48.20	5.1	28681	0.052	302	654
274.36	50.30	3.8	29915	0.052	340	654
308.06	62.75	4.6	37349	0.052	341	654

O^- in O_2

E/N (Td)	ND_L ($\times 10^{18}$/cm sec)	Standard Deviation (Per Cent)	D_L (cm^2/sec)	Pressure (Torr)	Run Number	Positions
3.97	1.94	9.1	236	0.261	322	543
4.91	1.97	8.0	236	0.261	321	543
5.70	1.99	3.3	310	0.209	318	543
6.14	1.94	4.0	231	0.261	320	543
7.73	2.04	3.8	253	0.261	319	543
8.73	2.01	4.6	300	0.209	316	543
11.54	2.10	3.9	327	0.209	315	543
13.73	2.11	7.5	342	0.209	314	543
17.04	2.05	4.8	311	0.209	317	543
17.33	2.53	3.3	375	0.209	263	432
19.15	3.62	3.9	187	0.627	260	321
21.86	2.97	2.1	442	0.209	264	543
24.37	3.18	5.7	625	0.157	270	321
30.94	4.30	6.0	640	0.209	265	543
34.42	4.22	2.0	831	0.157	271	432
38.96	5.95	0.4	1777	0.105	276	421
43.67	7.19	3.4	1071	0.209	266	654
46.68	9.05	2.2	1787	0.157	272	432
55.70	12.02	6.0	3599	0.105	277	532
61.70	14.78	2.6	2204	0.209	267	654
68.97	18.63	6.3	3690	0.157	273	432
77.30	22.36	4.0	6665	0.105	278	321
86.69	28.51	2.8	11282	0.078	279	652
96.72	27.95	6.0	16787	0.052	283	432
109.27	37.80	1.2	14981	0.078	280	432
122.64	38.76	1.6	11525	0.105	275	654
137.65	42.01	8.2	24502	0.052	284	432
174.85	48.33	5.4	28687	0.052	285	543

O_2^- in O_2

E/N (Td)	ND_L ($\times 10^{18}$/cm sec)	Standard Deviation (Per Cent)	D_L (cm^2/sec)	Pressure (Torr)	Run Number	Positions
3.94	1.27	10.1	73	0.522	334	432
4.03	1.28	1.1	64	0.627	349	432
4.96	1.31	6.2	66	0.627	348	543
5.47	1.52	4.6	85	0.522	333	432
6.20	1.40	8.2	67	0.627	347	432
6.85	1.40	4.3	80	0.522	332	432
7.70	1.45	9.6	105	0.418	305	321
8.70	1.48	5.9	88	0.522	342	543
9.66	1.60	9.5	78	0.627	350	654
10.84	1.56	7.0	111	0.418	306	432
12.01	1.65	9.1	82	0.627	298	543
12.32	1.74	7.4	104	0.522	343	543
13.66	1.78	10.1	88	0.627	351	654
15.41	1.61	4.9	118	0.418	307	432
17.44	1.72	2.4	103	0.522	344	654
19.35	1.78	9.4	88	0.627	352	654
21.82	1.85	8.9	137	0.418	308	543
24.68	1.94	10.0	116	0.522	345	654
27.43	1.86	2.0	271	0.209	353	653
30.80	2.07	10.1	154	0.418	309	654
34.82	2.00	4.2	298	0.209	354	543
38.97	2.23	10.0	167	0.418	310	654
43.99	2.18	6.1	328	0.209	355	543
55.58	2.75	6.9	415	0.209	356	654
67.26	4.12	3.3	660	0.209	357	654
79.46	4.61	2.0	642	0.209	358	654

APPENDIX III

TABULATION OF THE ION-MOLECULE REACTION RATES

The following pages list the results of the ion-molecule reaction rate determinations discussed in Chapter VI. The results appear in order of increasing E/N for each reaction. The column headings Positions, Pressures, and E/N have the same meanings as in Appendix I. The notation 1-7 in the Positions column means that positions 1 through 7 inclusive were used. The Reaction Rate is the coefficient k, in units of cm^6/sec for O^- reacting to form O_3^- and in units cm^3/sec for O^- reacting to form O_2^-. The Error refers to the estimated per cent error in the determination of k. Technique refers to the method of analysis used to determine k. These methods are described in Chapter VI.

$$O^- + 2O_2 \rightarrow O_3^- + O_2$$

E/N (Td)	Reaction Rate (cm^6/sec)	Error (Per Cent)	Pressures	Positions	Technique
6.04	1.0×10^{-30}	±14	.836	1-7	Fall Off
6.82	7.9×10^{-31}		.836	6,5	Curve Fit
7.44	1.0×10^{-30}	±14	.836	1-7	Fall Off
8.98	1.0×10^{-30}	±14	.732	1-7	Fall Off
12.47	1.1×10^{-30}	±14	.732	1-7	Fall Off
12.76	8.5×10^{-31}		.732	6	Curve Fit
13.94	1.0×10^{-30}	±14	.523	1-7	Fall Off
15.44	1.1×10^{-30}	±14	.313	1-7	Fall Off
15.85	8.5×10^{-31}		.627	6,5	Curve Fit
17.49	1.0×10^{-30}	±14	.732	1-7	Fall Off
19.74	1.1×10^{-30}	±14	.523	1-7	Fall Off
20.02	9.4×10^{-30}		.523	6,5	Curve Fit
27.91	1.1×10^{-30}	±14	.523	1-7	Fall Off

$$O^- + O_2 \rightarrow O_2^- + O$$

E/N (Td)	Reaction Rate (cm^3/sec)	Error (Per Cent)	Pressures (Torr)	Positions	Technique
62	2.5×10^{-14}	±58	0.105 and 0.209	7,6	Curve Fit
67	6.0×10^{-14}	±40	0.105 and 0.209	7,6	Curve Fit
78	2.2×10^{-13}	±32	0.105 and 0.209	7,6,5	Curve Fit
87	4.6×10^{-13}	±28	0.105 and 0.209	7,6,5	Curve Fit
98	7.8×10^{-13}	±28	0.105 and 0.209	7,6,5	Curve Fit
124	2.5×10^{-12}	±21	0.105 and 0.209	7,6,5	Curve Fit
140	3.4×10^{-12}	±19	0.105 and 0.209	7,6,5	Curve Fit

APPENDIX IV

THE TRANSPORT EQUATION AND ITS SOLUTION FOR IONS UNDERGOING DEPLETING REACTIONS

The transport equation and its solution, for the geometry of the present experiment, for ions undergoing only a depletion reaction has been reported by Moseley and Gatland[57,58] and will be outlined here.

Consider an ion population created at one end of a cylindrically symmetric drift space filled with gas at a uniform pressure, in which there exists an externally applied uniform electric field $\vec{E}$ along the z axis. Assume that the number density of the ion swarm, $n(\vec{r},t)$, is low enough that the space charge field is negligible. For this situation, Wannier[41] has shown that the ionic current density is given by

$$\vec{j}(\vec{r},t) = \vec{v}_d n(\vec{r},t) - \overleftrightarrow{D} \cdot \vec{\nabla}_r n(\vec{r},t). \qquad (119)$$

where $\overleftrightarrow{D}$ is a 3 x 3 diagonal tensor, the first two components of which (corresponding to the directions perpendicular to $\vec{E}$) are equal. If no gain in numbers of the species under consideration during the movement down the drift tube is allowed, but the loss of these ions through ion-molecule reactions with frequency α is considered, then the ion swarm is subject to a continuity equation of the form

$$\frac{\partial n}{\partial t} + \vec{\nabla} \cdot \vec{j} + \alpha n = 0. \tag{120}$$

If we denote the first two (transverse) components of $\overleftrightarrow{D}$ by D_T and the third (longitudinal) component by D_L, and add a source term, $\beta(\vec{r},t)$, to represent the source of ions at the initial end of the drift space, the equation for consideration becomes, in rectangular coordinates,

$$\frac{\partial n(x,y,z,t)}{\partial t} = D_T\left[\frac{\partial^2 n}{\partial x^2} + \frac{\partial^2 n}{\partial y^2}\right] + D_L \frac{\partial^2 n}{\partial z^2} - v_d \frac{\partial n}{\partial z} - \alpha n + \beta(x,y,z,t). \tag{121}$$

In the present apparatus, for which this analysis was developed, the ions enter the drift space through a circular aperture lying in a plane normal to the drift tube axis and centered on the axis. If the coordinate system is taken to have its origin at the center of this aperture and the electric field along z is in such a direction as to cause the ions to drift in the positive z direction, then the solution to Equation (121) in unbounded space is

$$n(x,y,z,t) = \int_{-\infty}^{t} dt' \int_{-\infty}^{\infty} dx' \int_{-\infty}^{\infty} dy' \int_{-\infty}^{\infty} dz' \frac{\beta(x',y',z',t')}{[4\pi(t-t')]^{3/2} D_T D_L^{1/2}} \tag{122}$$

$$\times \exp\left[-\alpha(t-t') - \frac{(x-x')^2 + (y-y')^2}{4 D_T(t-t')} - \frac{[z-z' - v_d(t-t')]^2}{4 D_L(t-t')}\right].$$

That (122) is indeed a solution to (121) can easily be verified by direct substitution.

Suppose the input β is given by

$$\beta(r',z',t') = \frac{b}{\pi r_o^2} S(\bar{r}_o - \bar{r}')\delta(z')\delta(t'), \tag{123}$$

where $S(\phi) = 0$ if $\phi < 0$, $S(\phi) = 1$ otherwise. This function describes an axially thin disk source of b ions with uniform surface density and radius r_o, being created instantaneously at $t' = 0$ in the plane $z' = 0$. Let $b/\pi r_o^2 = s$, the planar source density. Then (in cylindrical coordinates)

$$n(r,z,t) = \frac{s\, e^{-\alpha t} \exp\left(-(z-v_d t)^2/4D_L t\right)}{(4\pi t)^{3/2} D_T D_L^{1/2}} \int_o^{r_o} r'dr' \times \tag{124}$$

$$\int_o^{2\pi} d\theta' \exp\left[-\frac{r^2+r'^2 - 2rr'\cos\theta'}{4 D_T t}\right].$$

The remaining two integrals can be performed to yield

$$n(r,z,t) = \frac{s}{(4\pi D_L t)^{1/2}} \exp\left[-\alpha t - \frac{(z-v_d t)^2}{4D_L t}\right] X \tag{125}$$

$$\left[1 - \sum_{m=0}^{\infty} \sum_{i=0}^{m} \frac{1}{m!i!} \left(\frac{r^2}{4D_T t}\right)^m \left(\frac{r_o^2}{4D_T t}\right)^i \exp\left(-\frac{r_o^2 + r^2}{4D_T t}\right)\right].$$

Equation (125) is an expression for the ion number density at any given time at any point in space for an ion swarm which (1) was instantaneously created with uniform density across an axially thin disk, (2) drifts in unbounded space under the influence of a constant electric field, and (3) possibly undergoes a depleting reaction with the neutral gas molecules.

Since the apparatus to be considered here samples the ion swarm on the axis, the quantity of interest is the axial number density

$$n(0,z,t) = \frac{s\, e^{-\alpha t}}{(4\, D_L t)^{1/2}} [1 - \exp(-r_o^2/4D_T t)] \exp[-(z-v_d t)^2/4D_L t] \qquad (126)$$

where s is the initial ion surface density of the delta-function input of ions and r_o is the radius of the ion entrance aperture.

The quantity measured experimentally is the flux Φ of ions leaving the drift tube through the exit aperture of area A at a fixed distance z from the source plane:

$$\Phi(0,z,t) = Aj(0,z,t), \qquad (127)$$

where j(0,z,t) is the z-component of the ionic current density in the drift tube, on the axis, at the end of the drift distance z.

The ionic current density is related to the ionic number density by Equation (13), so that

$$j(0,z,t) = -D_L(\partial n/\partial z) + v_d n, \qquad (128)$$

where n(0,z,t) is given by (126). Differentiation and substitution into (127) gives

$$\phi(0,z,t) = \frac{A\ s\ e^{-\alpha t}}{4(\pi D_L t)^{1/2}} (v_d + z/t)[1 - \exp(-r_o^2/4D_T t)]\ \exp[-(z-v_d t)^2/4D_L t]. \tag{129}$$

In summary, Equation (129) gives the flux of ions passing through the exit aperture of the drift tube as a function of the time t and drift distance z. All of the ions of the species under consideration are assumed to be introduced from the ion source in periodic delta-function bursts, and none are produced by reactions in the drift space. However, loss of the ions in reactions producing other species is allowed, the rate of loss being described by the frequency α.

APPENDIX V

ANALYTIC EXPRESSION FOR THE INTEGRATED INTENSITY ON AXIS

Previous investigations in this laboratory made use of the integrated intensity on axis, I(z), in the study of transverse diffusion and depletion reactions. I(z) was determined from the following integration

$$I(z) = \int_0^\infty \Phi(0,z,t)dt \tag{130}$$

where $\Phi(0,z,t)$ is defined by Equation (129). This integration was previously performed numerically, but during the course of the present experiment the integration was performed analytically.

I(z) can be expressed as the sum of four integrals whose integrands are as follows:

$$[Asv_d e^{-\alpha t}/4(\pi D_L t)^{1/2}]\exp[-(z-v_d t)^2/4D_L t]\,, \tag{131}$$

$$-[Asv_d e^{-\alpha t}/4(\pi D_L t)^{1/2}]\exp[-r_o^2/4D_T t]\exp[-(z-v_d t)^2/4D_L t]\,, \tag{132}$$

$$[Asze^{-\alpha t}/4(\pi D_L t^3)^{1/2}]\exp[-(z-v_d t)^2/4D_L t]\,, \tag{133}$$

and

$$-[Asze^{-\alpha t}/4(\pi D_L t^3)^{1/2}]\exp[-r_o^2/4D_T t]\exp[-(z-v_d t)^2/4D_L t]. \tag{134}$$

These four integrals are put in a form so that the following expression can be used[85]

$$\int_0^\infty dx\ \exp(-a^2x^2 - b^2/x^2) = \frac{\pi^{1/2}}{2a} e^{-2ab}. \qquad (135)$$

The integral of integrand (131) can be written as

$$\frac{Asv_d}{4(\pi D_L)^{1/2}} \int_0^\infty \frac{dt}{t^{1/2}} \exp\left[- \frac{z^2}{4D_L t} + \frac{2zv_d t}{4D_L t} - \frac{v_d^2 t^2}{4D_L t} - \alpha t \right]. \qquad (136)$$

Make a change of variables, $x = t^{1/2}$, and define $a^2 = \alpha + v_d^2/4D_L$ and $b^2 = z^2/4D_L$; then Equation (136) can be written as

$$\frac{Asv_d}{2(\pi D_L)^{1/2}} \exp(zv_d/2D_L) \int_0^\infty \exp[-b^2/x^2 - a^2x^2]dx. \qquad (137)$$

The integration can be performed to yield

$$\frac{Asv_d \exp[zv_d/2D_L]}{4D_L^{1/2}[v_d^2/4D_L + \alpha]^{1/2}} \exp\left[- \frac{z(\alpha + v_d^2/4D_L)^{1/2}}{D_L^{1/2}} \right]. \qquad (138)$$

Examination of the integral of integrand (132) shows that it is the same as that for (131) except for the definition of b^2. b^2 is now defined by $b^2 = z^2/4D_L + r_o^2/4D_T$. The resulting integration of (132) yields

$$\frac{-Asv_d \exp[zv_d/2D_L]}{4D_L^{1/2}[v_d^2/4D_L+\alpha]^{1/2}} \exp\left[-2\left\{\frac{z^2}{4D_L}+\frac{r_o^2}{4D_T}\right\}^{1/2}\left\{\frac{v_d^2}{4D_L}+\alpha\right\}^{1/2}\right]. \qquad (139)$$

The integral of integrand (133) can be expressed as

$$\frac{Asz}{4(\pi D_L)^{1/2}} \int_0^\infty \frac{dt}{t^{3/2}} \exp\left[-\frac{z^2}{4D_L t}+\frac{2zv_d t}{4D_L t}-\frac{v_d^2 t^2}{4D_L t}-\alpha t\right]. \qquad (140)$$

Make a change of variables $x = t^{-1/2}$ and define $a^2 = z^2/4D_L$ and $b^2 = \alpha + v_d^2/4D_L$; then Equation (140) can be written in the form of Equation (135). Therefore the integral of (133) yields

$$\frac{As}{2} \exp(zv_d/2D_L)\exp\left[-\frac{z}{D_L^{1/2}}(\alpha + v_d^2/4D_L)^{1/2}\right]. \qquad (141)$$

Performance of the integral of (134) yields

$$\frac{-Asz \exp(zv_d/2D_L)}{4D_L^{1/2}\left\{\frac{z^2}{4D_L}+\frac{r_o^2}{4D_T}\right\}^{1/2}} \exp\left[-2\left\{\frac{z^2}{4D_L}+\frac{r_o^2}{4D_T}\right\}^{1/2}\left\{\frac{v_d^2}{4D_L}+\alpha\right\}^{1/2}\right]. \qquad (142)$$

Summation of Equations (138), (139), (141), and (142) yields for I(z) the following

$$I(z) = \frac{As\ \exp(zv_d/2D_L)}{4D_L^{1/2}} \left\{ \left[2D_L^{1/2} + \frac{v_d}{(\alpha + v_d^2/4D_L)^{1/2}} \right] \exp\left[\frac{-z}{D_L^{1/2}} \left(\frac{v_d^2}{4D_L} + \alpha \right)^{1/2} \right] \right.$$

$$\left. - \left[\frac{z}{(z^2/4D_L + r_o^2/4D_T)^{1/2}} + \frac{v_d}{(\alpha + v_d^2/4D_L)^{1/2}} \right] \times \right. \tag{143}$$

$$\left. \exp\left[-2 \left(\frac{z^2}{4D_L} + \frac{r_o^2}{4D_T} \right)^{1/2} \left(\frac{v_d^2}{4D_L} + \alpha \right)^{1/2} \right] \right\} .$$

BIBLIOGRAPHY

1. L. G. H. Huxley, R. W. Crompton, and M. T. Elford, Bull. Inst. Physics and Physical Soc. 17, 251 (1966).

2. E. W. McDaniel, Collision Phenomena in Ionized Gases (John Wiley and Sons, Inc., New York, 1964), p. 427.

3. Ibid., p. 38.

4. T. M. Miller, Ph.D. Dissertation, Georgia Institute of Technology, Atlanta, Georgia, 1967 (unpublished), p. 83.

5. S. Chapman and T. G. Cowling, The Mathematical Theory of Non-Uniform Gases, Second Edition (Cambridge University Press, London, 1952).

6. J. Zeleny, Phil. Trans. Roy. Soc. A195, 193 (1901).

7. J. Franck, Verh. d. D. Phys. Ges. 12, 291 (1910).

8. N. E. Bradbury, Phys. Rev. 40, 508 (1932).

9. R. A. Nielsen and N. E. Bradbury, Phys. Rev. 51, 69 (1937).

10. R. W. Crompton and M. T. Elford, Proc. Phys. Soc. (London) 74, 497 (1959).

11. A. Z. Doehring, Naturforsch 7a, 253 (1952).

12. E. C. Beaty, Proceedings of the Fifth International Conference on Phenomena in Ionized Gases, Munich, 1961 (North Holland Publishing Co., Amsterdam, 1962), Vol. 1, p. 183.

13. R. N. Varney, Phys. Rev. 89, 708 (1953).

14. E. Huber, Phys. Rev. 97, 267 (1955).

15. E. Schulz-DuBois, Z. Physik 145, 269 (1956).

16. E. W. McDaniel, op. cit., p. 463, 514.

17. D. S. Burch and R. Geballe, Phys. Rev. 106, 183 (1957).

18. E. W. McDaniel and H. R. Crane, Rev. Sci. Instr. 28, 684 (1957).

19. E. W. McDaniel and M. R. C. McDowell, Phys. Rev. 114, 1028 (1959).

20. R. Maushart, Ann. Physik (7) 1, 264 (1958).

21. L. M. Chanin, A. V. Phelps, and M. A. Biondi, Phys. Rev. 128, 219 (1962).

22. H. Eiber, Z. Angew. Phys. 15, 103, 461 (1963).

23. M. H. Mentzoni, Phys. Rev. 134, A80 (1964).

24. J. A. Rees, Australian J. Phys. 18, 41 (1964).

25. R. E. Voshall, J. L. Peck, and A. V. Phelps, J. Chem. Phys. 43, 1990 (1965).

26. E. C. Beaty, L. M. Branscomb, and P. L. Patterson, Bull. Am. Phys. Soc. 9, 535 (1964).

27. J. A. R. Samson and G. L. Weissler, Phys. Rev. 137, A381 (1965).

28. L. G. McKnight, Bull. Am. Phys., Soc., 12, 228 (1967).

29. C. Shafter and E. C. Beaty, Bull. Am. Phys. Soc. 14, 264 (1968).

30. J. Dutton and P. Howells, Proc. Phys. Soc. B1, 1160 (1968).

31. I. A. Fleming and J. A. Rees, Proc. Phys. Soc. B2, 432 (1969).

32. R. N. Varney, Twenty Second Annual Gaseous Electronics Conference, Gatlinburg, Tennessee, October, 1969, Paper U3.

33. L. G. McKnight and J. M. Sawina, Twenty Second Annual Gaseous Electronics Conference, Gatlinburg, Tennessee, October, 1969, Paper U4.

34. L. G. McKnight (private communication).

35. E. W. McDaniel, Collision Phenomena in Ionized Gases (John Wiley and Sons, Inc., New York, 1964), pp. 491.

36. D. S. Burch and R. Geballe, Phys. Rev. 106, 188 (1957).

37. J. H. Yang and D. C. Conway, J. Chem. Phys. 40, 1729 (1964).

38. H. Eyring, J. O. Hirschfelder, and H. S. Taylor, J. Chem. Phys. 4, 479 (1936).

39. M. W. Zemansky, Heat and Thermodynamics (McGraw-Hill, New York, 1957), pp. 232.

40. J. L. Moruzzi and A. V. Phelps, J. Chem. Phys. 45, 4617 (1966).

41. G. H. Wannier, Bell System Technical Journal, 32, 170 (1953).

42. D. A. Durden, P. Kebarle, and A. Good, J. Chem. Phys. 50, 805 (1969).

43. S. B. Woo (private communication).

44. F. C. Fehsenfeld, P. D. Goldan, A. L. Schmelfekopf, and E. E. Ferguson, Planet. Space Sci. 13, 579 (1965).

45. M. J. Copsey, D. Smith, and J. Sayers, Planet, Space Sci. 16, 243 (1968).

46. F. C. Fehsenfeld, A. L. Schmeltekopf, H. I. Schiff, and E. E. Ferguson, Plant Space Sci. 15, 373 (1967).

47. F. C. Fehsenfeld, E. E. Ferguson, and D. K. Bohme, Planet. Space Sci. 17, 1759 (1960).

48. D. L. Albritton, Ph.D. Dissertation, Georgia Institute of Technology, Atlanta, Georgia, 1967 (Unpublished).

49. Miller, op. cit., Chap. II.

50. J. T. Moseley, Ph.D. Dissertation, Georgia Institute of Technology, Atlanta, Georgia, 1968 (unpublished), Chap. II.

51. McDaniel, op. cit., p. 457.

52. R. W. Crompton, M. T. Elford, and J. Gascoigne, Aust. J. Phys. 18, 409 (1965).

53. D. MacNair, Rev. Sci. Instr. 38, 124 (1967).

54. Albritton, op. cit., p. 40.

55. A. O. Nier, Rev. Sci. Instr. 18, 398 (1947).

56. R. L. Fitzwilson, J. N. Fox, and E. W. Thomas, J. of Physics E 3 (formerly J. Sci. Instr.), 36 (1970).

57. J. T. Moseley, I. R. Gatland, D. W. Martin, and E. W. McDaniel, Phys. Rev. 178, 234 (1969).

58. J. T. Moseley, Ph.D. Dissertation, Georgia Institute of Technology, Atlanta, Georgia, 1968 (unpublished), Chapter IV.

59. I. R. Gatland, Georgia Tech Technical Report GIT-4-PU, Headquarters Project Squid at Purdue University (1968).

60. M. Abramowitz and I. A. Stegun, Handbook of Mathematical Functions (National Bureau of Standard, 1965), p. 378.

61. A. Papoulis, The Fourier Integral and Its Application (McGraw-Hill, New York, 1962), p. 279.

62. I. R. Gatland (private communication).

63. R. C. Amme and N. G. Utterback, Proc. Intern. Conf. Phys. of Electron. Atomic Collisions, 1st Univ. Coll. London, 1963 (North-Holland Publishing Company, Amsterdam, 1964), p. 847.

64. J. W. McGowan and L. Kerwin, Can. J. Phys. 42, 2086 (1964).

65. C. E. Brion, J. Chem. Phys. 40, 2995 (1964).

66. B. R. Turner, R. F. Mathis, and J. A. Rutherford, J. Chem. Phys. 49, 2051 (1968).

67. R. K. Curran, J. Chem. Phys. 38, 2974 (1963).

68. D. K. Bohme, D. B. Dunkin, F. C. Fehsenfeld, and E. E. Ferguson, J. Chem. Phys. 51, 863 (1969).

69. E. H. Fink and K. H. Welge, Z. Naturforsch. 23a, 358 (1968).

70. J. T. Herron and H. I. Schiff, Can. J. Chem. 36, 1159 (1958).

71. D. C. Frost and C. A. McDowell, Advan. Mass Spectrometry 1, 413 (1959).

72. G. J. Schulz, Phys. Rev. 128, 178 (1962).

73. J. T. Moseley, op. cit., p. 81-97.

74. D. L. Albritton, op. cit., p. 169.

75. T. M. Miller, op. cit., p. 147.

76. J. T. Moseley, op. cit., p. 135.

77. J. T. Moseley, op. cit., p. 147.

78. J. T. Moseley, op. cit., p. 98.

79. J. T. Moseley, op. cit., p. 227.

80. J. T. Moseley, op. cit., p. 202.

81. J. T. Moseley, op. cit., p. 165.

82. T. M. Miller, op. cit., p. 171.

83. J. T. Moseley, op. cit., p. 105.

84. J. T. Moseley, op. cit., p. 101.

85. M. Abramowitz and I. A. Stegun, op. cit., p. 304.

VITA

Robert Marvin Snuggs, III was born in Montgomery, Alabama, on November 27, 1942. He is the first of three sons of Mr. and Mrs. Robert M. Snuggs, Jr. He was married to Wanda Hughes on August 14, 1965.

Mr. Snuggs was graduated from Bay County High School in Panama City, Florida, in 1960. He entered Georgia Institute of Technology in that year. During his undergraduate program, he was a Co-operative student with the United States Naval Research and Development Laboratory at Panama City, Florida. He received the degree of Bachelor of Science in Physics, with honor, in 1964. He immediately began graduate study, and received the degree of Master of Science in Physics in 1966. He held a NASA fellowship for three years of his graduate study.

Mr. Snuggs is a member of Sigma Xi, the American Physical Society, Phi Kappa Phi, Sigma Pi Sigma, and Tau Beta Pi.